Polyploidy in Liver Regeneration and Adaptation to Chronic Liver Injury

by

Patrick David Wilkinson

Bachelor of Science, Saint Vincent College, 2014

Submitted to the Graduate Faculty of

School of Medicine in partial fulfillment

of the requirements for the degree of

Doctor of Philosophy

University of Pittsburgh

2019

UNIVERSITY OF PITTSBURGH

SCHOOL OF MEDICINE

This thesis/dissertation was presented

by

Patrick David Wilkinson

It was defended on

April 17, 2019

and approved by

Joseph Locker, Professor, Department of Pathology

Wendy Mars, Associate Professor, Department of Pathology

Satdarshan (Paul) Singh Monga, Professor, Department of Pathology

Edward Prochownik, Professor, Department of Microbiology and Molecular Genetics

Dissertation Director: Andrew Duncan, Assistant Professor, Department of Pathology

Polyploidy in Liver Regeneration and Adaptation to Chronic Liver Injury

Patrick David Wilkinson, PhD

University of Pittsburgh, 2019

The liver contains diploid and polyploid hepatocytes (tetraploid, octaploid, etc.), with polyploids comprising ≥90% of the hepatocyte population in adult mice. Moreover, polyploid hepatocytes form multipolar spindles in mitosis, leading to individual chromosome gains and/or losses and random aneuploidy. The molecular mechanisms that regulate polyploidization have been well-characterized; however, it is unclear if diploid and polyploid hepatocytes function similarly in multiple contexts. The effect of aneuploidy on liver function is also unknown and the degree of liver aneuploidy is debated, with reports showing aneuploidy affects 5-60% of hepatocytes.

We used mice lacking *E2f7* and *E2f8* in the liver (LKO), which have a polyploidization defect. We found diploid hepatocytes were enriched 20-fold in LKO livers and nearly all LKO hepatocytes were euploid compared to control hepatocytes, which were mostly aneuploid, suggesting polyploids are required for production of aneuploid progeny. Livers from LKO mice maintained normal function but became highly tumorigenic when challenged with tumor-promoting stimuli, suggesting that tumors in LKO mice were driven, at least in part, by diploid hepatocytes capable of rapid proliferation. Indeed, LKO hepatocytes were more proliferative and out-competed control hepatocytes in competitive repopulation studies. To eliminate potentially confounding effects associated with *E2f7/E2f8* deficiency, diploid and polyploid hepatocytes from wild-type mice were examined. The wild-type diploid cells also showed a proliferative advantage, entering and progressing through the cell cycle faster than polyploid cells, both *in vitro* and during liver regeneration. Finally, to investigate the role of diploids and polyploids in chronic injury we

bred LKO mice onto a tyrosinemia background, a disease model where the liver can develop disease-resistant, regenerative nodules. Survival was significantly reduced in tyrosinemic LKO mice, compared to controls, but they maintained the ability to form regenerative nodules. Molecular analyses revealed that the nodules in the tyrosinemic livers were generated via aneuploidy and inactivating mutations.

In summary we identified diverse, context-specific roles for diploids and polyploids in liver function, demonstrating diploid hepatocytes are the most proliferative and have the highest capacity for liver regeneration, and polyploid hepatocytes are required for the formation of aneuploid progeny and facilitate adaptation to chronic liver disease.

Table of Contents

List of Tables

List of Figures

Acknowledgements

There are a multitude of people I would like to acknowledge for providing support and assistance to me throughout my research experiences in and outside of graduate school. First, I want to thank my primary advisor and mentor Dr. Andy Duncan for all of the support and guidance he showed me. His support has been absolutely critical to my success as he helped me plan and execute experiments, offered insightful tips in designing and giving presentations, and enhanced my ability to write and think like a biomedical researcher. Most importantly, I appreciate that I was able to communicate with him on a daily basis, and that he goes above and beyond in making time to regularly meet with everyone in his lab. I credit Dr. Andy Duncan immensely for making my graduate studies a productive, enjoyable and overall gratifying experience.

Second, I would like to recognize all of the other members of my committee for their support in providing pivotal guidance for my research. I would like to thank Dr. Joe Locker for serving as chairperson of my committee and posing thought-provoking questions that helped steer my research. I would also like to thank Dr. Paul Monga and Dr. Ed Prochownik for their insightful comments and assistance that helped stimulate experimental design and drive my dissertation. I would also like to thank Dr. Wendy Mars, who along with serving on my committee, provided advice and support that helped make my time as a graduate student productive and successful.

Third, I would like to thank those who gave me teaching opportunities while in graduate school. I am grateful to Dr. Wendy Mars for giving me the opportunity to serve as a teaching assistant and tutor for first year IBGP graduate students for the Foundations of Biomedical Science class. I would also like to thank Dr. Georgia Duker and Dr. Gerry Apodaca for giving me the opportunity to teach medical students as a histology teaching assistant for the Tissues in Health

and Disease course. Additionally, I want to thank all of the graduate and medical students who were in my classes and made my teaching experiences enriching and engaging.

Fourth, I want to recognize all of my friends and peers who helped make my time in graduate school enjoyable and successful. I would especially like to thank Drew Bradshaw, Sarah Dremel, Karis Kosar, Laura Molina, Morgan Preziosi, Jackie Russell, Abby Stahl, Kyle Sylakowski and Dan Zuppo for your friendship and never-ceasing support. I would also like to thank the wonderful friends I made while working at Bridgeside Point II including Patrick Chan, Leonid Emerel, Maria Giovanna Francipane, Lynda Guzik, Bing Han, Jen Hill, Aimon Iftikhar, Jenna Kuhn, Sam LoPresti, Alexis Nolfi, Tara Richards and Clint Skillen. Additionally, I wish to thank Dr. Michael Oertel for his collaboration and my previous mentors at the University of Pittsburgh including Dr. J. Rich Chaillet, Dr. Steven Dobrowolski and Dr. Hideho Okada for their support. I would also like to thank my past advisors and friends from Saint Vincent College who positioned me for success in graduate school including Dr. Bruce Bethke, Dr. Matt Fisher, Dr. Jim Kellam, Thomas Octave, Jonathon Jacobeen, Michael Parisi, Michelle Koenig Parisi, Lauren Stanley and Michael Villavicencio.

Most importantly, I am grateful for the support and encouragement I received from my lab colleagues including Frances Alencastro, Evan Delgado, Madeleine Leek, Nairita Roy and former members Whitney Brown, Maelee Chen, Hong-yun Gong, Justin Moroney and Matt Weirich. The best part about working in the Duncan Lab was the people and each of you made my lab experience very enjoyable and successful. I will never forget all the wonderful memories we made working together.

Finally, I am grateful for all the support and encouragement I have received from my family and close friends. I would like to thank my parents Amy and David for their unwavering love and

making sure I always have the tools to succeed, my sister Elizabeth and brother Jeffrey for their help and support, and of course my buddy Baxter. I also appreciate the encouragement provided by my grandparents Jim and Janet Duch and David and Mary Ellen Wilkinson, along with numerous other family members. Additionally, I want to thank Connie Cauvel, Jim and Linda Moorhead, Bill and Jacquie Smith, as well as George Petree, Eric Wojnar, Corey Bierer, Zak Jones, Ralph Lemmon, Tammy Hampshire, Brad Bernas, Gary McWilliams, Bob Temple, Dr. Salvatore Orlando, Dr. Peter Shaw and several other people whom I simply do not have the space to list, for helping shape my path. I look back on the past with fond memories, and I know that my future will always be bright because of the special people in my life.

1.0 Introduction

Chapter 1 is adapted from one book chapter:

Delgado ER[1], Stahl EC[1], Roy N[1], **Wilkinson PD[1]**, Duncan AW[1]. Polyploidy in Liver Function, Mitochondrial Metabolism and Cancer. In: Arias I, editor. The Liver: Biology and Pathobiology, 6th Edition: Wiley; 2019. (*In press*).

[1] Department of Pathology, McGowan Institute for Regenerative Medicine, Pittsburgh Liver Research Center, University of Pittsburgh, 450 Technology Drive, Suite 300, Pittsburgh, PA 15219.

1.1 Polyploidy in the Liver

Most mammalian cells are diploids and have a nucleus containing two sets of chromosomes. However, there exists cells and whole organisms described as polyploid; a phenomenon characterized by variations in chromosome number. Polyploidy is defined as a chromosome number that is a whole number greater than twice the haploid chromosome content (1). For over 100 years the existence of polyploid cells, often containing two nuclei, have been documented in the liver (2). Hepatocytes, the parenchymal cells of liver tissue, have been shown to be the cells that are polyploid in liver. Polyploid hepatocytes are generated by a failure to complete the final stage of mitosis, known as cytokinesis, which results in a daughter cell containing more than 2 sets of chromosomes (3). While liver polyploidy has been well

documented, it is only recently that studies have begun to shed light on the mechanisms and genetic regulators of polyploidization.

1.1.1 Polyploidy in nature

Polyploid organisms and cell types have been documented in a variety of species including fungi, insects and plants (4-8). Polyploidy is most common in the plant kingdom as 30-80% of angiosperm (flowering) plant species are reported to be polyploid, with several being allopolyploids and containing multiple chromosome sets from more than one species (9, 10). Polyploidy is less common among animal species, possibly due to differences in gene regulation and sex determination factors (11). However, whole organismal polyploidy has been documented in animal species, including fish (i.e., *Salmonidae*) (12) and amphibians (i.e., *Xenopus*) (13). Mammals, on the other hand, usually only exhibit polyploidy in certain types of tissues, such as muscle and liver. Compared to plants, polyploid cells in mammals are usually autopolyploid because they contain multiple chromosome sets from only one species (7).

1.1.2 Polyploidy in mammalian somatic tissues and the liver

The majority of mammalian cells have a diploid (2n) nuclear content and contain two sets of chromosomes. However, polyploid cells, with a nuclear ploidy content greater than 2n, are an innate component of many mammalian species, including rodents and humans (1, 8). The formation and location of these polyploid cells is tissue-dependent. For example, myofibrils and osteoclasts become multinucleate, polyploid cells via cell fusion (14, 15). Others, including megakaryocytes and trophoblast giant cells, become polyploid through endoreduplication. Here,

proliferating cells progress through the cell cycle and replicate their DNA, but fail to complete nuclear division during mitosis, resulting in a polyploid cell with a single nucleus (6, 16). On the other hand, failure of cytokinesis (the final step of cell division where the parent cell's cytoplasm divides to produce two daughter cells) primarily drives the generation of polyploid cardiomyocytes and hepatocytes (1, 3, 17).

1.1.3 Hepatocyte polyploidization

Polyploidy levels change profoundly during liver growth and maturation. In the early stages of liver development, the liver is primarily populated with small, uniform diploid (2n) hepatocytes (18, 19). As the hepatocytes proliferate, the diploids fail to complete cytokinesis, and in turn generate a daughter cell with two diploid nuclei (2n x 2n), referred to as a binucleate tetraploid (Figure 1). Next, tetraploid cells with two diploid nuclei replicate their DNA and generate two mononucleate tetraploid (4n) daughter cells by successfully completing cytokinesis. Mononucleate tetraploid cells can produce mono- and binucleate octaploid (8n and 4n x 4n) hepatocytes through subsequent cell divisions with complete and incomplete cytokinesis. The process continues, producing hexadecaploid (16n) cells and hepatocytes with even greater ploidy states (1) (Figure 1). While failure to complete cytokinesis is the most common mechanism by which hepatocytes increase ploidy states, heterotypic cell fusion between macrophages and hepatocytes has been shown to occur, albeit infrequently (at approximately 1/100,000 hepatocytes) (20). In general, as the liver matures the hepatocyte population becomes increasingly heterogeneous in size, function and nuclear content, including number of nuclei per cell and chromosome sets per nucleus (1, 3, 21).

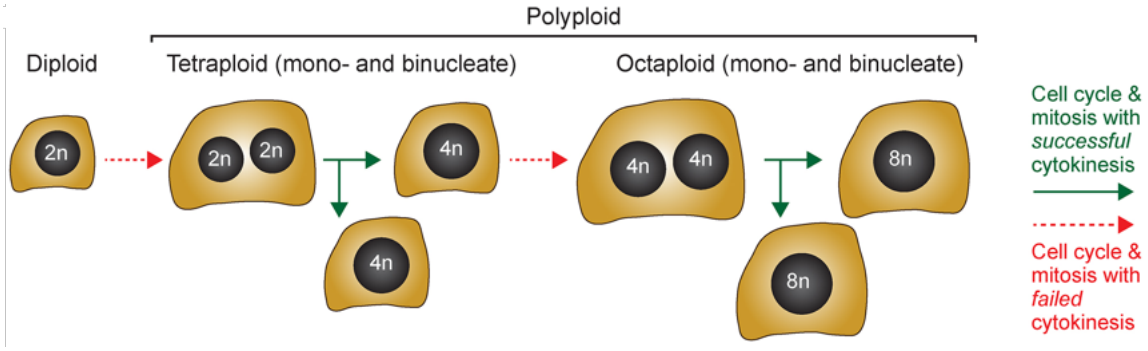

Figure 1. Polyploidy in the liver.

Hepatocytes are mononucleate or binucleate, and ploidy is determined by the number of nuclei per cell and DNA content of each nucleus. Cell division associated with failed cytokinesis drives hepatic polyploidization. The cartoon shows how a single diploid hepatocyte can give rise to mononucleate and binucleate tetraploid and octaploid hepatocytes. Note that in humans, diploid (2n) nuclei contain 46 chromosomes, tetraploid (4n) nuclei contain 92 chromosomes and octaploid (8n) nuclei contain 184 chromosomes.

The rate and percentage of liver polyploidization differs between species (1). At birth, the majority of human hepatocytes in the liver are diploid, with polyploids representing less than 10% (22). Notably, tetraploid hepatocytes appear within the first few weeks of development, followed by octaploid hepatocytes at 2-3 months after birth (23). By adulthood, the percentage of polyploidy is nearly doubled to 20%, and after the age of 60, approximately 50% of the human liver is comprised of polyploid hepatocytes (22, 24). Alternatively, the livers of mice are already 50% polyploid at weaning, whereas the livers of rats begin to polyploidize upon weaning, triggered by changes in insulin AKT-dependent signaling that result in cytokinesis failure (25). By 8-12 weeks of age both mouse and rat livers become 80% polyploid, a faster rate than human polyploidization, making rodents a useful model to study polyploidization in the span of a few weeks (26). The signals regulating the steady accumulation of polyploid hepatocytes in developing and aging humans remain unknown but may also be related to the insulin-AKT pathway. Interestingly, the

frequency of cells within each ploidy state remains relatively constant among individuals of the same age, suggesting the existence of a ploidy sensor to maintain homeostasis in the liver.

1.1.4 Genetic regulation of liver polyploidy

In addition to insulin/PI3K/Akt signaling, several other genes have been shown to influence and regulate hepatic polyploidization. Since acytokinetic cell division is the primary way hepatocytes become polyploid, many of the genes shown to regulate polyploidization are those involved in cell cycling and proliferation. In 2016 Hsu et al. demonstrated microRNAs regulate polyploidy as they showed deletion of the microRNA *Mir122* resulted in mouse livers with a ~2-fold reduction in polyploid hepatocytes (27). Further analysis showed that miR-122 negatively regulates *RhoA*, *Mapre1* and *Iqgap1*, all pro-cytokinesis genes. Additionally, deletion of *Mir122* led to increased expression of *Cux1*, which has been shown to positively regulate *Racgap1*, *Ect2* and *Kif23/Mklp1*, members of the centralspindlin complex that are involved in cell abscission and cleavage furrow ingression (27, 28).

The E2F transcription factor family has also been shown to influence hepatic polyploidization through cell cycle regulation. The E2F family, which consists of activators (E2F1, E2F2 and E2F3a/b), repressors (E2F4, E2F5 and E2F6) and atypical repressors (E2F7 and E2F8), regulates DNA replication, cell cycle progression and apoptosis primarily through a CDK-RB-E2F interaction (29). E2F1, which promotes entry into S-phase and DNA replication, has been demonstrated to negatively regulate polyploidization as livers of transgenic mice overexpressing E2F1 were enriched with diploid hepatocytes (30). In 2012 Chen et al and Pandit et al showed the atypical repressors E2F7 and E2F8, which antagonize E2F1 and promote the G1/S transition of the cell cycle, are highly expressed in livers of mice between weeks 1 and 7 of postnatal

development, the period corresponding to hepatocyte polyploidization (31, 32). Deletion of *E2f7* and *E2f8* in the liver, using a Cre recombinase system driven by the liver specific albumin-promoter, resulted in livers that had significantly reduced levels of binucleate and polyploid hepatocytes, but otherwise exhibited normal function, regeneration and development (32). Gene expression analyses indicated that E2F7 and E2F8 likely regulate hepatic polyploidy by disrupting E2F1 activity and downregulating expression of genes involved in mitosis (*Aurka/b* and *Ccnb1*) and those that promote cytokinesis (*Ect2*, *Mklp1* and *Racgap1*) (32).

Table 1 provides a summary of the many genes, including *Mir122*, E2F family members (*E2f1, E2f7* and *E2f8*) and cell cycle checkpoint regulators (*Rb1* and *Trp53*) that have been shown to affect liver ploidy (27, 31-34). Manipulating hepatic ploidy levels through the use of genetic knockout models has proven useful in studying the role of polyploidy in liver function and disease. However, it often remains difficult to separate phenotypic differences based on genetic deficiency and those due to ploidy disruptions, thus necessitating careful interpretation of the observations made from such studies.

Table 1. Genetic Regulators of Hepatic Polyploidy

Gene	Model	Hepatocyte Ploidy	Reference
Anln	siRNA knockdown in mouse	Increased	(35)
Cdk1	Deletion via knockout mouse	Increased	(36)
Cdkn1a/p21	Overexpressed in transgenic mouse	Increased	(37)
c-Myc	Deletion via knockout mouse	Decreased	(38)
	Overexpressed in transgenic mouse	Increased	(30)
E2f1	Deletion via knockout mouse	Increased	(32)
	Overexpressed in transgenic mouse	Decreased	(30)
E2f7, E2f8	Deletion via knockout mouse	Decreased	(31) (32)
Ercc1	Deletion via knockout mouse	Increased	(39) (40)
Mir122	Deletion via knockout mouse	Decreased	(27)
Rb1	Deletion via knockout mouse	Increased	(34)
Skp2	Deletion via knockout mouse	Increased	(41)
Ssu72	Deletion via knockout mouse	Increased	(42)
Survivin/Birc5	Deletion via knockout mouse	Increased	(43)
Trp53	Deletion via knockout mouse	Increased	(33)

1.1.5 Location of ploidy populations in the liver

In the mammalian liver, hepatocytes are arranged in discrete units called hepatic lobules. Blood from the portal vein mixes with the oxygen rich blood of hepatic arteries and flows toward the central vein of the lobule, bringing nutrients and other substances to hepatocytes. The uneven distribution of nutrients and oxygen, along with other factors including Wnt signaling gradients, divides the lobule into 3 zones: periportal (zone 1), mid-lobular (zone 2) and perivenous (zone 3) (44). Hepatocyte gene expression and metabolic function is often related to the zonal location of the cell (45).

One important question regarding liver architecture is whether polyploid hepatocytes are evenly distributed among all zones of liver lobules. Asahina et al. separated rat hepatocytes based on centrifugal fractionation and found that cells with metabolic gene expression consistent with hepatocytes of the periportal region were predominantly small, mononuclear diploid hepatocytes (46). On the other hand, Margall-Ducos et al. observed similar frequencies of incomplete cytokinesis among hepatocytes in the periportal and perivenous regions of developing rat livers between 15-25 days post-birth, and found binucleate hepatocytes were present in similar proportions between the two regions (3). Using a tamoxifen-inducible genetic tracing system, Wang et al. observed Axin2+ hepatocytes, which are located in the pericentral zone, could self-renew and give rise to progeny hepatocytes that moved in a pericentral-periportal direction. Moreover, they observed that the majority of the pericentral Axin2+ cells were diploids, suggesting Axin2+ diploid hepatocytes were the source of new hepatocytes under homeostatic and uninjured conditions (47). In 2017 Tanami et al. stained liver tissue and generated 3-dimensional profiles of hepatic nuclei to identify ploidy populations across the lobule. They observed polyploidization occurred rapidly in mice between weeks 3 and 4 post-birth and that polyploids were slightly

enriched in the mid-lobule region of adult livers (48). Together these studies demonstrate that polyploids are located in all regions of the lobules, but whether polyploids are enriched in specific zones remains an active area of research.

1.2 Polyploidy in Liver Function and Regeneration

The liver is a vitally important organ situated to metabolize hundreds of molecules for energy regulation and drug toxicity, as well as to produce digestive bile acids and regulate blood composition (49). These processes require the orchestration of complex gene networks and necessitate the maintenance of liver function for survival. As such, the liver has a robust capacity to adapt to injury and undergo complete regeneration. The impact of polyploidy on gene expression and liver regeneration is just beginning to be understood.

1.2.1 Polyploidy in hepatocyte gene expression and liver function

While the mechanisms that produce polyploid hepatocytes have been well characterized, the relationship between ploidy and gene expression remains unclear. Experiments have shown that polyploidy is associated with specific gene expression patterns in yeast (50). In regards to mammals, studies have demonstrated that nuclear content affects expression levels of genes regulating megakaryocyte differentiation (51) and that giant trophoblast cells could exhibit biallelic X-chromosome gene expression due to incomplete X-inactivation (52). Additionally, a large-scale genome comparative study illustrated that cardiac stress genes were expressed at different levels between diploid and polyploid cardiomyocytes (53).

It has been postulated that hepatic ploidy state could affect gene expression. One hypothesis is that gene expression levels increase proportionally with ploidy. In this case, tetraploids and octaploids would have 2X and 4X greater gene expression levels, respectively, compared to diploids. Thus, tetraploid and octaploid cells would also potentially contain 2X and 4X the total RNA and protein content as diploid cells (1). Another hypothesis is that diploid and polyploid hepatocytes exhibit differential gene expression. In this scenario, gene expression levels would vary on a gene-to-gene basis between ploidy populations, with polyploids exhibiting greater expression of specific genes versus diploids and vice versa. A 2007 study by Lu et al. compared gene expression between quiescent diploid, tetraploid and octaploid hepatocyte populations isolated by flow cytometry. Surprisingly, the study found gene expression was mostly equivalent between ploidy populations, and the magnitude of difference was small for those genes with different expression levels (54). This suggested that few genes are differentially expressed, at least in quiescent hepatocytes. Further studies are needed to determine if differential gene expression occurs in disease conditions or in response to specific stimuli because variations at the molecular level could ultimately endow certain ploidy subsets with unique functional capabilities (1, 55).

1.2.2 Polyploidy and liver regeneration

The regenerative capacity of the liver has been well documented, but the role of polyploidy in this process remains unclear. It is hypothesized that diploid and polyploid populations could play unique roles in the process. Originally, it was believed that polyploid hepatocytes were mature, terminally differentiated cells with little proliferative capacity. This was suggested from studies demonstrating that hepatocytes in livers of mice and rats become increasingly polyploid with age, and that >99% of hepatocytes in adult livers were quiescent (56, 57). Moreover,

hepatocyte turnover has been shown to be slow, with cell lifespan ranging from 200 to 300 days in adults (58). However, polyploids have been observed to proliferate in response to partial hepatectomy (PH), the surgical removal of up to two-thirds of the liver mass (59). While these experiments confirmed that polyploid hepatocytes can proliferate, it is unclear if the proliferative capacities of diploids and polyploids are equivalent. One study demonstrated that livers from rats that had undergone PH had increased polyploidy levels and changes associated with cell senescence and aging (60). Another study showed that mice with drug-induced necrosis and cirrhosis developed regenerating nodules enriched with diploid hepatocytes (61). The idea that diploids are more proliferative than polyploid hepatocytes is also supported by observations that diploid hepatocytes are enriched in patients and rodents with hepatocellular carcinomas (HCC) (61-64). In contrast, it was shown that transplanted octaploid and diploid hepatocytes proliferated equivalently in the *Fah*$^{-/-}$ liver repopulation model. However, a limitation of this study was that the ploidy states of the transplanted cells changed as the octaploid cells underwent ploidy reversal (proliferating octaploids generated daughter hepatocytes with reduced ploidy) and the diploids polyploidized during the course of repopulation (26). Taken together, these experiments illustrate that further studies are needed to determine the precise proliferative capacities of diploid and polyploid hepatocyte populations, and the mechanisms regulating proliferation of each ploidy population.

1.2.3 Polyploidy in aging and impaired liver regeneration

Aging is known to lead to the accumulation of senescent cells in multiple tissues and organ systems, including the liver (65). Senescence is the irreversible exit of the cell cycle, driven by the shortening of telomeres (i.e., the protective caps of chromosomes) through exhaustive replication

or other stressors. Many hypothesize that senescence is a protective mechanism against tumorigenesis that might arise from genomic instability, but senescence also has the effect of limiting tissue regeneration and promoting the secretion of inflammatory mediators that can be damaging to surrounding tissue (66). Aged octaploid cells were found to express a higher proportion of senescence markers compared to tetraploid and diploid cells, including p16, p21 and p53, which also serve important tumor suppressor roles (67). Methods to deplete senescent cells in aged organs and tissues, such as the INK-ATTAC mouse, were not capable of depleting senescent cells in the liver but reduced the spontaneous occurrence of liver tumors by depleting senescent cells at peripheral sites, thus demonstrating the role of the aged microenvironment in the etiology of liver cancers and other age-related diseases (65, 66).

Unlike senescent diploid cells, which must be cleared by the immune system, senescent polyploid cells have the unique capacity to undergo ploidy reversal (67). Aged hepatocytes that undergo ploidy reversal also downregulate expression of senescence markers, acting as a type of cell rejuvenation (67). Ploidy reversal might partially explain the capacity of the aged liver to regenerate, although regeneration is substantially reduced in elderly individuals. After PH in mice, hepatocytes in aged livers have delayed cell cycle entry and the livers are significantly deficient in the number of proliferating hepatocytes (68-70). The age-related decline in hepatocyte proliferation has been attributed to transcription factor C/EBPα complexing with Brm, a chromatin remodeling protein detected only in aged livers (71), which inhibits E2F-regulated gene expression (72). Notably, when the circulatory systems of young and aged mice are connected through heterochronic parabiosis, the number of hepatocytes undergoing proliferation increased in the aged livers. While the ploidy of the rejuvenated hepatocytes was not documented, a reduction in the C/EBPα-Brm complexes was observed (71).

When aged diploid or octaploid hepatocytes are implanted into young *Fah*$^{-/-}$ mice, the octaploid hepatocytes undergo ploidy reversal, giving rise to lower hepatic ploidy states that no longer express markers of senescence (26, 67). This study not only implicated the ability of a young systemic environment to rejuvenate hepatocyte proliferative capacity, but also suggested that hepatocytes with differential ploidy states have equivalent proliferation kinetics during long-term repopulation. Future studies will be needed to decipher the role of cell intrinsic factors, such as ploidy and gene stability, mitochondrial function and autophagy, versus extrinsic factors in the local or systemic environment, in the process of hepatocyte function and regeneration after injury and during aging.

1.3 The Ploidy Conveyor Generates Genetic Diversity

A high degree of diversity exists among the liver hepatocyte population as hepatocytes vary in terms of the number of nuclei per cell (typically 1 or 2) and the DNA content of each nucleus (diploid, tetraploid, octaploid, etc.). While hepatocytes are heterogeneous in regard to the number of chromosome sets, they also demonstrate diversity at the individual chromosome level. Hepatocytes exhibiting aneuploidy, where single chromosomes are gained or lost, have also been documented in the liver. Polyploidization, ploidy reversal and aneuploidy, which are collectively called the “ploidy conveyor”, prominently drive hepatocyte heterogeneity that is important for liver function and adaptation to chronic liver injury (1).

1.3.1 Liver aneuploidy

While hepatocytes are heterogeneous in regard to number of chromosome sets, they also exhibit diversity at the individual chromosome level. G-banding, fluorescence *in situ* hybridization and single cell DNA sequencing studies have indicated 5-50% of hepatocytes in healthy livers of mice and humans are aneuploid, having gained or lost individual chromosomes (Figure 2) (22, 26, 73). Recently, it was shown that the livers of mice deficient in microRNA-122 had reduced polyploid levels, were enriched with diploid hepatocytes and had abnormally low aneuploidy levels (74). Additionally, studies have shown that polyploidy and aneuploidy levels follow similar trends, as both increase with age and are the highest in adult mouse and human livers (1, 75). The degree of aneuploidy plateaus in mice from 4-15 months of age (26). Similarly, in humans, hepatic aneuploidy levels remain stable between the ages of 10 and 60 years (22).

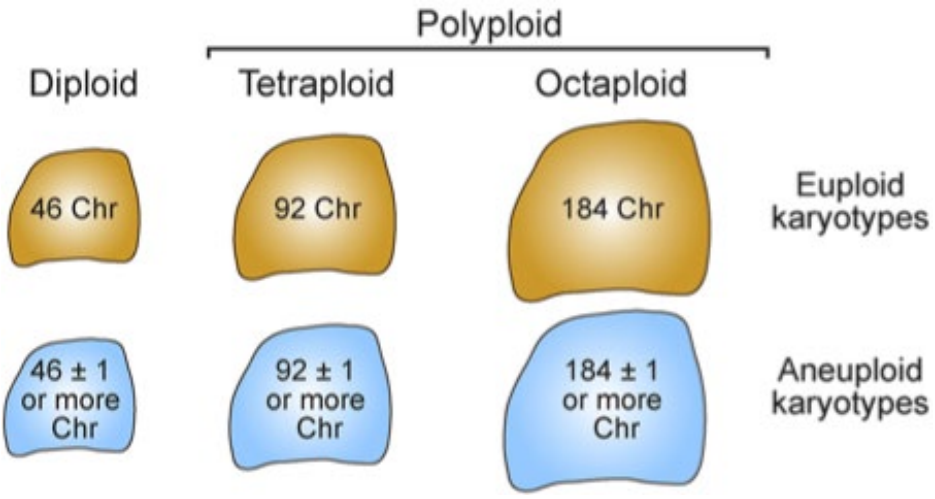

Figure 2. Polyploidy and aneuploidy in the liver.

In humans, diploid (2n), tetraploid (4n) and octaploid (8n) hepatocytes contain 46, 92 and 184 chromosomes (Chr), respectively. Euploid karyotypes contain balanced sets of chromosomes, whereas aneuploid karyotypes contain one or more random chromosome gains and/or losses.

In most cases, dividing polyploid hepatocytes, both mononucleates and binucleates, undergo mitosis using a bipolar spindle arrangement. Here, the centrosomes arrange themselves in a bipolar orientation, the nuclear membrane breaks down and the chromosomes condense and arrange themselves along the midline. Nuclear segregation then occurs in a bipolar fashion, with the chromosomes of specific pairs pulled toward opposite ends of the cells. In the case of a dividing tetraploid cell, successful cytokinesis results in two mononucleate ~tetraploid cells while acytokinetic division results in a binucleate ~octaploid cell (Figure 3, left panel). However, polyploid hepatocytes can complete mitosis using a multipolar spindle arrangement, and undergo "reductive mitosis," or a reduction in nuclear content, a process called "ploidy reversal" (Figure 3, middle and right panels). One example of ploidy reversal is illustrated with a proliferating tetraploid hepatocyte that forms a tripolar spindle during mitosis (Figure 3, middle panel). The chromosomes of the dividing cell are pulled toward three poles, resulting in two daughter cells

with ~diploid nuclei and one daughter cell with a ~tetraploid nucleus. Additionally, polyploid cells can perform ploidy reversal by undergoing double mitosis (Figure 3, right panel). In this case, proliferating tetraploids can generate up to four ~diploid daughter cells and octaploids can generate up to eight ~diploid daughter cells (26, 76, 77). Chromosome segregation errors can occur during bipolar division of polyploid hepatocytes but are most common during cell division with multipolar spindles (26, 76). For instance, microtubules associated with the outer poles occasionally attach to the same kinetochore during multipolar spindle construction. If left unchecked, this error prevents chromosomes from migrating to discrete poles during anaphase. Consequently, these "lagging" chromosomes are frequently excluded from the daughter cell nuclei and form what is considered a micronucleus. Cytogenetic analyses of hepatocytes have shown that liver aneuploidy is widespread, with chromosome gains and losses occurring in an unbiased fashion (22, 78).

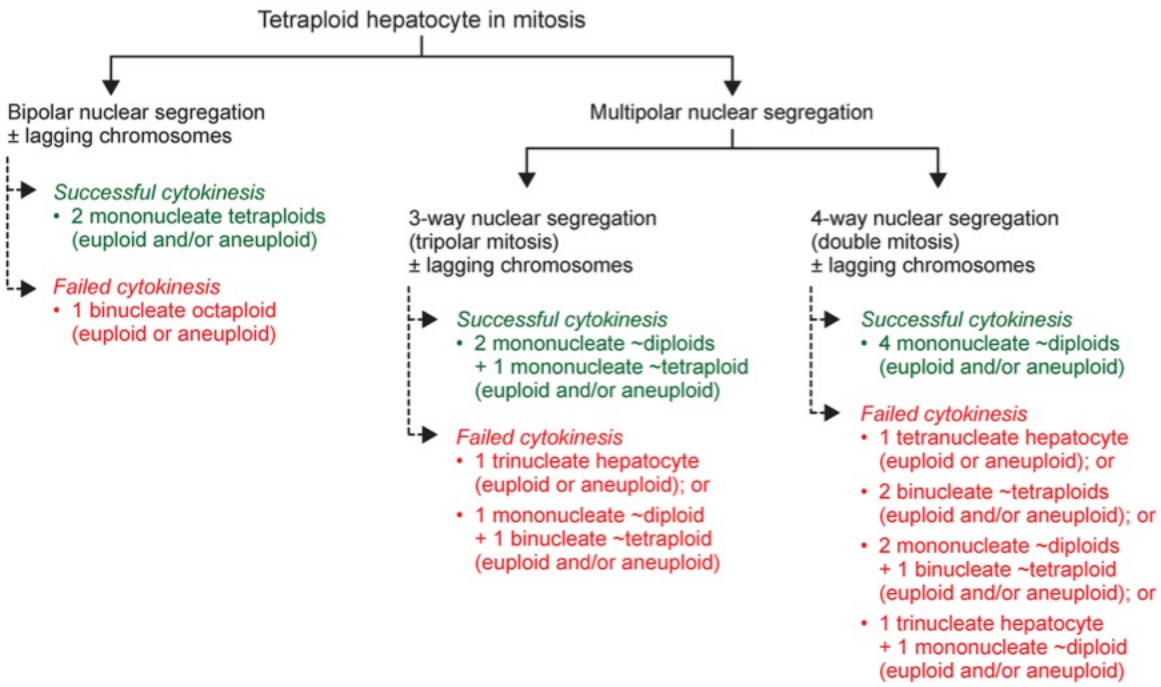

Figure 3. Types of daughter cells generated by a dividing tetraploid hepatocyte.

Polyploid hepatocytes can undergo chromosome segregation errors (e.g., lagging chromosomes) and multipolar cell divisions to generate aneuploid daughter cells with reduced ploidy. The flowchart outlines the various types of daughter cells that can be generated by a dividing tetraploid hepatocyte undergoing bipolar (left) or multipolar (middle and right) nuclear segregation.

1.3.2 Liver ploidy supports hepatic adaptation

It has been hypothesized that the diverse population of polyploid and aneuploid hepatocytes endows the liver with the ability to adapt to a variety of environmental stresses (78). Interestingly, studies have shown that budding yeast strains with specific chromosome numbers are able to survive toxic insults and deleterious mutations (79, 80). In the context of the liver, it has been demonstrated that aneuploid hepatocytes could protect against chronic liver disease. Notably, a study illustrated that mice suffering from tyrosinemia due to loss of FAH, an enzyme in the tyrosine catabolic pathway, developed resistance to the disease partially through hepatic

aneuploidy (78) (Figure 4). Mice suffering from tyrosinemia can be treated and kept healthy by blocking the tyrosine catabolic pathway upstream of FAH using the drug 2-(2-nitro-4-trifluoro-methylbenzoyl)-1,3-cyclo-hexanedione (NTBC) or deleting the enzyme homogentisic acid dioxygenase (HGD) (81, 82). In the aforementioned study, NTBC was withdrawn from $Fah^{-/-}$ $Hgd^{+/-}$ mice and, contrary to the expectation that all mice would succumb to liver failure, some mice developed numerous small, healthy nodules in their livers. Karyotyping and array comparative genomic hybridization analyses revealed that many of the healthy nodules were comprised of aneuploid hepatocytes lacking a copy of chromosome 16, which contains the wild-type copy of *Hgd*. Thus, the healthy liver nodules were populated with *Hgd*-deficient hepatocytes. It was hypothesized that chronic injury was toxic to the majority of hepatocytes except those that had previously lost the chromosome with the *Hgd* wild-type copy. The disease-resistant hepatocytes (monosomic for chromosome 16), proliferated and repopulated the liver and restored normal liver function (78).

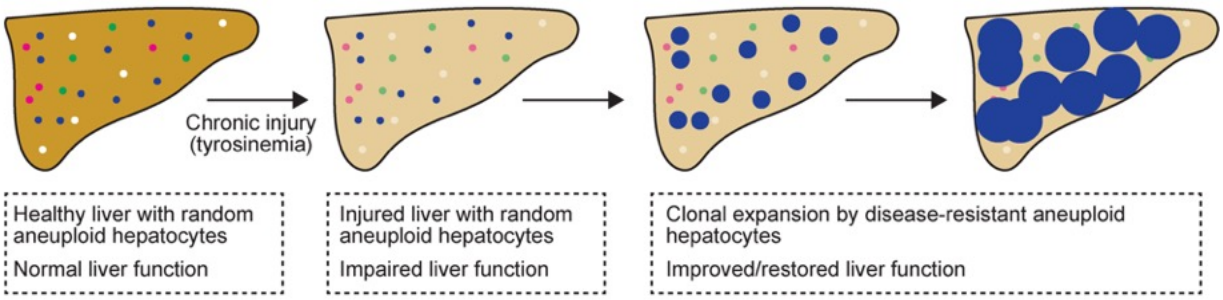

Figure 4. Proof-of-concept studies demonstrated that disease-resistant aneuploid hepatocytes promote adaptation to chronic liver injury.

Healthy mouse livers contain randomly aneuploid hepatocytes, which are illustrated by multicolored cells. In response to chronic injury (induced by tyrosinemia in *Hgd*$^{+/-}$ *Fah*$^{-/-}$ mice), liver function was severely impaired. Hepatocytes lacking chromosome 16 (blue) were resistant to the injury and capable of proliferation. Clonal expansion by these injury-resistant hepatocytes spontaneously repopulated the liver and restored liver function.

1.4 Polyploidy and Liver Pathology

Liver disorders affect 30 million people in the United States and are the 10th leading cause of death in the country (83-85). Each year 40,000 people are diagnosed with end-stage liver disease, resulting in nearly 30,000 patient deaths. In most cases the only effective treatment for patients with end-stage liver disease is whole organ replacement. However, donor liver availability falls far short of demand, as only 6,000 patients of the 16,000 Americans that need liver transplants will receive transplants (86). Moreover, nearly 1,400 patients will die before a suitable liver becomes available and many liver transplant recipients, particularly elderly patients, often suffer from transplant-related complications (87). Although much progress has been made toward understanding mechanisms of liver disease and repair, a lack of alternative therapies to whole organ replacement illustrates that new strategies are urgently needed (1, 88, 89).

Several studies have shown ploidy levels become atypical (increased/decreased) in many liver disease states including hepatocellular carcinoma, cirrhosis and viral hepatitis (62, 90, 91). Additionally, liver polyploidy has been observed to change when the liver is subjected to oxidative stress (92). However, the effects these changes in hepatic ploidy levels have on liver disease remain poorly defined. It remains unclear as to whether polyploidy contributes to disease development and progression, or functions as a protective mechanism. Ultimately, uncovering the role of polyploidy in liver pathologies will provide for the improvement of existing therapies and development of novel treatments.

1.4.1 Polyploidy and aneuploidy in liver cancer

HCC is the most common form of liver cancer and is associated with high mortality and morbidity worldwide (95). Work through the 1990s and early 2000s observed that HCC tumors from patients contained more diploid cells than polyploid cells (93). Consistent with these observations, work conducted on rats exposed to diethylnitrosamine (DEN) or 2-acetyl-aminofluorene indicated that the cells within the diseased, HCC tissue became predominately diploid (64, 94, 95). It is unclear if this shift from polyploid to diploid cells after malignant HCC transformation is a cause or effect in pathogenesis, but a potential explanation for the enrichment of diploid hepatocytes in HCCs is that polyploid hepatocytes protect from oncogenic transformation. This concept is counterintuitive, however, because polyploidy is traditionally associated with increased disease severity in other cancers (96).

Recent studies support the idea that polyploidy plays a protective role in the liver. Using a tunable system for altering hepatic ploidy *in vivo*, Zhu and colleagues showed that *Anln* deficient mice with highly polyploid livers were protected from HCC in the DEN tumor initiation model,

whereas *E2f8* deficient mice with predominately diploid livers were predisposed to HCC formation (35). Most importantly, these studies revealed that the polyploid state protects from transformation by providing extra tumor suppressor alleles. With two homologous chromosomes per cell, diploid hepatocytes have two alleles of each tumor suppressor. If one tumor suppressor allele is mutated and inactivated, the cell is protected by only one functional allele. However, the cell is highly susceptible to tumorigenesis if the second allele is subsequently inactivated. In contrast, polyploid hepatocytes have four or more homologous chromosomes and a corresponding number of tumor suppressor alleles. When a single tumor suppressor is inactivated in a polyploid hepatocyte, the cell is protected or "buffered" by three or more functional alleles. Thus, even if a second mutation event inactivates a remaining allele, the cell still retains a minimum of two functional alleles and can maintain tumor suppressor activity. Taken together, studies in patients and rodent models strongly support the notion that diploid hepatocytes are more susceptible to oncogenic transformation, while polyploid hepatocytes provide a protective mechanism against HCC formation.

Previous work from Michalopoulos and others found 461 copy number variations (CNVs) in 98 human HCC samples, demonstrating that chromosomal variations are common in liver cancer (97). The CNVs identified in this study contained discrete genomic amplifications and deletions but not gains or losses of entire chromosomes. While aneuploidy in patient HCC tumors is not well studied, hepatoblastoma tumors have been extensively characterized and shown to contain near-diploid or near-tetraploid cells that have gained or lost entire chromosomes (98). Additionally, underlying pathologies of hepatocellular carcinogenesis, such as chronic Hepatitis B virus infection, aflatoxin exposure and oxidative damage, are associated with chromosomal variations (99, 100).

It is largely accepted that increased aneuploidy, or chromosome instability (CIN), associates with worse disease prognosis (101). Unexpectedly, patients with lung, breast, ovarian and gastric cancers with the highest degree of CIN were reported to have better outcomes than patients with moderate CIN (101). One potential explanation is that high-degree CIN leads to mitotic catastrophe and cell death, which effectively kills tumors with the most aneuploidy. It is difficult to determine if aneuploidy is advantageous for HCC cancer cell survival because experimentally induced aneuploidy and chromosomal rearrangements have produced ambiguous and conflicting results (101). Recent work suggests that the relationship between aneuploidy and HCC can be studied by modulating miR-122 levels *in vitro* and *in vivo* because *Mir122* deficiency results in an increase in mononucleate hepatocytes with a concomitant reduction in aneuploidy (74). To effectively investigate if aneuploidy contributes to HCC development, the ability to manipulate ploidy in cancer models is critical. Ultimately, the development of innovative strategies that can eliminate and treat tumors in the liver will depend upon determining the relationship between polyploidy, aneuploidy and cancer cell survival.

1.4.2 Polyploidy in liver disease

Recently, several studies have concentrated on elucidating the role of polyploidy in liver disease and injury. One such study found that polyploid hepatocytes exhibited higher infection rates of the malaria parasite *Plasmodium* than diploids. Here, it was demonstrated that *Plasmodium* parasites preferentially infected polyploid hepatocytes compared to diploids (102). Other studies have looked at the relationship between liver polyploidy and Hepatitis B (HBV) and Hepatitis C viral infections (HCV). Reductions and increases in hepatic polyploidy have been observed in patients with hepatitis infections, making it unclear if polyploidy contributes to disease progression

or resistance. Moreover, many of these patients have other liver complications, including cirrhosis and hepatocellular carcinoma, making it difficult to disentangle the ploidy phenotypes strictly related to hepatitis infection (62, 90, 91).

Polyploidy levels have been shown to increase in cases of metabolic and oxidative stress. Gentric et al. observed increases of hepatic polyploidy in mouse models of nonalcoholic fatty liver disease (NAFLD) and patients with nonalcoholic steatohepatitis (NASH) (92). Cell cycle analysis demonstrated a significant increase in polyploid hepatocytes and tissue microscopy showed dramatic enrichment for mononucleate cells with high nuclear content. However, it was unclear as to whether these highly polyploid hepatocytes, which the authors termed "pathological polyploidy", were contributing to disease progression or resistance (103). Hepatic polyploidy has also been shown to be higher in livers affected by metabolic overload. Madra et al. observed increased levels of polyploidy in mice administered high doses of iron (104). Additionally, it was seen that Long Evans Cinnamon rats, which accumulate copper in the liver due to a genetic defect in a copper transporter gene, had increased hepatic polyploidy (105). As certain diseases and disorders are characterized by hepatic accumulation of iron (thalassemias, hereditary hemochromatosis and chronic blood transfusion) (106) and copper (Wilson's disease) (107), it is important that studies investigate the relationship between polyploidy and metabolic overload.

2.0 Polyploidy in Hepatocyte Proliferation and Liver Regeneration

Chapter 2 is adapted from one published research manuscript:

Wilkinson PD[1], Delgado ER[1], Alencastro F[1], Leek MP[1], Roy N[1], Weirich MP[1], Stahl EC[1], Otero PA[1], Chen MI[1], Brown WK[1], Duncan AW[1]. The Polyploid State Restricts Hepatocyte Proliferation and Liver Regeneration in Mice. Hepatology 2019. 69:1242-1258.

[1] Department of Pathology, McGowan Institute for Regenerative Medicine, Pittsburgh Liver Research Center, University of Pittsburgh, 450 Technology Drive, Suite 300, Pittsburgh, PA 15219.

The liver contains a mixture of hepatocytes with diploid or polyploid (tetraploid, octaploid, etc.) nuclear content. Polyploid hepatocytes are commonly found in adult mammals, representing ~90% of the entire hepatic pool in rodents. The cellular and molecular mechanisms that regulate polyploidization have been well-characterized; however, it is unclear if diploid and polyploid hepatocytes function similarly in multiple contexts. Answering this question has been challenging because proliferating hepatocytes can increase or decrease ploidy, and animal models with healthy diploid-only livers have not been available. Mice lacking *E2f7* and *E2f8* in the liver (LKO) were recently reported to have a polyploidization defect but were otherwise healthy. Herein, livers from LKO mice were rigorously characterized, demonstrating a 20-fold increase in diploid hepatocytes and maintenance of the diploid state even after extensive proliferation. Livers from LKO mice maintained normal function but became highly tumorigenic when challenged with tumor-promoting stimuli, suggesting that tumors in LKO mice were driven, at least in part, by diploid hepatocytes capable of rapid proliferation. Indeed, hepatocytes from LKO mice proliferate faster

and out-compete control hepatocytes, especially in competitive repopulation studies. In addition, diploid or polyploid hepatocytes from wild-type mice were examined to eliminate potentially confounding effects associated with *E2f7/E2f8* deficiency. The wild-type diploid cells also showed a proliferative advantage, entering and progressing through the cell cycle faster than polyploid cells, both *in vitro* and during liver regeneration. Diploid and polyploid hepatocytes responded similarly to hepatic mitogens, indicating that proliferation kinetics are unrelated to differential response to growth stimuli. ***Conclusion:*** Diploid hepatocytes proliferate faster than polyploids, suggesting that the polyploid state functions as a growth suppressor to restrict proliferation by the majority of hepatocytes.

2.1 Introduction

Most mammalian somatic cells are diploid and contain pairs of each chromosome, but there are also polyploid cells such as skeletal muscle, megakaryocytes, trophoblast giant cells, cardiac myocytes and hepatocytes that contain additional sets of chromosomes (1, 108, 109). Polyploid hepatocytes are among the best described, and in adult humans and mice, polyploids comprise more than 50% and 90%, respectively, of the hepatocyte population (22, 26). Polyploidization begins at day 14 in mice when proliferating hepatocytes fail to complete cytokinesis and produce binucleate tetraploid daughter cells containing two diploid nuclei (3, 27, 110). In turn, these binucleate tetraploid hepatocytes begin cycling, and, upon successful cytokinesis, generate a pair of mononucleate tetraploid daughters. This process continues, generating octaploid and even higher ploidy hepatocytes. The polyploid state is also reversible. Proliferating polyploid hepatocytes can undergo multipolar cell division to generate diploid or near-diploid daughters, a

process termed the ploidy conveyor (26). Thus, the adult liver contains a heterogeneous mixture of diploid and polyploid hepatocytes, but it is unknown whether these different hepatic subsets perform specialized functions in normal homeostasis or liver regeneration.

The E2F family of transcription factors regulates progression through the cell cycle (111). In the liver, E2F1-6 are expressed at low levels throughout life, whereas E2F7 and E2F8 are elevated between weeks 1 and 7 of postnatal development, a period correlating with hepatocyte polyploidization (32). The role of E2F7 and E2F8 was studied using liver-specific *E2f7/E2f8* double knockout mice (31, 32). Livers in these mice were reported to function normally through several months of age, but they were significantly depleted of polyploid hepatocytes. Similar, albeit less pronounced, phenotypes were seen in *E2f7* and *E2f8* single knockout mice. E2F7 and E2F8 regulate hepatic ploidy in two primary ways (32). First, E2F7 and E2F8 antagonize E2F1 activity, and, consistent with this relationship, transgenic mice overexpressing E2F1 were enriched for diploid hepatocytes, which is similar to the phenotype of *E2f7/E2f8* double knockout mice (30). Secondly, E2F7 and E2F8 negatively regulate genes involved in cytokinesis. Since cytokinesis failure is the primary method hepatocytes become polyploid (3), loss of E2F7 and E2F8 promotes successful cytokinesis of proliferating mononucleate diploid cells.

Here, we utilized liver-specific *E2f7/E2f8* double knockout (LKO) mice to investigate functional differences between diploid and polyploid hepatocytes. Similar to published reports, LKOs contained ~20 times more diploids and 3 times fewer polyploids. The reduced-polyploidy phenotype was stable at 2.5 and 5 months of age and following extensive hepatocyte proliferation. When adults were treated with a tumor induction/promotion model, LKO mice developed abundant liver tumors whereas control mice were resistant to tumorigenesis. We speculated that tumors in LKO mice were driven, at least in part, by diploid hepatocytes capable of rapid

proliferation. Using *in vivo* and *in vitro* approaches, we showed that hepatocytes from LKO livers proliferated faster and could out-compete hepatocytes from control livers, especially in competitive repopulation. We also compared diploid and polyploid hepatocytes from WT mice. Cell culture and liver regeneration assays showed that diploids entered and completed the cell cycle earlier than polyploids. Diploid and polyploid hepatocytes responded similarly to hepatic mitogens, indicating that proliferation kinetics were unrelated to differential response to growth stimuli. Together, the data show for the first time that diploid hepatocytes proliferate faster than polyploids, suggesting that the polyploid state functions as a growth suppressor to restrict proliferation by the majority of hepatocytes.

2.2 Methods

2.2.1 Mouse strains

The Institutional Care and Use Committee of the University of Pittsburgh approved all mouse experiments. Mice were maintained in a standard 12-hour light/dark system. They were housed in Optimice cages (AnimalCare Systems, Centennial, CO) with Sani-Chip Coarse bedding (P. J. Murphy, Montville, NJ) and provided *ad libitum* access to water and standard mouse chow (LabDiet, St. Louis, MO, Purina ISO Pro Rodent 3000). Mice were provided huts and running wheels for enrichment. All animals were sacrificed between 9 am and noon daily. *E2f7/E2f8* liver-specific knockout mice (LKO) were a kind gift from Alain deBruin and Gustavo Leone (31, 32). LKO mice, which were a mixed background but predominantly FVB, contained floxed E2f7 and E2f8 alleles, a Rosa26-*lacZ* reporter (R26R-*lacZ*) and Cre recombinase driven by the albumin

promoter (Alb-Cre): *E2f7*$^{loxP/loxP}$ *E2f8* $^{loxP/loxP}$ *R26R*$^{lacZ/lacZ}$ *Alb-Cre*$^{Tg/0}$. Control mice were negative for Alb-Cre: *E2f7*$^{loxP/loxP}$ *E2f8* $^{loxP/loxP}$ *R26R*$^{lacZ/lacZ}$. FRGN mice (*Fah*$^{-/-}$ *Rag2*$^{-/-}$ *Interleukin 2 common Gamma chain*$^{-/-}$ Nod background) were used for liver repopulation studies (Yecuris, Inc., Tualatin, OR) (112, 113). FRGN mice were maintained on 8 mg/l 2-(2-nitro-4-trifluoro-methylbenzoyl)-1,3-cyclo-hexanedione (NTBC) in their drinking water (Ark Pharm, Libertyville, IL). Wild-type (WT) C57BL/6J mice were from Jackson Labs (Bar Harbor, ME). Unless noted, male mice were used for experiments.

2.2.2 Hepatocyte isolation

Primary hepatocytes were isolated using a 2-step collagenase perfusion (114). Briefly, following general anesthesia induction, a catheter was inserted into the portal vein or inferior vena cava and 0.3 mg/ml collagenase II (Worthington, Lakewood, NJ) was circulated through the liver. Digested livers were placed in DMEM-F12 with 15 mM HEPES (Corning, Corning, NY) + 5% FBS (Sigma-Aldrich, St. Louis, MO), passed through a 70 μm cell strainer and washed twice using low-speed centrifugation (55g for 2 min) to remove non-parenchymal cells. Hepatocyte viability, determined by trypan blue staining, was typically >80%. Hepatocytes from FRGN transplantation recipients were isolated as described above, except the collagenase II concentration was increased to 1 mg/ml.

2.2.3 Ploidy analysis

For detection of ploidy populations, freshly isolated primary hepatocytes were washed twice in PBS, adjusted to a density of 1-2 million cells/ml and incubated on ice with 2 μl/ml Fixable

Viability Dye (FVD) eFluor 780 (eBioscience, San Diego, CA). Following 2 washes with PBS, hepatocytes were fixed with 2% PFA, washed an additional 2 times with PBS and incubated with permeabilization buffer (0.1% saponin and 0.5% BSA in PBS) + 15 μg/ml Hoechst 33342 (Life Technologies, Carlsbad, CA). Cells were washed twice and stored in PBS until flow cytometry analysis. We also detected Ki-67 in hepatic ploidy populations. Hepatocytes were prepared using the same methods as above except following FVD 780 incubation they were fixed with Foxp3 fixation buffer (eBioscience) at room temperature, washed twice with permeabilization buffer (eBioscience) and incubated in permeabilization buffer with mouse anti-Ki-67 eFluor 660 antibody (Invitrogen, Carlsbad, CA) + 15 μg/ml Hoechst 33342. Cells were washed twice with PBS and stored in permeabilization buffer until flow cytometry analysis.

Ploidy populations are indicated with *chromatid number* "c" (2c, 4c, 8c) or *chromosome number* "n" (2n, 4n, 8n). We used *chromatid number* in Fig. 7 and Fig. 8 since the gated cells contain a mixture of quiescent and proliferating cells, although >99% of adult hepatocytes are quiescent (e.g., a 4c cell is either a diploid in G2/M-phase or a tetraploid in G0/G1-phase). We used *chromosome number* in Fig. 11, Fig. 16, Fig 17 and Fig. 18 because quiescent cells are specifically gated (e.g., a 4n cell is a tetraploid).

2.2.4 Liver enzymes

Serum was collected from experimental animals and the levels of circulating serum enzymes, including alanine transaminase (ALT), aspartate transaminase (AST) and alkaline phosphatase (ALP), as well as direct bilirubin and total bilirubin were determined by the University of Pittsburgh Medical Center Clinical Laboratory.

2.2.5 Body weight and LW/BW

Livers from experimental animals were excised, washed in PBS and weighed. The percentage of the weight occupied by the liver was determined by dividing the liver weight by the total body weight of the mouse.

2.2.6 High fat diet treatment

LKO and control mice were placed on a high fat diet (HFD) for 8 weeks in which the chow was given *ad libitum* and replaced weekly. The mice were given an adjusted calorie diet in which 42% of the calories were from fat (TD.88137 Adjusted calories diet, Teklad Research Diets, Envigo, Indianapolis, IN). The mice were weighed regularly and after 8 weeks the mice were sacrificed following overnight fasting. The livers were isolated, washed in PBS, weighed to determine a final LW/BW and embedded in optimal cutting temperature (OCT) compound (Sakura Finetek, Torrance, CA). To identify neutral lipids, sections were stained with Oil Red O by the McGowan Institute for Regenerative Medicine Histology Core Lab. The percentage of the liver tissue area that was stained with Oil Red O was quantified using ImageJ software (NIH).

2.2.7 β-galactosidase (β-gal) activity assay

β-galactosidase (β-gal) activity was detected in LKO and control liver tissue and cells. Livers were embedded in OCT compound (Sakura Finetek) and cryosectioned at a thickness of 10 μm. Frozen liver sections were fixed with 0.2% glutaraldehyde, 2% paraformaldehyde (PFA) and stained overnight with Xgal solution (2 mM Xgal in DMSO, 4 mM $K_3Fe(Cn)_6$, 4 mm $K_4Fe(Cn)_6$-

H_2O, 2 mM $MgCl_2$, 0.02% NP-40, 0.01% sodium deoxycholate, 10 mM HEPES and PBS) in a 37°C humid incubator. The tissue was counterstained with Nuclear Fast Red and mounted with Permount (Fisher, Pittsburgh, PA). Cells were isolated via perfusion, seeded at 40,000 viable cells/well in 24-well Primaria Cell Culture plates (Corning) in seeding media and then fixed with 0.5% glutaraldehyde. The cells were stained overnight with Xgal solution (same as above) in a 37°C humid incubator.

2.2.8 General processing of paraffin embedded tissue

Livers from LKO and control mice were fixed in 10% neutral buffered formalin (NBF), embedded in paraffin and sectioned at a thickness of 4 μm. Sections were deparaffinized using xylene and graded ethanol (100-95%) washes and incubated in citric-acid based antigen retrieval (Vector, Burlingame, CA).

2.2.9 Quantification of mono- and binucleate hepatocytes in liver sections

Following paraffin embedding, sectioning and antigen retrieval, liver sections were blocked with 2% BSA. For quantification of mono- and binucleate hepatocytes, sections were stained with mouse anti-β-catenin primary antibody (Santa Cruz, Dallas, TX) followed by goat anti-mouse AlexaFluor 594 secondary antibody (Invitrogen, Carlsbad, CA). The sections were counterstained with Hoechst 33342 and mounted with Fluoromount-G (Southern Biotech, Birmingham, AL). A minimum of 700 hepatocytes/sample was scored.

2.2.10 Proliferation marker staining in liver sections

To measure Ki-67 (G1/S/G2/M-phases) in postnatal development, tissue sections were treated with 3% hydrogen peroxide to quench endogenous peroxidase and blocked with Avidin/Biotin blocking solution (Vector SP-2001). Sections were stained with rabbit anti-Ki-67 (Abcam, Cambridge, MA) followed by biotinylated goat anti-rabbit secondary antibody and Avidin-conjugated peroxidase (Vector ABC kit PK-6100); staining was visualized with ImmPACT DAB Peroxidase Substrate (Vector SK-4105). Sections were counterstained with hematoxylin, dehydrated with ethanol and xylene washes and mounted with Permount (Fisher).

To measure Ki-67 in regenerating livers following PH, liver sections were blocked with 2% BSA and stained with rabbit anti-Ki-67 primary antibody (Abcam) and mouse anti-E-cadherin primary antibody (BD Biosciences, San Jose, CA) followed by species-specific secondary antibodies: goat anti-rabbit AlexaFluor 594 and goat anti-mouse AlexaFluor 488 secondary antibody (both from Life Technologies). The sections were counterstained with Hoechst 33342 to visualize nuclei and mounted with Fluoromount-G (Southern Biotech). For PCNA (S-phase) and bright phospho-histone H3 (PHH3) (M-phase) staining, tissue sections were permeabilized with 0.1% Triton X-100 and blocked with 5% normal goat serum. The sections were then co-stained with rabbit anti-PHH3 primary antibody (Invitrogen), mouse anti-PCNA primary antibody (IgG2a, Santa Cruz) and mouse anti-β-catenin primary antibody (IgG1, Santa Cruz) followed by species and isotype specific secondary antibodies: goat anti-rabbit AlexaFluor 647, goat anti-mouse IgG2a AlexaFluor 488 and goat anti-mouse IgG1 AlexaFluor 594 (all from Life Technologies). The sections were counterstained with Hoechst 33342 to visualize nuclei and mounted with Fluoromount-G (Southern Biotech). A minimum of 600 hepatocytes/sample was scored to determine the percentage of $Ki67^+$, $PCNA^+$ and bright $PHH3^+$ cells.

2.2.11 Liver zonation staining

Following paraffin embedding, sectioning and antigen retrieval, liver sections were permeabilized using 1% Saponin followed by blocking in 2% BSA. Tissues were co-stained with primary antibodies mouse anti-glutamine synthetase (GS, Santa Cruz, Dallas, TX), goat anti-Cyp1A2 (Santa Cruz) and rabbit anti-β-catenin (Santa Cruz) followed by species-specific secondary antibodies: donkey anti-mouse AlexaFluor 647, donkey anti-rabbit AlexaFluor 488 and donkey anti-goat AlexaFluor 594 (all from Life Technologies). The sections were counterstained with Hoechst 33342 to visualize nuclei and mounted with Fluoromount-G (Southern Biotech). Pericentral (GS^+ $Cyp1A2^+$), mid-lobule (GS^- $Cyp1A2^+$) and periportal (GS^- $Cyp1A2^-$) regions were identified and the percentage of binucleate hepatocytes in each region was quantified. A minimum of 200 cells were counted in each region.

2.2.12 DEN tumor induction model

Control and LKO (6-week-old) mice were injected intraperitoneally with 90 mg/kg DEN (Sigma-Aldrich). Three weeks following the injection, mice were fed a standard rodent diet containing 0.05% Phenobarbital-Sodium Salt (LabDiet) for an additional 3, 6 or 9 months. Following paraffin embedding, sectioning and antigen retrieval, liver sections were treated with 3% hydrogen peroxide to quench endogenous peroxidase and blocked with Avidin/Biotin blocking solution (Vector SP-2001). Sections were stained with rabbit anti-glutamine synthetase primary antibody (Abcam) followed by biotinylated goat anti-rabbit secondary antibody and Avidin-conjugated peroxidase (Vector ABC kit PK-6100); staining was visualized with ImmPACT DAB Peroxidase Substrate (Vector SK-4105). Sections were counterstained with hematoxylin,

dehydrated with ethanol and xylene washes, and mounted with Permount (Fisher). Hematoxylin & Eosin (H&E) staining was performed by the Development Laboratory in the University of Pittsburgh Department of Pathology. Glutamine synthetase positive (GS^+) and negative tumors (GS^-) were quantified and measured.

2.2.13 RNA isolation, qRT-PCR and PCR

Total RNA was isolated from liver tissue using Trizol (Life Technologies, Carlsbad, CA) or RNeasy Plus Mini Kit (Qiagen, Germantown, MD) and subjected to qRT-PCR to quantify the expression of protein-coding genes. Total RNA was reverse-transcribed into complementary DNA (cDNA) using M-MLV (Life Technologies) and quantitative PCR reaction was performed with SYBR Green PCR Master Mix (Life Technologies). Primer sequences are listed in supporting table. Reactions were performed using a StepOnePlus System (Life Technologies). Relative expression was calculated using the ΔΔCT method. To determine presence or absence of *E2f7/E2f8* a PCR reaction was performed using cDNA, and PCR products were analyzed on a 1% agarose gel.

2.2.14 Liver repopulation using LKO or control hepatocytes

Hepatocytes from 6-week-old LKO and control donor mice were isolated using a 2-step collagenase perfusion. 300,000 LKO or control donor ($H\text{-}2K^{q}+$) hepatocytes were intrasplenically injected into 6-8-week-old FRGN ($H\text{-}2K^{q}-$) recipients. Recipient mice were maintained on 8 mg/ml NTBC for 4 days following transplantation. The transplanted mice were cycled on/off NTBC to promote donor cell ($H\text{-}2K^{q}+$) proliferation. Following several cycles of NTBC

withdrawal, mice were considered highly repopulated when body weights stabilized at ~100% of the initial weight. Hepatocytes were isolated from repopulated mice using a 2-step collagenase perfusion as previously described. The isolated hepatocytes were stained with FVD 780, anti-mouse H-2K^{q} AlexaFluor 647 antibody (Biolegend, San Diego, CA) for donor-derived cells and counterstained with 15 μg/ml Hoechst 33342 following permeabilization with 0.5% Saponin (Sigma-Aldrich) in PBS. The ploidy of the donor cells (H-2K^{q}+) was determined using flow cytometry.

2.2.15 Competitive repopulation experiments

Hepatocytes from 6-week-old LKO and control mice were mixed in ~equal ratios (Group 1: LKO$^{60\%}$ and control$^{40\%}$) or skewed towards control hepatocytes (Group 2: LKO$^{17\%}$ and control$^{83\%}$). A combined total of 300,000 donor (Fah+) cells were intrasplenically injected into 6-8-week-old FRGN recipient mice. Recipient mice were maintained on 8 mg/ml NTBC for 4 days following transplantation. The transplanted mice were cycled on/off NTBC to promote donor cell proliferation. The mice were weighed regularly and re-started on NTBC when body weights decreased to 80% baseline to minimize morbidity and mortality. Following several cycles of NTBC withdrawal, mice were considered highly repopulated when body weights stabilized at ~100% of the initial weight when off NTBC. Hepatocytes were isolated from repopulated mice using 2-step collagenase digestion as previously described. To determine the extent of repopulation, hepatocytes were stained for Fah. Briefly, cells were seeded at 40,000 viable cells/well in 24-well Primaria Cell Culture plates (Corning) in seeding media, fixed in 4% PFA, and blocked with 5% normal donkey serum in 0.05% PBS-Tween 20. The cells were stained with custom rabbit anti-Fah primary antibody and donkey anti-rabbit AlexaFluor 555 secondary

antibody (Life Technologies), counterstained with Hoechst 33342 and mounted with Fluoromount-G (Southern Biotech). To determine the percentage of donor cells in the repopulated liver, β-gal activity was assessed in the isolated hepatocytes. The cells were seeded at 40,000 viable cells/well in 24-well Primaria Cell Culture plates (Corning) in seeding media, fixed with 0.5% glutaraldehyde and stained overnight with Xgal solution in a 37°C humid incubator using methods previously described. The ratio of LKO (β-gal+) to control (β-gal-) donor hepatocytes in the repopulated liver was measured.

2.2.16 Partial hepatectomy

A 2/3 partial hepatectomy (PH) was performed on adult C57BL/6J WT, LKO and control mice using methods similar to those described previously (115). Briefly, a small vertical incision was made directly below the sternum of anesthetized mice. The left anterior liver lobe was removed after tying it with a ligature, followed by removal of the right and left segments of the median lobe. This effectively removes 2/3 of the liver mass. For tissue analysis, livers were harvested post-surgery, weighed, fixed in 10% neutral buffered formalin, embedded in paraffin and sectioned at a thickness of 4 μm. The tissue sections were stained for Ki-67 and E-cadherin using previously described methods, and the number of proliferating ($Ki\text{-}67^{+}$) hepatocytes quantified. For FACS analysis, cells from the livers of C57BL/6J WT mice that had undergone 2/3 PH were isolated via 2-step collagenase perfusion and prepared for Ki-67 FACS analysis using methods previously described. FACS analysis was used to quantify the total number of proliferating ($Ki\text{-}67^{+}$) hepatocytes for each ploidy population.

2.2.17 *In vitro* proliferation using LKO and control hepatocytes

LKO or control hepatocytes from 14-day-old or adult mice were seeded at 40,000 viable cells/well in 24-well Primaria Cell Culture plates (Corning) in seeding media: DMEM-F12 with 15 mM HEPES (Corning), 5% FBS (Atlanta Biologicals, Atlanta, GA) and Antibiotic-Antimycotic Solution (Corning). After 4 hours, seeding media was replaced with growth media: DMEM-F12 with 15 mM HEPES (Corning), 0.5% FBS (Atlanta Biologicals), Antibiotic-Antimycotic Solution (Corning) and ITS Supplement (containing 1 μg/ml insulin, 0.55 μg/ml transferrin and 0.67 ng/ml sodium selenite; Gibco Life Technologies). For BrdU labeling, hepatocytes were cultured in growth media containing 1 mM BrdU (Sigma-Aldrich) for 12-24 hours prior to harvest (as indicated in each experiment), fixed in 4% PFA, washed in 1% Triton X-100 followed by 2 N HCl and 0.1 M Na_2B4O_7, and blocked with 0.5% skim milk. Next cells were incubated with mouse anti-BrdU primary antibody (BD Biosciences) and goat anti-mouse AlexaFluor 594 secondary antibody (Life Technologies), counterstained with Hoechst 33342, and mounted with Fluoromount-G (Southern Biotech). For phospho-histone H3 (PHH3) staining, cells were fixed in 4% PFA, blocked with 2% BSA in Normal Donkey Serum, stained with rabbit anti-PHH3 primary antibody (Invitrogen) and donkey anti-rabbit AlexaFluor 555 secondary antibody (Life Technologies), counterstained with Hoechst 33342 and mounted with Fluoromount-G (Southern Biotech). Nuclei with punctate PHH3 staining were considered to be in G2-phase. For measuring apoptosis, hepatocytes were cultured in growth media containing 0.5 μM NucView 488 substrate (a substrate for detecting active caspase-3, a marker of apoptosis; Biotium, Hayward, CA) for 30 minutes before harvest. Cells were fixed with 4% PFA, stained with Hoechst 33342 and mounted with Fluoromount-G (Southern Biotech). Approximately 100 cells/sample/time were scored for each stain. To measure molecular markers of proliferation, LKO and control hepatocytes from

adult mice were seeded at $1x10^6$ viable cells/well in 10-cm Primaria Cell Culture dishes (Corning) in seeding media. After 4 hours, seeding media was replaced with growth media. At each time point the cells were washed, trypsinized, and harvested. RNA was isolated using the RNeasy Plus Mini Kit (Qiagen) and prepared for qRT-PCR using methods previously described.

2.2.18 *In vitro* proliferation using WT hepatocytes, with and without mitogens

Hepatocytes from 20-day-old WT C57BL/6 mice were seeded at 100,000 viable cells/well in 6-well Primaria Cell Culture plates (Corning) in seeding media before switching to growth media 4 hours later. The cells were grown in growth media containing 1 mM BrdU for 12-24 hours prior to harvest, fixed in 4% PFA and stained for BrdU, PHH3 and active caspase-3 using methods stated previously. For growth factor stimulation, cells were seeded, switched to serum-free media and growth factors added 4 hours later. Growth factors included mouse HGF, human EGF, mouse FGF-acidic (FGF1), mouse FGF-basic (FGF2), human PDGF-AA, human TGFα (all 40 ng/ml: R&D Biosystems, Minneapolis, MN) and insulin (1 μg/ml). The cells were incubated with 1 mM BrdU for 12-24 hours prior to harvest, fixed in 4% PFA, and stained for BrdU using methods described previously. The number of positively stained mono- and binucleate hepatocytes was quantified by overlaying phase-contrast and fluorescent images. Approximately 350 cells/sample/time/growth condition were scored.

2.2.19 Flow cytometry

All FACS analyses were performed with a FACS Aria II-SORP (BD Biosciences) equipped with a 130 μm nozzle and running DiVa v8.0.2 software. FACS plots were generated using FlowJo 9.9.6 (Treestar, Ashland, OR).

2.2.20 Microscopy

Fluorescent images were captured with a Nikon TiU fluorescent microscope equipped with a monochrome camera. Non-fluorescent images were captured with a Nikon TS100 microscope equipped with a color camera. Gross morphology images were taken using a Nikon D3100 DSLR Digital Camera with 18-55mm f/3.5-5.6 Auto Focus-S Nikkor Zoom Lens. Images were processed with Nikon NIS Elements Basic Research software, NIH ImageJ software and Adobe Photoshop.

2.2.21 Statistical analysis

Statistical significance was calculated by GraphPad Prism 7.0.a or Microsoft Excel 16.16.6 using 2-tailed Student's *t* test. *P* values < 0.05 were considered significant.

Additional methods can be found in **Appendix A (page 136)**.

2.3 Results

2.3.1 Liver-specific deletion of *E2f7* and *E2f8* blocks hepatic polyploidy

To validate the effects of *E2f7* and *E2f8* deficiency in the liver, we obtained mice with floxed *E2f7* and *E2f8* alleles and a Rosa26-*lacZ* reporter (R26R-*lacZ*) that were crossed with Cre recombinase driven by the Albumin promoter (Alb-Cre) to specifically delete these genes in the liver (31, 32). *E2f7/E2f8* liver-specific knockout (LKO) and control mice were compared. Taking advantage of R26R-lacZ, control hepatocytes lacking Alb-Cre did not express β-galactosidase (β-gal), as expected, whereas hepatocytes from LKO mice were β-gal+ (Fig. 5A). Consistent with the literature, liver weight to body weight (LW/BW) ratio (Fig. 5B), circulating liver enzymes (Fig. 5C) and hepatic zonation (Fig. 5D-F) were comparable (31, 32). Additionally, gene signatures were equivalent between LKO and control mice at 3 and 16 weeks of age (e.g., gene ontology categories, cell cycle, metabolism, proliferation and differentiation) and in livers depleted of E2f8 alone (e.g., differentiation genes such as *Albumin*, *Foxa3* and *Hnf4a*; Cytochrome P450 family members; and cell cycle genes) (32, 35).

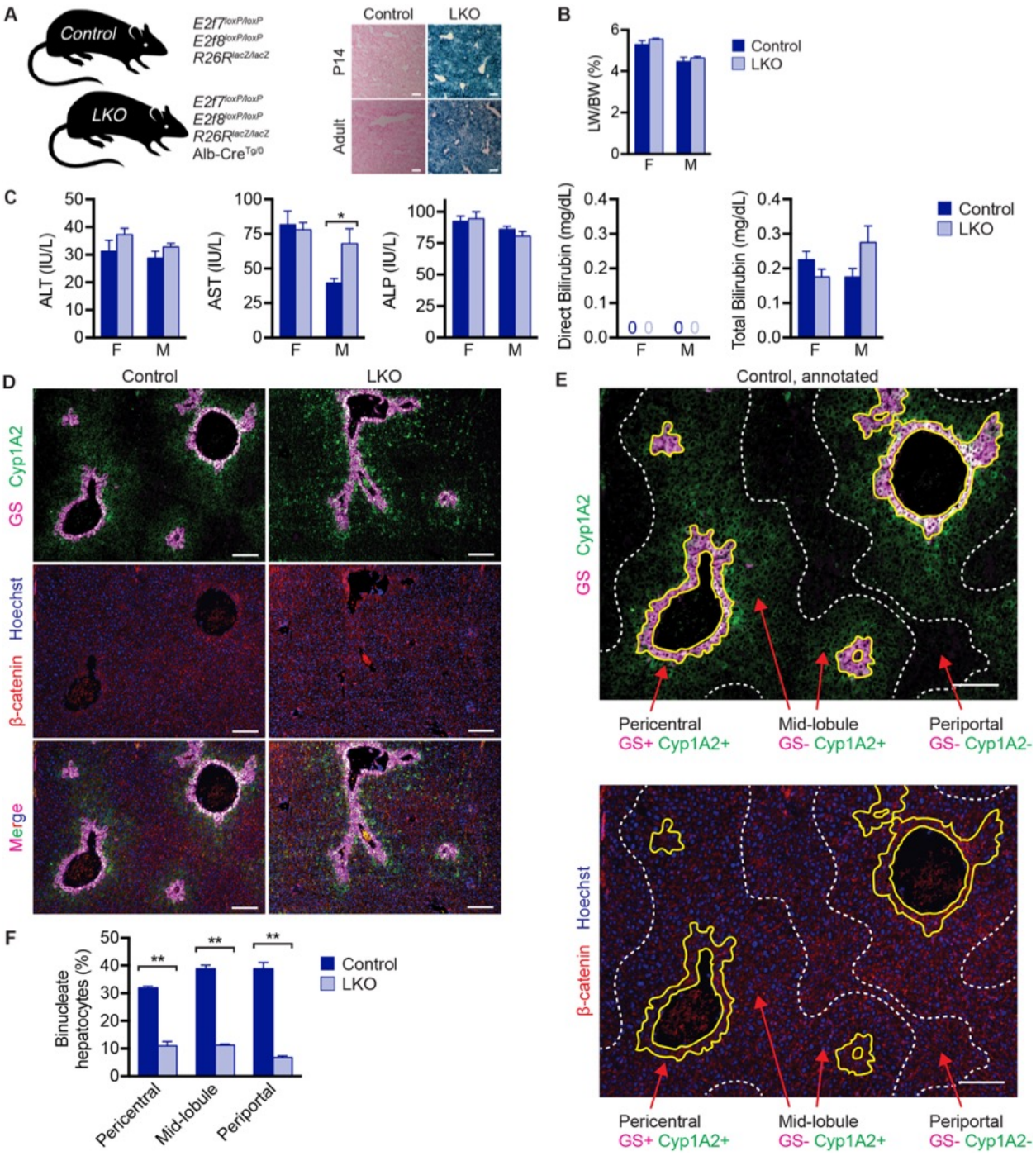

Figure 5. Liver-specific deletion of *E2f7/E2f8* as a hepatic polyploidy knockout model.

(A) Experimental mice contain floxed *E2f7* and *E2f8* alleles as well as R26R-lacZ. LKO mice are hemizygous for Alb-Cre and controls are negative. Livers isolated from 14-day-old (P14) and 2.5-month-old (adult) LKO and control mice were stained with X-gal to visualize β-gal (blue) and nuclear fast red to visualize nuclei (pink) (n = 3-4/genotype/age). β-gal activity confirms Cre activity in LKO livers. (B) LKO and control mice at 2.5 months have

similar LW/BW ratios. (C) LKO and control mice at 2.5 months have similar levels of ALT, ALP and direct/total bilirubin. AST levels are slightly elevated in male LKO mice (n = 4/genotype/age/gender; F, female; M, male). (D) Livers from 2.5-month-old male LKO and control mice were stained for Glutamine Synthetase (GS, a pericentral marker, pink), Cytochrome P450 1A2 (Cyp1A2, a pericentral and mid-lobule marker, green), β-catenin (cell membrane marker, red) and Hoechst dye (nuclear marker, blue). Representative images are shown as 2-color panels and as a 4-color merge. (E) The GS and Cyp1A2 expression pattern was used to define pericentral, mid-lobule and periportal regions. Within each region, mono- and binucleate hepatocytes were identified using β-catenin and Hoechst staining. Representative images are shown for a control mouse. Solid yellow lines indicate the pericentral region and dashed white lines highlight the mid-lobule area. (F) Mono- and binucleate hepatocytes were quantified in each zone. Overall, the percentage of binucleate hepatocytes is reduced in LKO livers. However, similar to control livers, binucleate hepatocytes in LKO livers are distributed evenly in all zones. * $P < 0.05$, ** $P < 0.001$. Graphs show mean ± sem. Scale bars are 100 μm.

To assess liver function following chronic injury, we maintained mice on high fat diet (HFD) for 8 weeks. LKO and control mice had equivalent ALT levels, proportional increases in body weight and LW/BW ratios (Fig. 6A-C). Gross liver morphology and accumulation of neutral lipids were the same (Fig. 6D,E). Thus, together with the observation by Pandit et al. that LKO and control mice respond equivalently to DDC diet (32), *E2f7/E2f8* deficient mice appeared to be functionally normal.

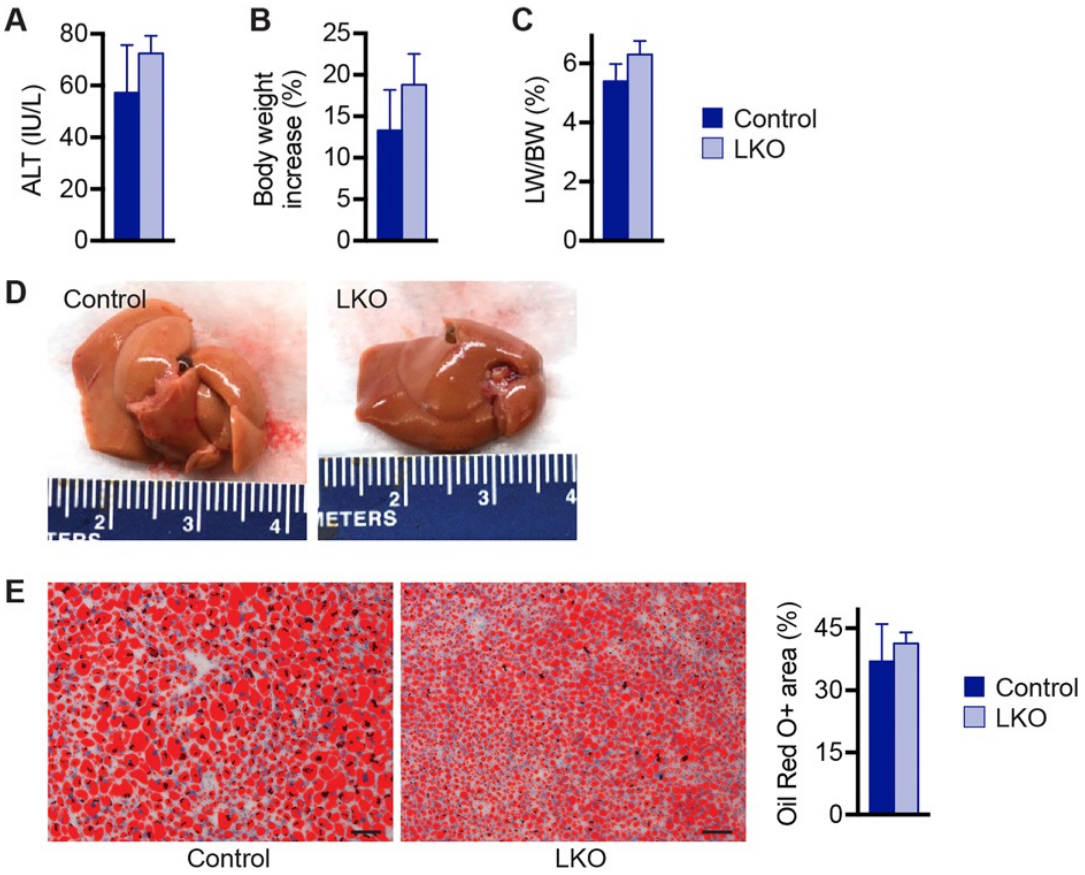

Figure 6. LKO and control mice respond to HFD equivalently.

(A-C) Approximately 3-month-old LKO (n = 8) and control mice (n = 3) were maintained on HFD for 8 weeks to model fatty liver disease. ALT levels (A), body weight increase (B) and LW/BW ratios (C) were the same. (D,E) Livers harvested after 8 weeks were similar in terms of gross morphology (D) and accumulation of neutral lipids, as seen by Oil Red O staining (E). Representative images are shown, and the percentage of Oil Red O+ tissue quantified. Graphs show mean ± sem. Scale bar is 100 μm.

The most striking effect associated with loss of *E2f7/E2f8* is altered hepatic ploidy. Binucleate hepatocytes were reduced 3-4-fold in LKO livers as early as day 20 and into adulthood (Fig. 7A), and they were distributed evenly between all zones in the liver, similar to controls (Fig. 5F). We determined cellular ploidy by quantifying nuclear content using flow cytometry. In control adult livers, diploid cells comprised only 3-4% of hepatocytes and polyploids comprised the rest. The ploidy spectrum was dramatically altered in LKO livers, with diploids representing 60-70% of hepatocytes. This observed 20-fold enrichment of diploid hepatocytes in LKO livers was seen in 2.5- and 5-month-old livers (Fig. 7B,C).

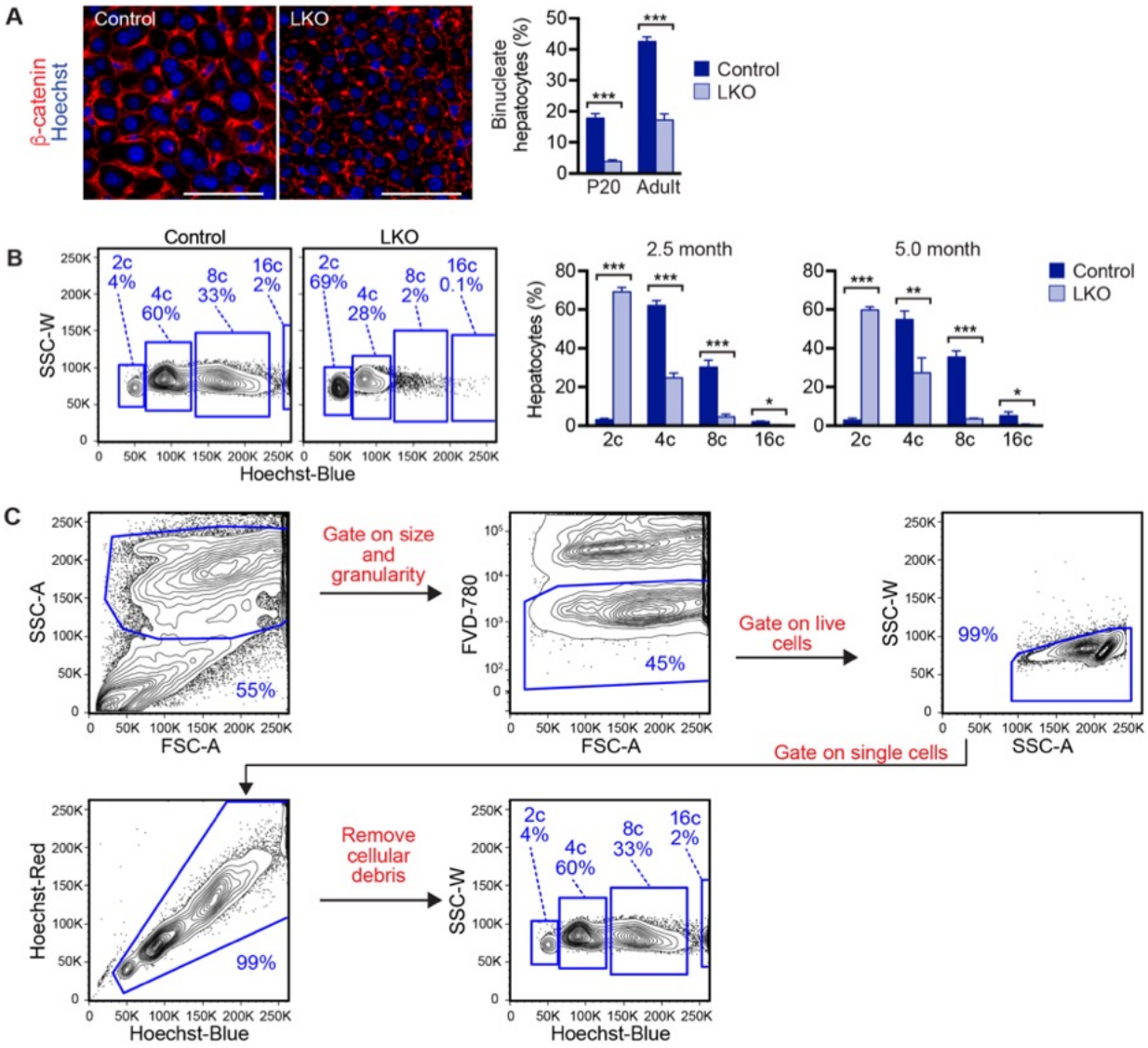

Figure 7. LKO mice are deficient in polyploid hepatocytes.

(A) Livers from 20-day-old (P20) and 2.5-month-old (adult) LKO and control mice were stained for β-catenin to mark cell membranes (red) and Hoechst dye (blue) to mark nuclei. The percentage of binucleate hepatocytes was quantified (n = 3-5 mice/genotype; mixed gender), and representative images are shown at 2.5 months. (B) Freshly isolated hepatocytes from 2.5- or 5.0-month-old LKO and control mice were loaded with Hoechst to determine hepatocyte ploidy by FACS analysis. Representative FACS plots are shown (at 2.5 months) and the percentage of diploid, tetraploid, octaploid and hexadecaploid hepatocytes (2c, 4c, 8c, 16c, respectively) are shown for each age (n = 3-6/genotype/age; males). Here, ploidy populations are marked with chromatid number "c" since they contain a mixture of cycling and quiescent cells (although >99% are quiescent). (C) Single cell suspensions of LKO and control

hepatocytes were stained with FVD-780 (a viability dye) + Hoechst dye and analyzed by flow cytometry. Cells were gated on the basis of size/granularity and viability. Subsequently, single cells were selected and cellular debris removed. Hepatic ploidy populations were determined by separating the cells based on incorporation of Hoechst using the Hoechst-blue channel. Ploidy populations are marked with chromatid number "c" since they contain a mixture of cycling and quiescent cells (although >99% are quiescent). Representative FACS plots are shown for a control mouse. * $P < 0.05$, ** $P < 0.01$, *** $P < 0.0004$. Graphs show mean ± sem. Scale bar is 50 μm.

We previously showed that diploid hepatocytes can polyploidize during therapeutic liver repopulation (26). We therefore wondered whether the LKO ploidy phenotype was stable during extensive proliferation. To test this, we utilized the fumarylacetoacetate hydrolase (Fah) liver repopulation model (Fig. 8A) (114). Mice lacking Fah develop liver failure but are kept alive and healthy by supplementing 2-(2-nitro-4-trifluoro- methylbenzoyl)-1,3-cyclo-hexanedione (NTBC) in the drinking water. Fah+ donor hepatocytes are transplanted into *Fah*$^{-/-}$ mice and NTBC is removed. In this environment, donor hepatocytes have a proliferative advantage, and cells proliferate 500-1000-fold to replace host hepatocytes. To prevent immune rejection of transplanted hepatocytes, which were a mixed background, we used immune deficient *Fah*$^{-/-}$ mice (termed "FRGN" for *Fah*$^{-/-}$ *Rag2*$^{-/-}$ *Interleukin 2 common Gamma chain*$^{-/-}$ Nod background) (112, 113). FRGN mice transplanted with adult LKO or control hepatocytes were completely repopulated (>99%), as seen by expression of the donor marker H-2K^{q} (Fig. 8B,C). Moreover, we noticed that LKO-transplanted recipients repopulated 25% faster than control-transplanted mice (Fig. 8A). After complete liver repopulation, control hepatocytes were >99% polyploid, and LKO hepatocytes remained predominantly diploid, indicating that the LKO ploidy phenotype is stable even after extensive *in vivo* proliferation (Fig. 8B). Together, the data show that LKO mice serve as a stable "hepatic polyploidy knockout" model.

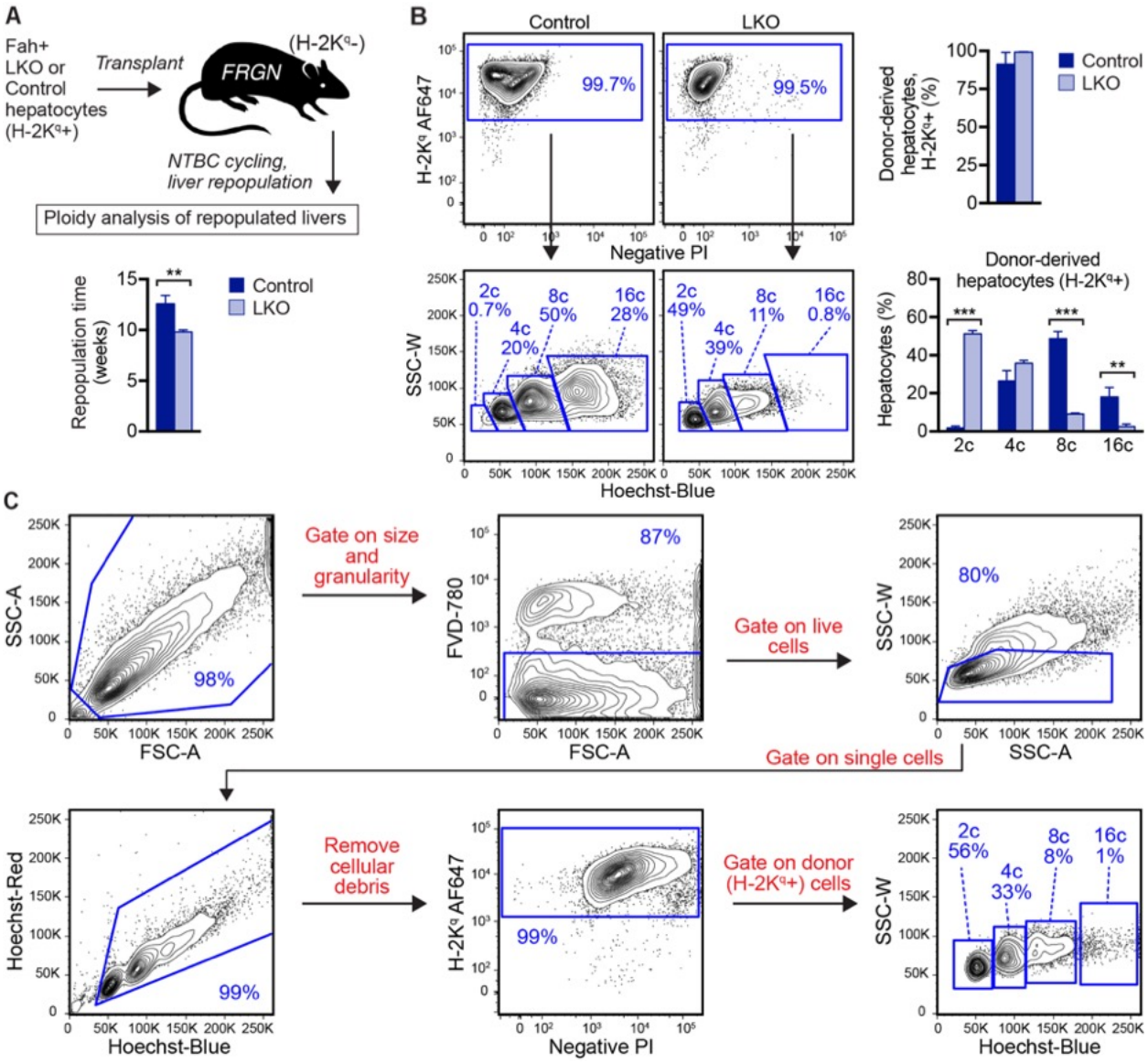

Figure 8. LKO hepatocytes remain predominantly diploid even after extensive proliferation.

(A,B) LKO or control hepatocytes from 2-month-old male mice were transplanted into female FRGN mice that were subjected to NTBC cycling and harvested upon complete repopulation (A). The time to repopulation, as defined by maintenance of 100% body weight in the absence of NTBC, is indicated (n = 6-7/genotype). Representative FACS plots and compiled data are shown (n = 4-5/genotype) (B). Hepatocytes from repopulated recipients were ≥99.5% positive for the donor marker H-2K^q, indicating that LKO and control hepatocytes repopulated equivalently (B, top). Ploidy analysis revealed that LKO-repopulated livers were highly enriched for diploid hepatocytes, whereas livers repopulated with control hepatocytes were predominantly polyploid (B, bottom). (C) Hepatocytes isolated from FRGN livers repopulated by LKO or control hepatocytes were stained with FVD-780 + H-2K^q-AF647 (a donor marker) +

Hoechst dye. Cells were gated on the basis of size/granularity and viability. Single cells were then selected and cellular debris removed. Donor-derived cells (H-2K^{q+}) were selected and hepatic ploidy populations determined. Representative FACS plots are shown for an FRGN mouse repopulated by LKO hepatocytes. ** $P < 0.01$, *** $P < 0.0004$. Graphs show mean ± sem.

2.3.2 DEN-induced liver tumors expand rapidly in LKO mice

Polyploidy is a hallmark of cancer that has been shown to promote genomic instability and dysregulated gene expression, frequently leading to cellular transformation and tumorigenesis (116, 117). Intriguingly, in the liver, polyploidy has been suggested to protect against tumorigenesis (35, 118). Since LKO mice function normally and are predominantly diploid, these mice provided an opportunity to assess the role of polyploidy in hepatocellular carcinogenesis. Six-week-old LKO or control mice were injected with a single dose of diethylnitrosamine (DEN) to initiate tumor formation and 3 weeks later mice were placed on a phenobarbital (PB) diet to promote tumor expansion (Fig. 9A) (119-122). LW/BW ratio was consistently higher in LKO mice (Fig. 9B). Macroscopically, tumors were not seen in control livers after 3, 6 or 9 months (Fig. 9C). In LKO livers, tumors were undetected after 3 months, discrete tumors were visible after 6 months, and by 9 months, livers were dramatically enlarged and filled with tumors. Liver tumors in the DEN/PB model typically contain activating β-catenin mutations, so we stained liver sections with H&E for general histology and glutamine synthetase (GS), a β-catenin target that serves as a surrogate marker for activated β-catenin (Fig. 9D) (120, 123, 124). LKO mice were highly enriched with GS- and GS+ liver tumors. Tumor number, size and area increased with time in the LKO mice (Fig. 9E).

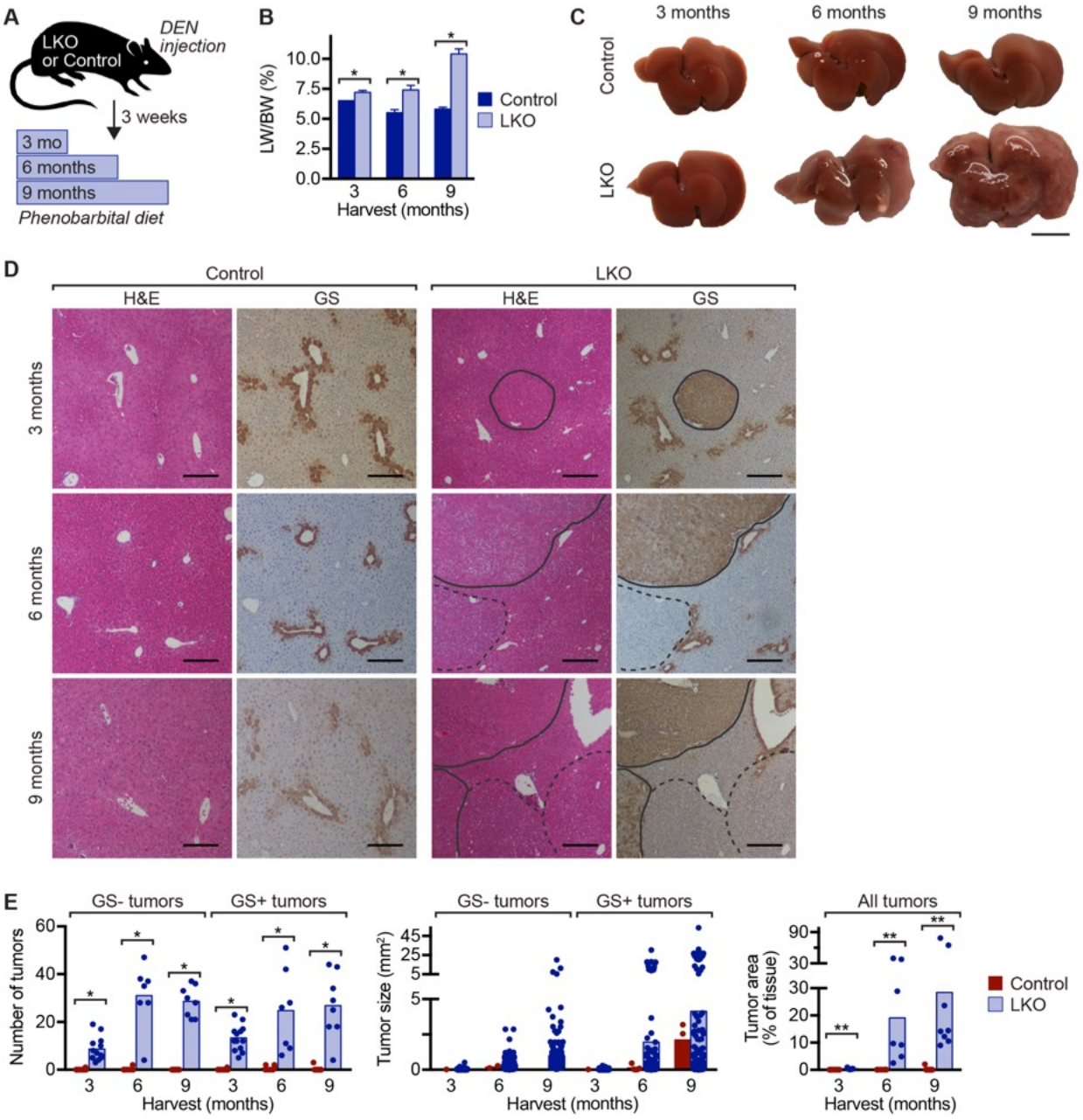

Figure 9. Liver tumors induced by the DEN model expand rapidly in LKO mice.

(A) Experimental design is shown. Six-week-old LKO and control mice were injected with DEN (90 mg/kg) to induce liver tumors, and after 3 weeks, they were maintained on chow supplemented with 0.05% phenobarbital for 3, 6 or 9 months to promote tumor expansion (n = 7-9 mice/genotype/time point; males). (B) LW/BW was elevated in LKO mice at all time points. Graph shows mean ± sem. (C) Control livers contained no macroscopic tumors after 3-9 months. In LKO livers, there were few macroscopic tumors at 3 months, and they increased in size and number over time. Gross morphology is shown for representative livers. (D) Serial liver sections were stained with H&E and GS

(brown) to identify liver tumors. GS- tumors (dashed line) and GS+ tumors (solid line) are indicated. (E) Compared to controls, tumors in LKO mice were more numerous (left), larger in size (middle) and occupied more liver tissue (right). Graphs show mean and dots represent individual mice (for tumor number and tumor area) or individual tumors (for tumor size). * $P < 0.002$, ** $P < 0.0008$. Scale bars are 1 cm (in C) or 200 μm (in D).

Genes involved in DEN metabolism (*Cyp2b10*) and PB-induced proliferation (*Car* and *Cyp2e1*) were expressed at similar levels, indicating that response to DEN/PB is not attributed to *E2f7/E2f8* deficiency (Fig. 10A,B) (125-127). ALT, AST and bilirubin levels were similar in both groups, although ALT was increased 2-3-fold in LKO mice after 9 months (Fig. 10C). Together, these data are consistent with other reports (35, 128) and show that LKO mice are highly susceptible to DEN/PB-mediated tumorigenesis, suggesting that the hepatic polyploid state protects the liver from tumor formation.

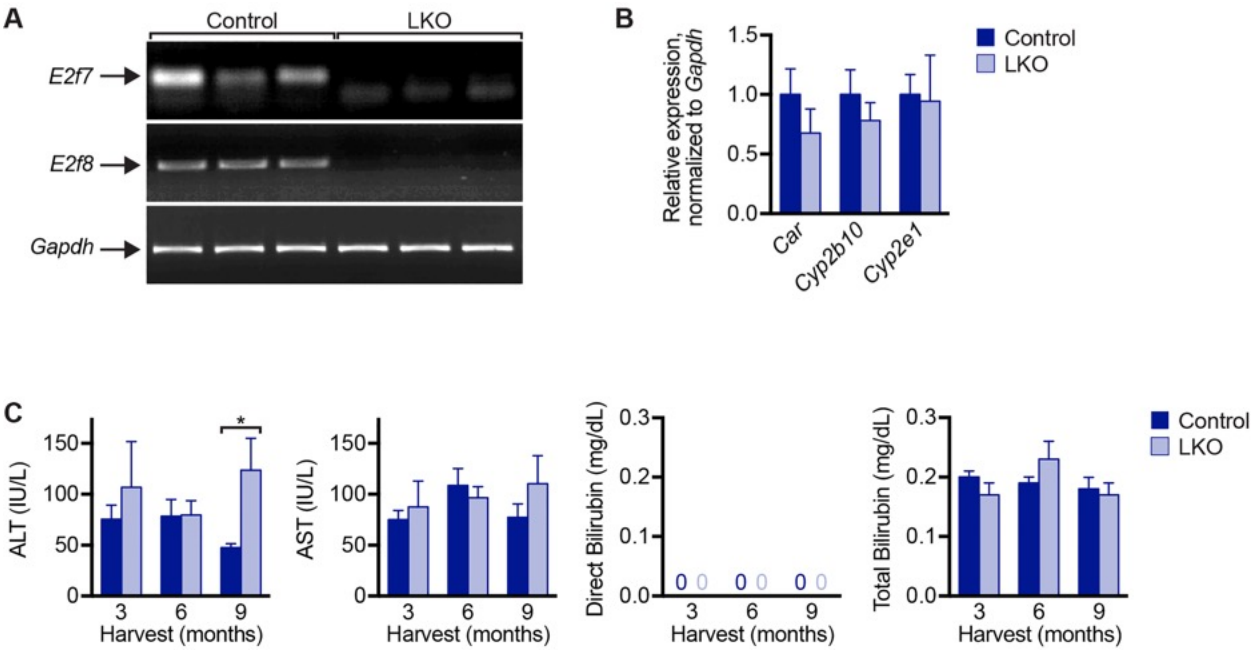

Figure 10. Characterization of LKO and control mice in the DEN/PB tumor model.

(A,B) Hepatocytes were isolated from 6-week-old LKO and control mice prior to DEN injection, as described in Fig. 7B,C (n = 3-4; males). As expected, *E2f7* and *E2f8* were expressed by control hepatocytes but not by LKO hepatocytes (A). Genes involved in DEN metabolism (*Cyp2b10*) and PB-induced proliferation (*Car* and *Cyp2e1*) were equivalently expressed. Gene expression was normalized to *Gapdh* (B). (C) Liver enzyme levels were determined after 3, 6 and 9 months of PB treatment (n = 7-13/genotype/time point). ALT levels were equivalent at 3 and 6 months, and they were 2-3-fold elevated at 9 months. AST and total/direct bilirubin were equivalent. * $P = 0.02$. Graphs show mean ± sem.

2.3.3 Adult LKO hepatocytes transit through the cell cycle rapidly *in vitro*

We observed that transplanted LKO hepatocytes repopulated FRGN livers 25% faster than control hepatocytes (Fig. 8A). Therefore, since LKO hepatocytes are predominantly diploid, we hypothesized that diploid hepatocytes are more proliferative than polyploids, which drives tumor formation in DEN/PB-treated LKO mice. To test this idea, we compared proliferation of LKO and control hepatocytes *in vitro.* First, we measured cell cycle progression using hepatocytes from 14-day-old mice where LKO and controls are equivalent in terms of ploidy (96% diploid) and cell cycle status (83% quiescent) (Fig. 11A,B). Therefore, any variations in proliferation *in vitro* are unrelated to ploidy states or basal proliferation rates.

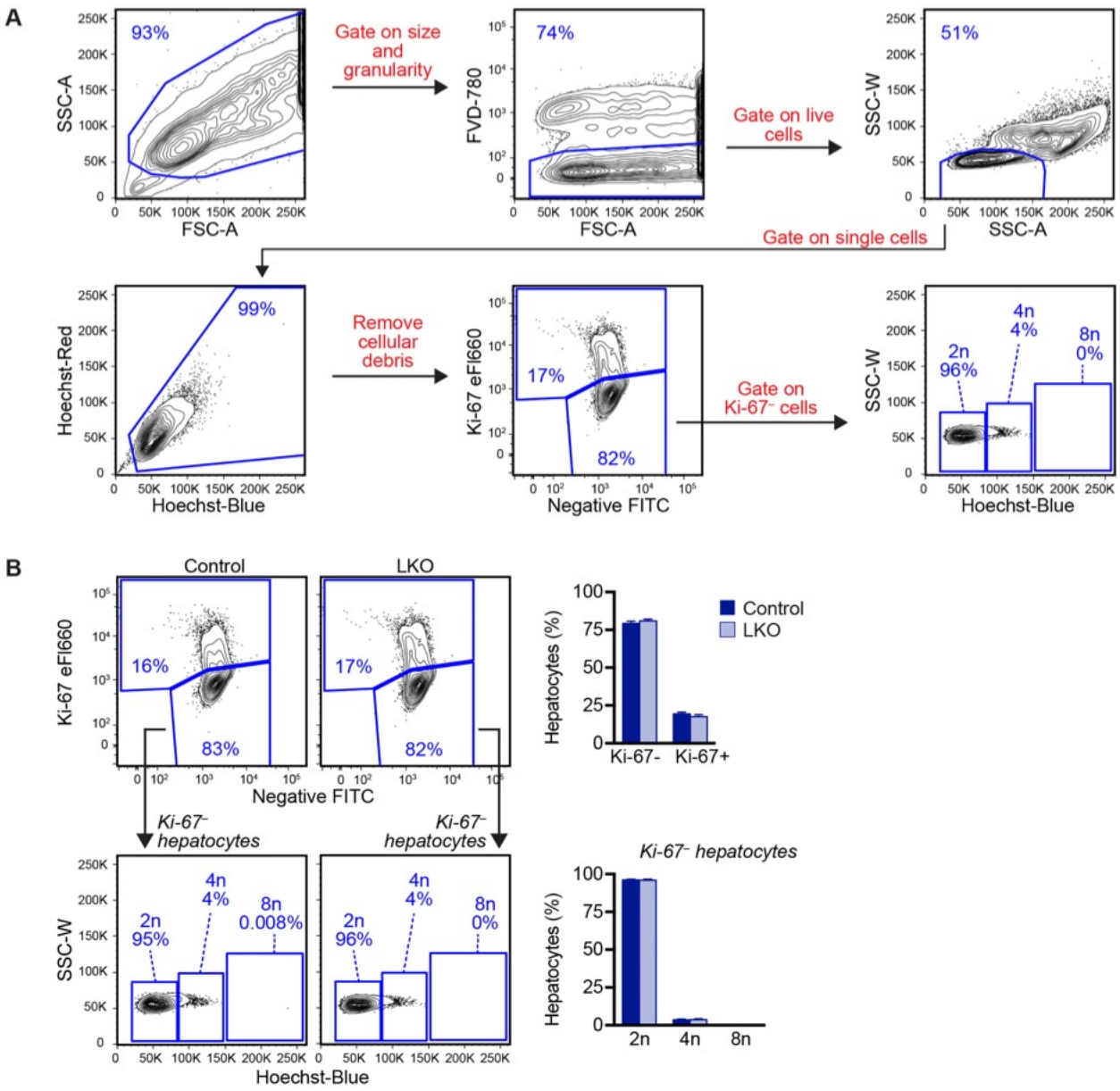

Figure 11. Hepatic ploidy is equivalent in 14-day-old LKO and control mice.

(A,B) Single cell suspensions of freshly isolated LKO and control hepatocytes were stained with FVD-780, fixed/permeabilized, stained with Ki-67-AF647 + Hoechst dye and analyzed by flow cytometry. Cells were gated on the basis of size/granularity and viability. Next, single cells were selected and cellular debris removed. Finally, cells were separated based on Ki-67 expression and ploidy was determined for the Ki-67- subset. Here, ploidy populations are marked with chromosome number "n" since they contain quiescent cells only (e.g., 2n, 4n, 8n). The gating strategy is shown for a representative LKO mouse (A). Ki-67 expression and ploidy are comparable in LKO and control mice

(n = 3-4 mice/genotype). Representative FACS plots are shown and the data summarized (B). Graphs show mean ± sem.

Freshly isolated hepatocytes were seeded in cell culture dishes, and cells and nuclei in S-phase (BrdU incorporation), G2-phase (speckled phospho-histone H3 staining, PHH3) and undergoing apoptosis were tracked (Fig. 12A). Compared to controls, the percentage of LKO hepatocytes in S-phase was increased at all time points (Fig. 12B and Fig. 13A). LKO hepatocytes in G2-phase were modestly elevated at 24-48 hours, reduced at 72 hours and equivalent at 96 hours (Fig. 12C and Fig. 13B). There were slightly fewer LKO apoptotic hepatocytes throughout the culture period (Fig. 12D). Next, we tracked proliferation in 2.5-month-old adult hepatocytes. The percentage of LKO hepatocytes in S-phase (48-96 hours) and G2-phase (24-72 hours) was elevated throughout the culture period, while cell death was nearly equivalent (Fig. 12B-D and Fig. 13A,B). To compare LKO proliferation kinetics between 14-day-old and 2.5-month-old adult hepatocytes, we normalized LKO values in each phase of the cell cycle to control values (Fig. 12E). The data indicate that cell cycling is modestly increased in 14-day-old LKO hepatocytes, whereas hepatocytes in S- and G2-phases in LKO adults are elevated consistently and to a greater extent.

Consistent with the cellular markers of proliferation, cyclin genes including *Ccnd1*, *Ccne1*, *Ccna2* and *Ccnb1*, which are enriched at defined cell cycle stages, were also upregulated by proliferating LKO hepatocytes (Fig. 13C). Since 14-day-old hepatocytes are inherently more proliferative than adult hepatocytes we cannot exclude the possibility that genotype-specific differences are masked at young ages. Nonetheless, the data suggest that non-ploidy differences contribute minimally to altered cell cycle kinetics by LKO hepatocytes and hepatic ploidy differences play a dominant role.

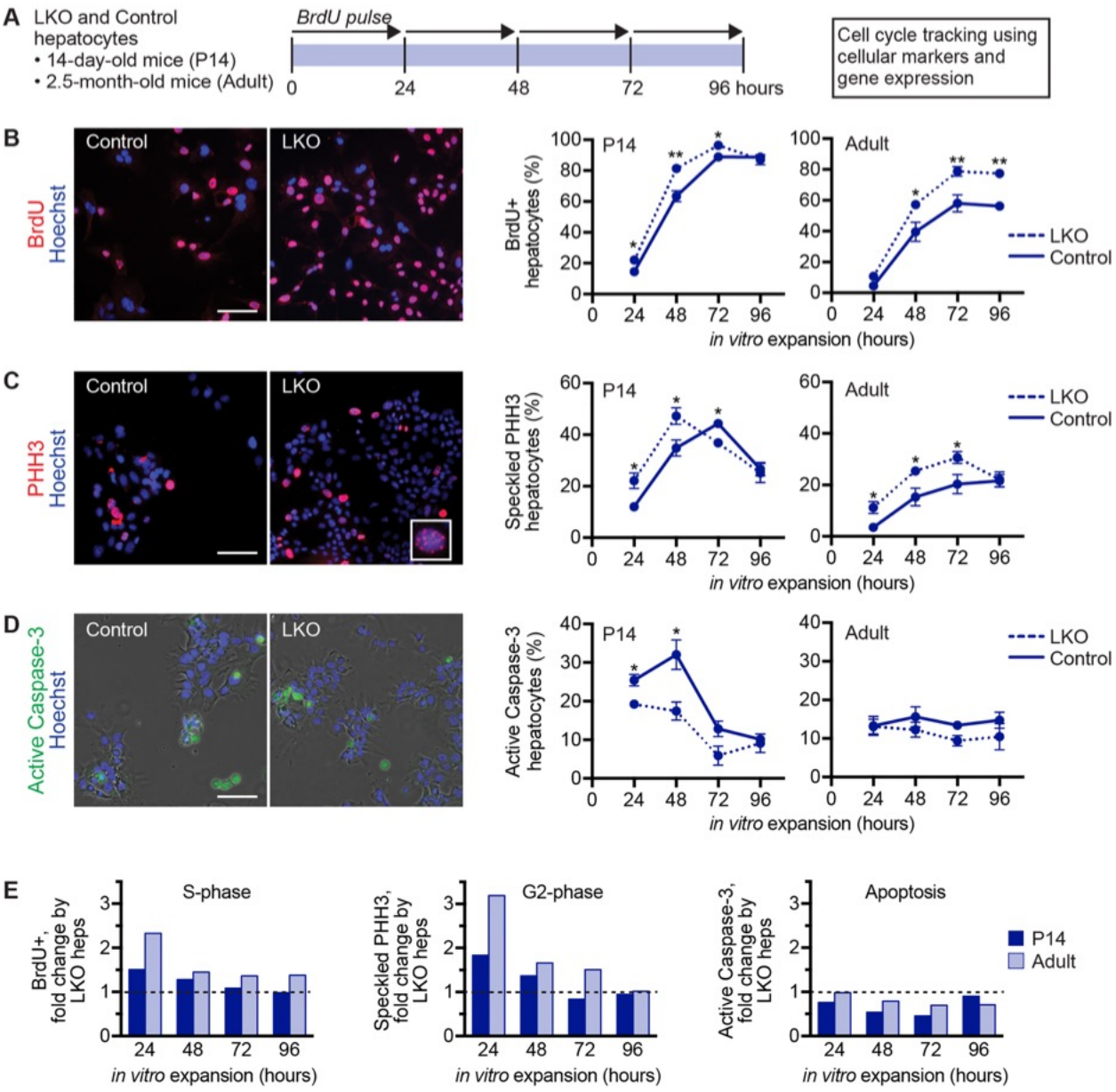

Figure 12. LKO hepatocytes that are predominantly diploid cycle faster than control hepatocytes.

(A) Experimental design is shown. LKO and control hepatocytes isolated from 14-day-old (n = 3-5/genotype/time point) or 2.5-month-old mice (n = 4-6/genotype/time point; female) were seeded in cell culture dishes and harvested after 24, 48, 72 or 96 hours of proliferation to determine S-phase via BrdU incorporation, G2-phase via speckled PHH3 staining and apoptosis via active caspase-3 staining. For BrdU incorporation, cells were pulsed with BrdU for 24 hours prior to harvest. (B-D) Representative images are shown for cells after 72 hours in culture. Cells were stained for BrdU (red) (B), PHH3 (red, inset shows speckled staining pattern) (C) and active caspase-3 (green, overlaid with phase contrast) (D). Nuclei were stained with Hoechst dye (blue). Graphs show the percentage of positive cells at each

time point; see Fig. 13 for the percentage of positive nuclei. (E) LKO proliferation kinetics by hepatocytes isolated from 14-day-old mice were compared to 2.5-month-old mice by calculating the fold-change of LKO hepatocytes in each phase of the cell cycle versus control values. The dashed lines indicate a normalized value of 1. * $P < 0.04$, ** $P < 0.008$. Graphs show mean ± sem (B-D) or mean only (E). Scale bars are 100 μm.

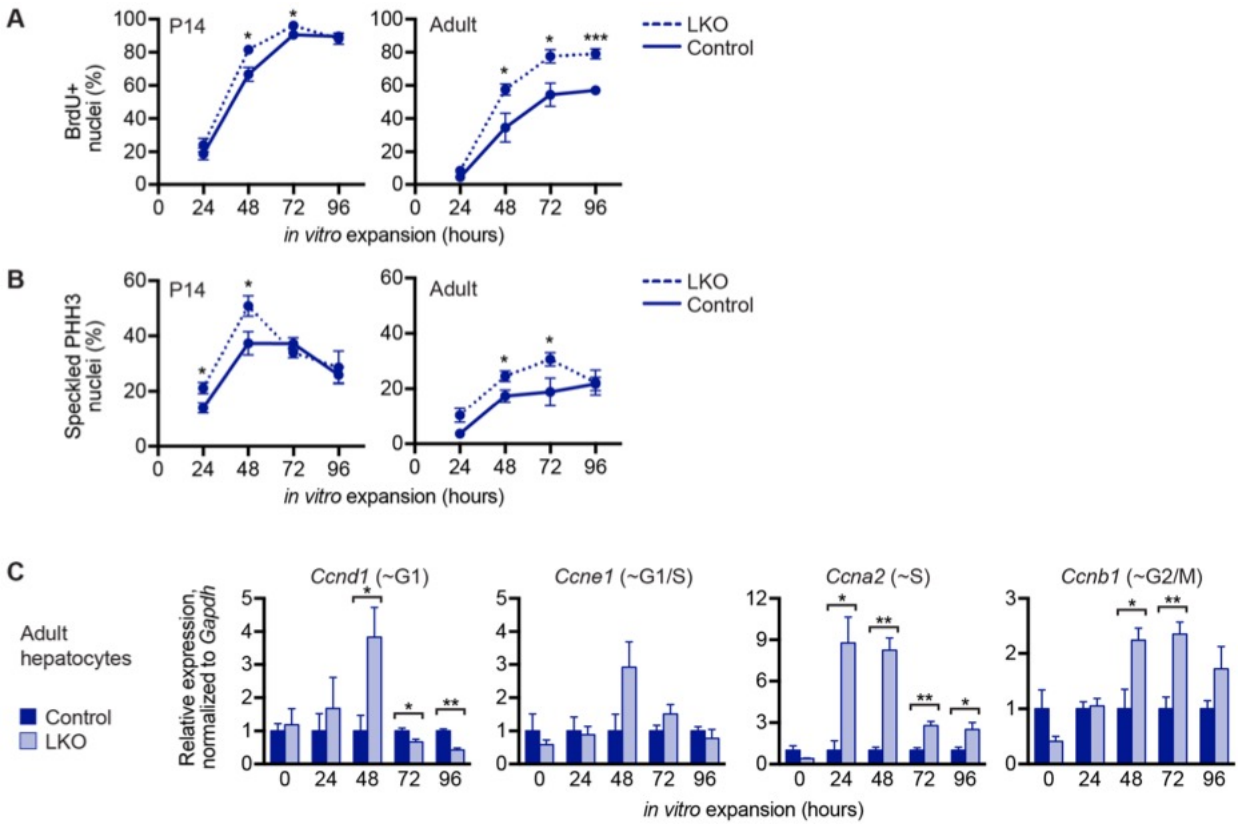

Figure 13. LKO hepatocytes cycle faster than control hepatocytes, as measured by nuclear proliferation markers and mRNA expression of cyclin family members.

(A,B) BrdU and PHH3 stained cells from Fig. 12 were evaluated for BrdU+ nuclei (A) and speckled PHH3 nuclei (B). The percentage of positive nuclei at each time point correlates with the percentage of positive cells in Fig. 12. (C) LKO and control hepatocytes from 2.5-month-old adults were cultured as described in Fig. 12A and harvested at each time point to measure mRNA expression of cyclin family members (n = 3-4/genotype/time point; male). The approximate phase of the cell cycle corresponding to each gene is indicated. CyclinD1 (*Ccnd1*) is enriched in G1-phase; CyclinE1 (*Ccne1*) is enriched at G1/S transition; CyclinA2 (*Ccna2*) is enriched at S/G2 transition; and CyclinB1 (*Ccnb1*) is enriched in G2/M (92, 129, 130). Cyclin expression was normalized to *Gapdh* and control values were set to 1.0 at each time point. * $P < 0.05$, ** $P < 0.008$, *** $P = 0.0006$. Graphs show mean ± sem.

2.3.4 LKO hepatocytes proliferate faster than controls *in vivo*

Since LKO hepatocytes progressed through the cell cycle faster than controls *in vitro,* we next characterized hepatocyte proliferation *in vivo.* First, we compared proliferation during postnatal liver development. LKO and control livers were harvested at 15-75 days of age and stained for Ki-67, a marker of G1/S/G2/M phases of the cell cycle. The percentage of Ki-67+ hepatocytes was equivalent at all ages (Fig. 14A). Next, we compared proliferation during liver regeneration in response to 2/3 partial hepatectomy (PH). In this classic procedure, 2/3 of the liver mass is surgically removed and the remaining liver tissue undergoes a wave of proliferation to restore the liver mass (131-133). LW/BW recovery and the percentage of Ki-67+ (G1/S/G2/M), PCNA+ (S-phase) and bright PHH3+ (M-phase) hepatocytes was nearly equivalent at all time points (Fig. 14B,C). While we cannot exclude the possibility that LKO hepatocytes entered the cell cycle earlier than controls between 0 and 48 hours, there was a trend toward increased Ki-67+ and PCNA+ hepatocytes in LKO livers at later time points, particularly at 72 hours (Fig. 14C).

In contrast to relatively mild proliferative programs during postnatal liver development and PH (where each hepatocyte divides 1-2 times to restore the liver mass), we compared hepatocyte proliferation using the Fah liver repopulation model where transplanted donor hepatocytes undergo 9-10 population doublings. We mixed LKO and control hepatocytes in ~equal ratios (Group 1: $LKO^{60\%}$ and $control^{40\%}$) and transplanted mixtures of donor cells into FRGN recipients. Upon completed repopulation, we isolated hepatocytes and determined the degree of chimerism (Fig. 14D). More than 90% of hepatocytes were Fah+, indicating high-level repopulation (Fig. 14E). Since LKO hepatocytes express the β-gal reporter, we then quantified β-gal+ (LKO) and β-gal- (control) cells. The majority of cells were β-gal+ (93%), representing 1.5-fold expansion by LKO hepatocytes during liver repopulation (Fig. 14F and Appendix A Fig. 32A). We also performed

competitive transplants with the donor mixture skewed toward control hepatocytes (Group 2: $LKO^{17\%}$ and $control^{83\%}$) (Fig. 14D). After repopulation, Fah+ donor hepatocytes comprised >90% of the livers (Fig. 14E) and 92% of hepatocytes were β-gal+, representing 5.4-fold expansion by LKO hepatocytes during liver repopulation (Fig. 14F and Appendix A Fig. 32B).

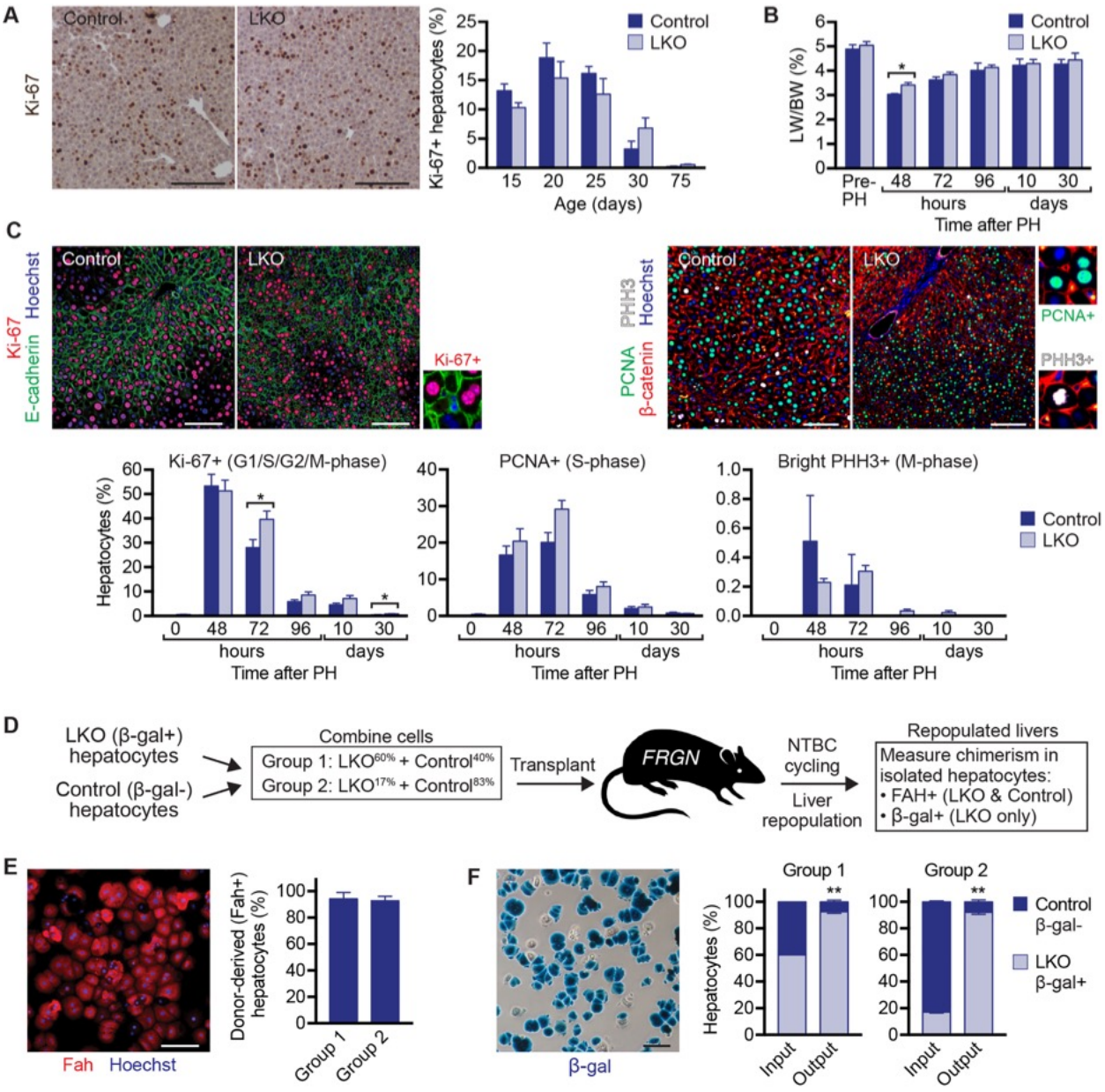

Figure 14. LKO hepatocytes proliferate faster than controls during liver regeneration and repopulation.

(A) LKO and control livers harvested during postnatal development (15, 20, 25 and 30 days) and in adults (75 days), were stained for Ki-67 (brown) as a marker for proliferation (n = 4-5 mice/genotype/age; mixed gender). Representative micrographs are shown for 20-day-old mice (left), and percentage of Ki-67+ hepatocytes is shown for all ages (right). (B-C) Two-thirds PH was performed on 2.5-month-old LKO and control mice to induce liver regeneration. Livers were harvested before PH and at the indicated time points after PH (n=3-8 mice/genotype/age; mixed gender). LW/BW is shown (B). On the left, liver sections were stained with Ki-67 (red), E-cadherin (green, to mark cell membranes) and Hoechst (blue, to mark nuclei). On the right, liver sections were stained with β-catenin

(red, to mark cell membranes), PCNA (green), PHH3 (white) and Hoechst (blue, to mark nuclei). Representative images are shown 48 hours after PH, and magnified insets depict Ki-67+ (G1/S/G2/M-phase), PCNA+ (S-phase) and bright PHH3+ (M-phase) nuclei. The percentage of hepatocytes in each phase of the cell cycle for all time points is indicated (bottom) (C). (D-F) Liver repopulation was compared using competitive transplantation. Hepatocytes from 2.5-month-old male LKO and control mice were mixed in defined ratios and transplanted into FRGN recipients. Group 1 contained 60% LKO and 40% control (n = 5 recipients); Group 2 contained 17% LKO and 83% control (n = 7 recipients). Mice were cycled off/on NTBC for ~3 months to promote expansion of donor cells. Following completed liver repopulation, hepatocytes were isolated and chimerism was determined. Cartoon shows the experimental design (D). Isolated hepatocytes were heterogeneous, containing Fah+ donor cells (LKO and control) and Fah- recipient cells and the degree of repopulation was determined by Fah staining. Representative staining is shown for a repopulated recipient from Group 1 (Fah, red and Hoechst, blue), and the graph shows the percentage of Fah+ cells in each group (E). Hepatocytes were stained with X-gal to visualize β-gal (blue). Representative image is shown for a repopulated recipient from Group 1. The graphs summarize the percentages of β-gal- and β-gal+ hepatocytes at the time of transplant (marked as "input") and after liver repopulation (marked as "output") (F). See Appendix A Fig. 32 for data from individual recipients. * $P < 0.03$, ** $P < 0.001$. Graphs show mean ± sem. Scale bars are 100 μm.

To reconcile the observed cell proliferation differences between LKO and control hepatocytes during liver regeneration and competitive repopulation assays, we performed a modeling analysis. We compared the impact of cell size and proliferation rate on liver volume production, considering rapid proliferation by relatively small LKO hepatocytes and slower proliferation by relatively large control hepatocytes (Fig. 15). Slower-cycling, large control hepatocytes contributed greater cell volume after 1 or 2 cell divisions; but after 3 cell divisions, faster-cycling, small LKO cells generated increased cumulative volume with each successive division. Taken together, the data indicate that LKO hepatocytes are more proliferative than control hepatocytes, especially when induced to divide extensively.

A

Calculations	Group 1 (40:60)		Group 2 (83:17)	
	Control	LKO	Control	LKO
i. Transplanted cells (300K total)	40% (120K)	60% (180K)	83% (249K)	17% (51K)
ii. Estimated number of cells engrafted (10% = 30K)	12K	18K	24.9K	5.1K
iii. Donor-derived cells in repopulated livers	7.5% (2.25M)	92.5% (27.75M)	7.9% (2.37M)	92.1% (27.63M)
iv. Fold expansion	187.5	1542	95.2	5420
v. Population doublings	7.6	10.6	6.6	12.4
vi. Population doubling time (relative units)	13.2	9.4	15.2	8.1
vii. Relative proliferation rate	**1.0**	**1.4**	**1.0**	**1.9**

B

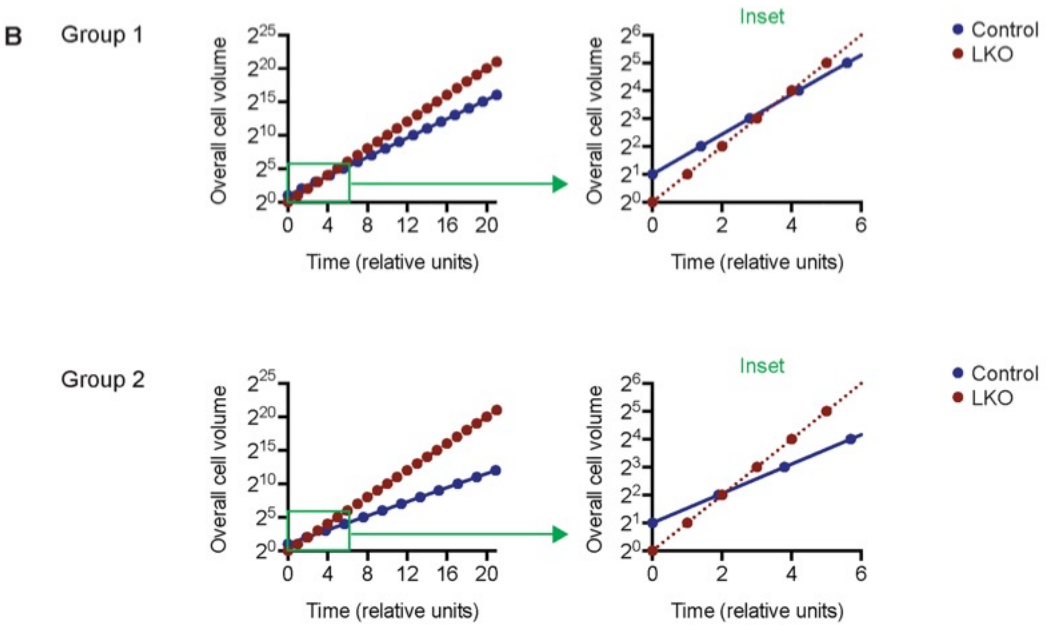

Figure 15. Impact of cell size and cell doubling time during control and LKO hepatocyte proliferation.

(A) Calculation to determine relative population doubling times. (i) In competitive repopulation experiments (Fig. 14D), a total of 300,000 hepatocytes from LKO and control mice were mixed and transplanted into FRGN recipients in defined ratios (Groups 1 and 2). (ii) Approximately 10% of transplanted cells engraft into liver parenchyma (114). (iii) Following complete liver repopulation, engrafted donor cells generate ~30 million hepatocytes. Percentages are derived from Appendix A Fig. 32. (iv) *Fold expansion* represents the fold increase of each cell type during repopulation and was calculated as follows: [# cells in repopulated liver / # engrafted cells]. (v) *Population doublings* refers to the number of doublings required to achieve the indicated fold expansion; calculated as [$\log_2$ (fold expansion)]. (vi) If time to complete repopulation is "100 relative units" and cells proliferate continuously, the *population doubling time* is calculated by [100 / # population doublings]. (vii) *Relative proliferation rate,* calculated as [1 / (doubling time for LKO / doubling time for control)], indicates that LKO population doublings are 1.4 (Group 1) or 1.9 (Group 2) times faster than population doublings by control hepatocytes. (B) Combined effect of proliferative capacity and cell size on production of liver mass. Diploid hepatocytes are smaller than polyploids, and, for simplicity,

it was assumed that LKO hepatocytes (mostly diploid) are half the size of control hepatocytes (mostly polyploid). Two population doubling times are considered, based on observations that population doublings by LKO hepatocytes are 1.4 (Group 1) or 1.9 (Group 2) times faster than population doublings by control hepatocytes. Graphs show the cumulative increase in cell volume over time. Together, the data show that slower cycling and larger control hepatocytes contribute greater cell volume after 1 or 2 cell divisions, but after 3 cell divisions, faster cycling and smaller LKO hepatocytes are more productive, generating increased cumulative volume with each successive division.

2.3.5 WT diploid hepatocytes enter the cell cycle earlier than polyploids during liver regeneration

We next hypothesized that the polyploid state reduces proliferative potential, which enables diploid hepatocytes to proliferate quicker than polyploids. To test this idea, we compared proliferation by WT diploid and polyploid hepatocytes. Specifically, we performed 2/3 PH on 2.5-month-old C57BL/6J WT mice, harvested hepatocytes during liver regeneration and assessed proliferation and ploidy by flow cytometry (Fig. 16A). As expected, hepatocytes were nearly completely quiescent 0-24 hours post PH, but by 36 hours ~60% of hepatocytes were Ki-67+, indicating cell cycle entry. The number of cycling hepatocytes remained high 48 hours after PH (~50%) and decreased by 72-96 hours (Fig. 16B,C). Twenty-eight days after PH most hepatocytes returned to quiescence. The overall distribution of hepatic ploidy subsets was equivalent before (0 hours) and after (28 days) liver regeneration (Fig. 16D).

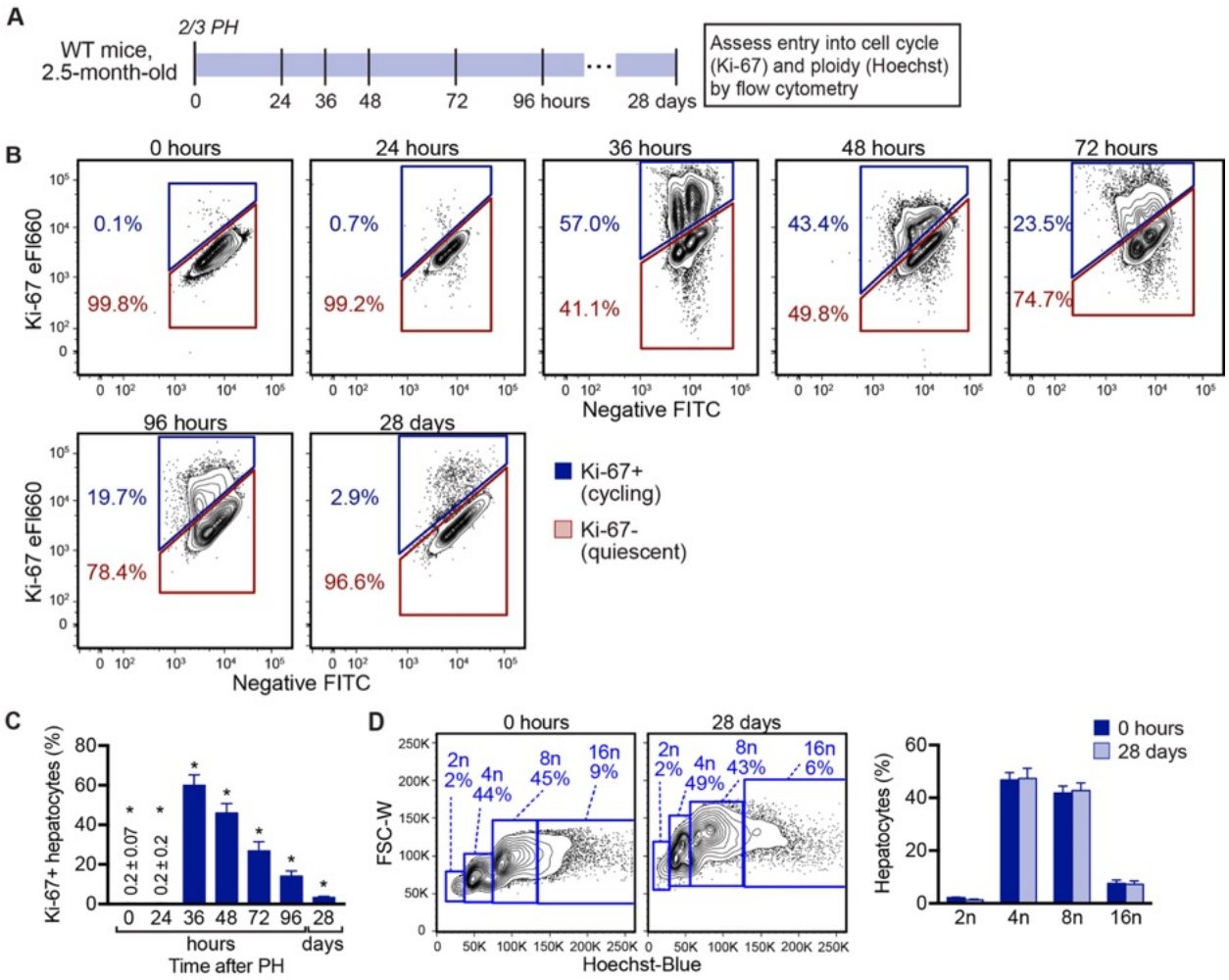

Figure 16. Diploid hepatocytes enter the cell cycle faster than polyploids during liver regeneration.

(A) Experimental design for comparing regeneration by diploid and polyploid hepatocytes. Livers from 2.5-month-old male WT C57BL/6J mice were induced to regenerate by 2/3 PH and hepatocytes isolated during liver regeneration (24-96 hours) and after complete regeneration (28 days). Live hepatocytes were stained for Ki-67 and ploidy. (B) Representative FACS plots show the percentage of Ki-67+ cycling and Ki-67- quiescent hepatocytes during liver regeneration induced by 2/3 PH (24-96 hours) and after complete liver regeneration (28 days) (n = 3-6/time point). (C) The percentage of Ki-67+ cells is indicated (n = 3-6/time point). (D) The ploidy spectrum is equivalent before (0 hours) and after (28 day) liver regeneration. Representative FACS plots are shown for Ki-67- hepatocytes (left) and the percentage of each ploidy population quantified (right, n = 4-5). * $P < 0.05$ in Fig. 16C for comparisons of Ki-67+ hepatocytes between each time point except 36 versus 48 hours and 36 versus 72 hours, which are not significant. Graphs show mean ± sem.

To determine the contribution of each ploidy subset *during* regeneration, we compared ploidy in quiescent and cycling cells. During early-stage regeneration (36-48 hours), ploidy subsets of cycling hepatocytes (Ki-67+) were right-shifted relative to quiescent cells (Ki-67-) in terms of Hoechst intensity (Fig. 17A,B). This increase in nuclear content by each cycling ploidy population indicates transition to S-phase and active DNA replication. In contrast, by late-stage regeneration (72-96 hours), ploidy profiles of cycling hepatocytes were more diffuse, consistent with cells in G1/S/G2/M phases, making it challenging to identify cycling populations with the same DNA content (e.g., cells with 4c DNA content could be diploids in G2 or tetraploids in G0/G1). We focused on early-stage regeneration where we could accurately identify all the ploidy populations. Qualitatively, at 36-48 hours the quiescent subpopulation contained few diploids and was enriched with tetraploid and octaploid hepatocytes. Ploidy distribution shifted markedly in the cycling subpopulation where there were more cycling diploids than quiescent diploids and fewer cycling octaploids than quiescent octaploids (Fig. 17B). We also quantified the percentage of hepatocytes within the quiescent and cycling subpopulations (Fig. 17C). At 36 hours, cycling diploid hepatocytes were increased 3-fold whereas cycling tetraploids, octaploids and hexadecaploids were unchanged or reduced. The trend was even more pronounced at 48 hours, with a 6-fold increase in cycling diploids and ploidy-dependent reduction in cycling cells. Although all hepatocytes proliferate in response to 2/3 PH (59), the data show that entry into the cell cycle is inversely proportional to hepatocyte ploidy. Thus, in response to regenerative stimuli, diploid hepatocytes enter the cell cycle quicker than polyploid hepatocytes.

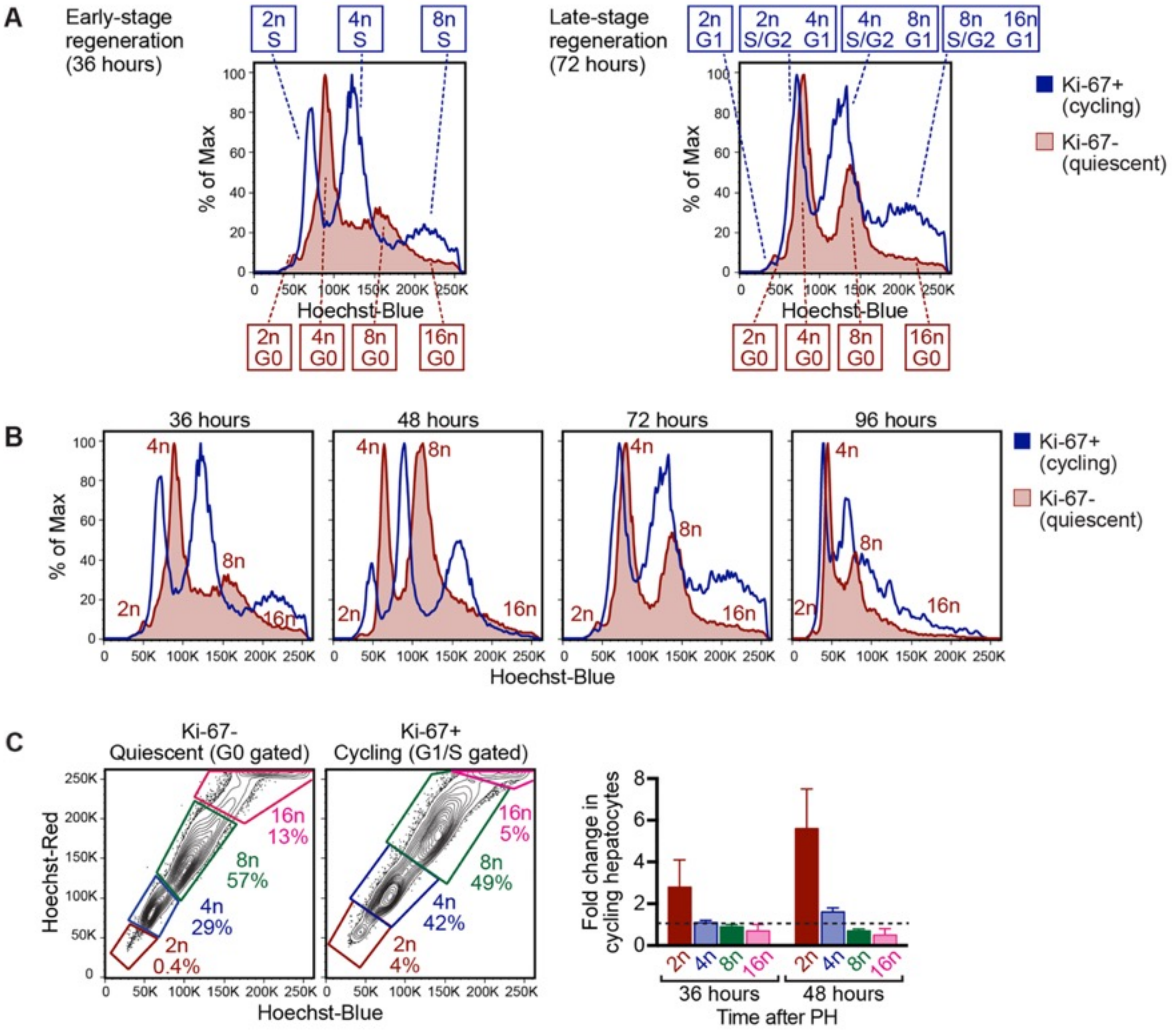

Figure 17. Contributions of ploidy subsets to liver regeneration.

(A) Representative histograms show ploidy overlays of Ki-67+ cycling and Ki-67- quiescent hepatocytes 36 and 72 hours after PH (n = 3-5). The cell population within each peak is annotated. (B) Representative histograms show ploidy overlays of Ki-67+ cycling and Ki-67- quiescent hepatocytes 36-96 hours after PH (n = 3-5). Individual ploidy populations are indicated for quiescent hepatocytes in Fig. 16B. (C) The percentage of each ploidy population was determined for quiescent and cycling hepatocytes during early-stage regeneration at 36 and 48 hours. Gates in the Ki-67- quiescent fraction represent cells in G0; gates in the Ki-67+ cycling fraction represent cells in G1/S. Representative FACS plots are shown at 48 hours (right) and the fold-change in cycling hepatocytes calculated (fold-change = Ki-67+/Ki-67-) for each ploidy population (left, n = 3-4). Dashed line represents fold-change of 1.

2.3.6 WT diploid hepatocytes proliferate faster than polyploids *in vitro*, and ploidy subsets respond to mitogenic signals equivalently

Liver regeneration is regulated by numerous signals that affect initiation, progression and termination of hepatocyte proliferation (134). To confirm our previous findings that diploid hepatocytes enter the cell cycle earlier than polyploids during liver regeneration, we compared proliferation by diploid and polyploid hepatocytes using a simplified culture model. We used hepatocytes from 20-day-old WT mice because, in contrast to adults, most mononucleate hepatocytes at this age are diploid, and nearly all binucleate hepatocytes are tetraploid (Fig. 18A-D). Thus, we quantified mono- and binucleate hepatocytes as a readout for diploid and tetraploid hepatocytes, respectively.

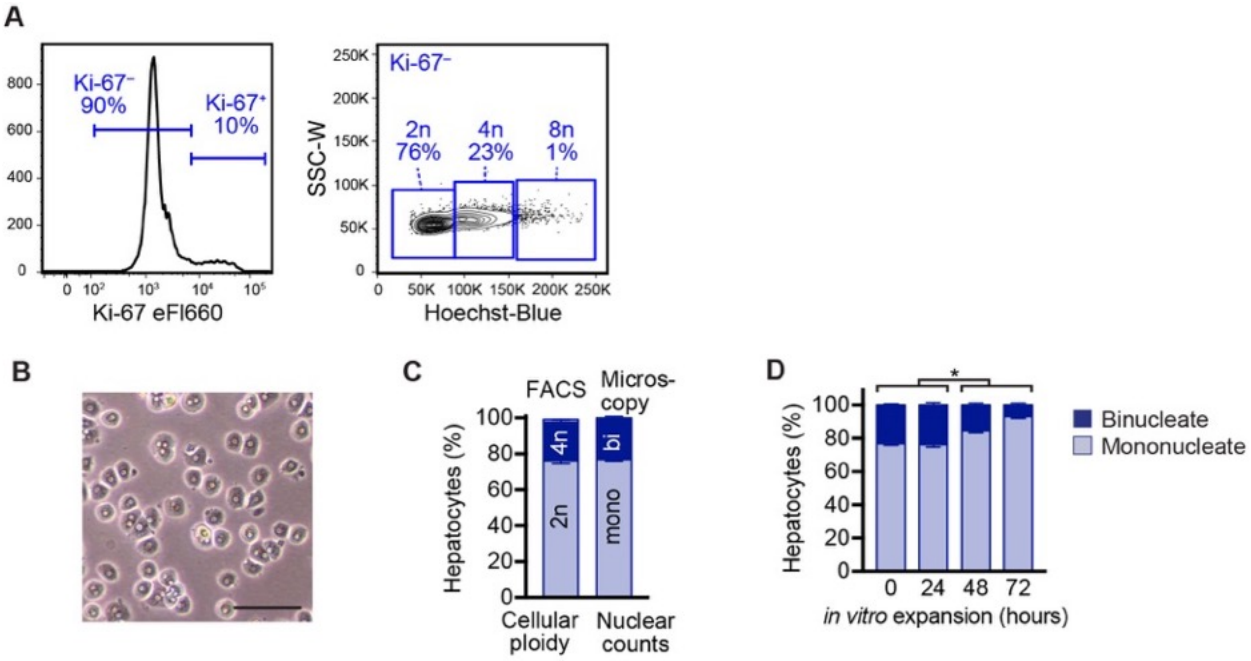

Figure 18. In 20-day-old WT livers, most mononucleate hepatocytes are diploid, and most binucleate hepatocytes are tetraploid.

(A-C) Hepatocytes isolated from 20-day-old mice were analyzed for Ki-67 expression and ploidy using flow cytometry (n = 6). Representative FACS plots are shown (A) and percentage of hepatic ploidy populations is graphed (C). See Fig. 11 for the gating strategy. Hepatocytes were seeded on cell culture dishes and mono- and binucleate hepatocytes were quantified 3-4 hours after attachment (n = 6). Representative micrograph is shown (B), and the percentage of mono- and binucleate hepatocytes is graphed (C). Together, the data show that 76% of quiescent hepatocytes are diploid and 22% are tetraploid; similarly, in terms of nucleation, 77% of hepatocytes are mononucleate and 23% are binucleate. (D) The percentage of mono- and binucleate hepatocytes is indicated throughout the culture period (n = 6). * $P < 0.0005$. Graphs show mean ± sem. Scale bar is 100 μm.

Freshly isolated hepatocytes were cultured for 12-72 hours, and cells in S-phase, G2-phase and undergoing apoptosis were tracked (Fig. 19A). Binucleate hepatocytes started incorporating BrdU at 24-48 hours, and the percentage of BrdU+ cells slowly increased through 72 hours (Fig. 19B). In contrast, mononucleate hepatocytes entered S-phase earlier. Mononucleates incorporated BrdU by 12 hours, and the percentage of BrdU+ cells increased sharply at 24-48 hours and plateaued around 72 hours. In addition to entering S-phase earlier, the number of BrdU+ cells was consistently higher in the mononucleate subset, although the magnitude decreased with time. A similar trend was seen with cells in G2-phase, and the degree of apoptosis was similar for mono- and binucleate cells (Fig. 19C,D). Together with the *in vivo* findings, the data indicate that while all ploidy subsets are proliferative, diploid hepatocytes enter and transit the cell cycle faster than polyploids.

Finally, we wanted to understand the mechanism by which diploid hepatocytes enter the cell cycle and proliferate faster than polyploid hepatocytes. Recently, Kreutz et al. showed that diploid hepatocytes bound insulin with greater affinity than polyploids, suggesting that hepatic ploidy subsets could respond to insulin stimulation in different ways (135). Therefore, we hypothesized that differential growth factor binding by diploid and polyploid hepatocytes could regulate hepatocyte proliferation in a ploidy-specific manner. To test this idea, we stimulated primary hepatocytes with growth factors in serum-free media and compared BrdU incorporation by mononucleate and binucleate hepatocytes (Fig. 19A). We focused on growth factors that have been implicated in liver regeneration, including primary mitogens (HGF, EGF and TGFα) and auxiliary mitogens (insulin, FGF1 and FGF2) (134, 136). In the absence of exogenous growth factors, hepatocytes from 20-day-old WT mice were highly proliferative. Mononucleate hepatocytes entered S-phase 12-24 hours earlier than binucleates, and the percentage of BrdU+

cells was consistently higher (Fig. 19E). As a negative control, we stimulated with PDGF, which is produced by hepatocytes during liver regeneration but acts on stellate cells, and found that S-phase kinetics for mono- and binucleates were equivalent to controls (134). When we treated hepatocytes with mitogens, the number of BrdU+ cells trended upward throughout the culture period (e.g., compare BrdU incorporation for control and growth factor treatment). However, growth factor stimulation induced proliferation by mono- and binucleate hepatocytes to a similar degree, indicating that neither mononucleate nor binucleate hepatocytes responded preferentially (although we cannot exclude the possibility of subtle ploidy-specific effects). Thus, the data indicate the rapid proliferation by diploid hepatocytes is not caused by differential sensitivity to the growth stimuli tested here.

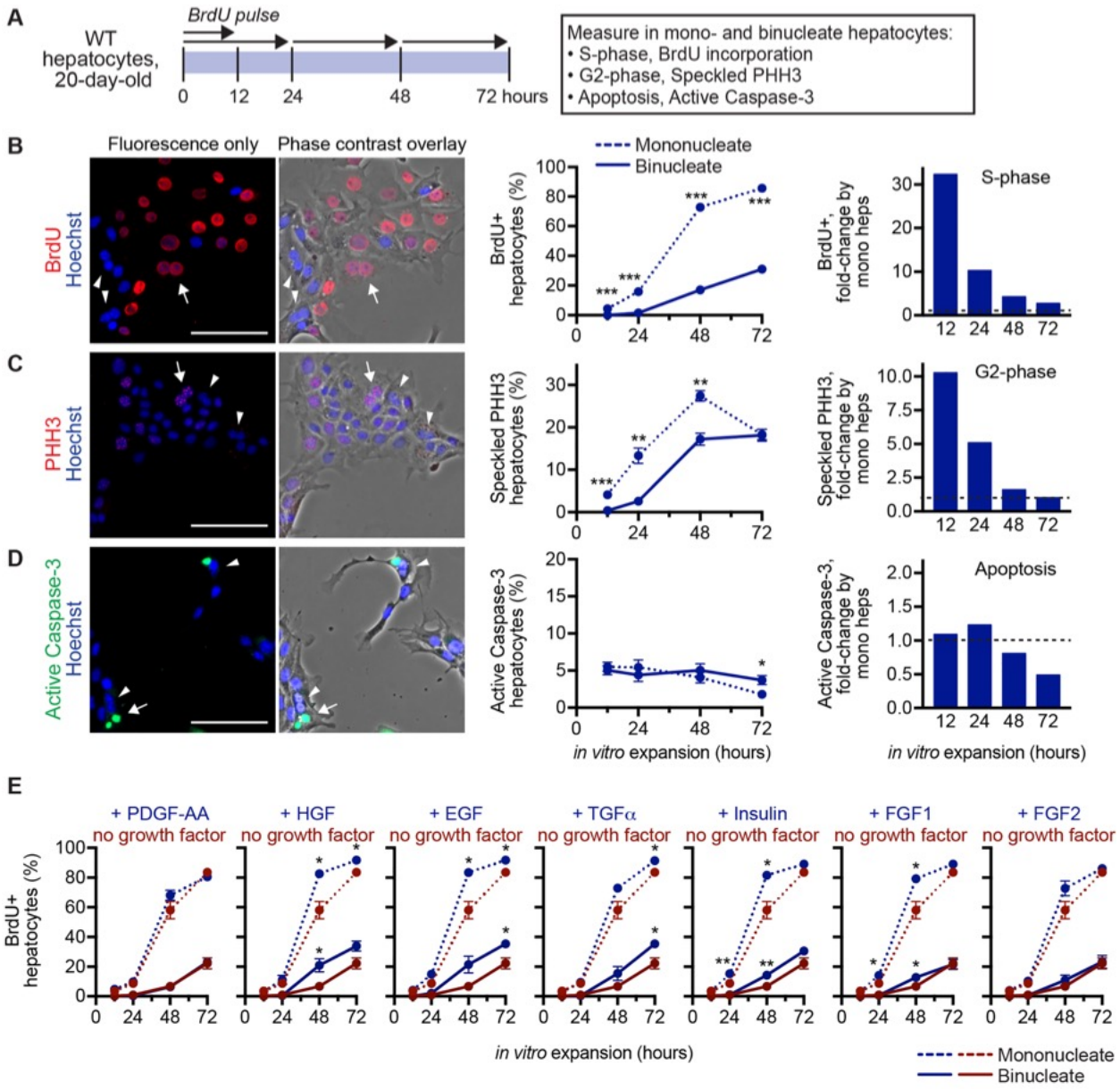

Figure 19. Diploid hepatocytes cycle faster than polyploids *in vitro*.

(A) Experimental design for comparing *in vitro* proliferation by mono- and binucleate hepatocytes. Hepatocytes isolated from 20-day-old WT C57BL/6J mice were cultured in growth media containing 0.5% FBS + 1 µg/ml insulin and harvested after 12, 24, 48 or 72 hours to determine S-phase via BrdU incorporation, G2-phase via speckled PHH3 staining and apoptosis via active caspase-3 staining (n = 2-4 males and 2 females/time point). For BrdU incorporation, cells were pulsed with BrdU for 12 or 24 hours prior to harvest, as indicated. (B-D) Cells were stained for BrdU (red) (B), PHH3 (red) (C) or active caspase-3 (green) (D), and nuclei were stained with Hoechst dye (blue). Representative images after 48 hours in culture show fluorescence only or fluorescence overlaid with phase contrast, which is helpful

for identifying mono- and binucleate cells (left panels). Binucleate cells are indicated with arrows (positive for BrdU, speckled PHH3 or active caspase-3) or arrow heads (negative for BrdU, speckled PHH3 or active caspase-3). Proliferation kinetics for mono- and binucleate hepatocytes are shown (middle panels). Additionally, graphs show the fold-change in positive mononucleate hepatocytes compared to binucleates (right panels). Normalized values for binucleates are indicated with a dashed line. (E) Hepatocytes isolated from 20-day-old WT C57BL/6J mice were cultured in serum-free media alone or with 40 ng/ml PDGF-AA, HGF, EGF, TGFα, FGF1, FGF2 or 1 μg/ml insulin for 12-72 hours (n = 2 males and 1 female/time point). Wells were harvested after BrdU pulse, as described in (A), and stained for BrdU incorporation. Each graph shows the percentage of BrdU+ mononucleate (dashed lines) and binucleate (solid lines) hepatocytes stimulated with (blue) and without (red) growth factor. * $P < 0.05$, ** $P < 0.002$, *** $P < 0.00002$. *P* values in (E) refer to comparisons between each population ± growth factor. Graphs show mean ± sem (B,C,D-middle, E) or mean only (B,C,D-right). Scale bars are 100 μm.

2.4 Discussion

The ability to study diploid and polyploid hepatocyte function *in vivo* is challenging. One reason is that the ploidy state of a hepatocyte can change during proliferation (26). Another reason is that, until recently, there have not been any loss-of-polyploidy genetic models that exhibit normal liver function. In 2012, Pandit et al. and Chen et al. described mice with liver-specific deletion of *E2f7* and *E2f8* and found the mice were depleted of polyploid hepatocytes (31, 32). We used liver-specific *E2f7/E2f8* knockouts (LKO) to further study the effects of polyploidy-deficiency. Consistent with previous findings, LKO mice were functionally equivalent to controls. Most strikingly, diploid hepatocytes were increased 20-fold and LKO hepatocytes remained predominantly diploid even after 500-1000-fold expansion. Thus, LKO mice represent a stable "polyploidy knockout" model for testing the consequences of loss-of-polyploidy *in vivo.*

Herein we compared proliferation by diploid and polyploid hepatocytes. In response to mild proliferative cues during liver postnatal development, LKO and control livers had equivalent numbers of proliferating cells. But, in response to stronger proliferative cues, diploid hepatocytes proliferated faster. This was first seen during liver regeneration induced by 2/3 PH where there was a modest increase in proliferating LKO hepatocytes 3 days post PH and upon completion of liver regeneration. The effect was most pronounced during competitive repopulation when LKO hepatocytes outperformed controls. We also compared proliferation by diploid and polyploid hepatocytes from WT mice *in vitro* and *in vivo.* In the early stages of liver regeneration induced by 2/3 PH, diploid hepatocytes started proliferating sooner than polyploids. Additionally, among polyploid hepatocytes, tetraploids entered the cell cycle faster than octaploids, and octaploids began cycling earlier than hexadecaploids, suggesting that cell cycle entry is inversely proportional to ploidy. Collectively, the data demonstrate that diploid hepatocytes enter the cell cycle earlier and progress through the cell cycle faster than polyploids. Considering that diploid hepatocytes are the minority, representing ≤10% of all hepatocytes in mice (26), it remains to be determined which ploidy population contributes the most during a regenerative response.

At first glance, our current findings appear to conflict with earlier work where we compared repopulation by diploid and octaploid hepatocytes using competitive repopulation (26). In our earlier work, genetically marked WT diploid and octaploid hepatocytes were isolated by FACS and co-transplanted in defined ratios into *Fah*$^{-/-}$ mice. After repopulation, the ratio of diploid-derived and octaploid-derived hepatocytes was equivalent to the ratio that was originally transplanted, indicating equivalent repopulation potential by each group. However, these results were difficult to interpret because the ploidy status of donor cells changed during liver repopulation — diploid hepatocytes became polyploid and octaploid hepatocytes became

tetraploid and diploid. We believe the current work provides a more accurate description of ploidy-dependent hepatocyte proliferation by focusing specifically on diploids and polyploids. Here we show that in response to proliferative cues, diploid hepatocytes enter the cell cycle earlier and progress through the cell cycle faster than polyploids. Taken together, we suggest that, at the level of individual cells (or even during clonal expansion), diploid hepatocytes cycle faster than polyploids. However, during extensive proliferation where diploid and polyploid hepatocytes generate mixed-ploidy daughters, these heterogeneous populations have equivalent proliferative capacity.

The molecular mechanisms by which diploid hepatocytes proliferate faster than polyploids are poorly understood. In 2007, Lu and colleagues compared gene expression between quiescent diploid and tetraploid hepatocytes from mice (54). Surprisingly, very few genes were differentially expressed, and the magnitude of change was small, suggesting that hepatic ploidy subsets are similar at the RNA level. Recently, it was reported that diploid hepatocytes bind insulin more effectively than polyploids, so we tested whether diploid and polyploid hepatocytes could have different responses to hepatic mitogens (135). We stimulated primary WT hepatocytes *in vitro* with growth factors associated with liver regeneration. Each growth factor induced hepatic proliferation, but the response by diploid and polyploid hepatocytes was equivalent, indicating that diploid hepatocytes are not hypersensitive to mitogenic stimulation. New work is necessary to determine how diploid hepatocytes proliferate faster than polyploids. We speculate that cell cycle regulation may be subtly different in diploids than polyploids (e.g., earlier replication licensing, shorter S-phase), which dramatically changes proliferation potential, especially over successive rounds of cell division. Additional mechanistic insights will come from understanding ploidy-

specific proliferation in response to different forms of liver injury and by characterizing the liver microenvironment in this process.

In addition to comparing proliferation between diploid and polyploid hepatocytes in cell culture and during liver regeneration and repopulation, we also examined oncogenic proliferation. LKO livers developed numerous tumors of various sizes, whereas control mice were relatively tumor-free. These results are consistent with a report by Kent, Leone and colleagues where LKO mice spontaneously developed liver tumors during aging and developed more tumors than controls in the DEN tumor induction model (128). A number of mechanisms could explain the sensitivity of LKO mice to liver tumorigenesis. First, the E2F family of transcription factors regulate cell cycle progression, and dysregulated expression could promote oncogenic expansion. E2F8 (deleted in LKO) has been suggested to function as a tumor suppressor, and E2F1 (upregulated in LKO) has been implicated as both a tumor suppressor and oncogene (128, 137). Secondly, the increased tumorigenesis in LKO mice is consistent with our finding that diploid hepatocytes proliferate faster than polyploids. LKO mice are enriched with the most proliferative cells (diploids), and upon tumor initiation, the large number of rapidly cycling diploid hepatocytes in LKO mice drive tumorigenesis. A third mechanism was recently described by Zhang, Zhu and colleagues where they showed that polyploid hepatocytes protect from liver cancer (35). In a series of elegant experiments, polyploid hepatocytes were found to "buffer" against loss of tumor suppressors. Inactivation of one copy of a tumor suppressor in a diploid cell leads to loss-of-heterozygosity and increased potential for transformation. However, in the case of polyploid hepatocytes, the additional sets of chromosomes effectively provide "backup" copies of the tumor suppressor, which reduce the likelihood of transformation. We suggest that the large number of liver tumors in the LKO models arise through a combination of the aforementioned mechanisms.

Notably, hepatocellular carcinomas (HCC) in humans and rodents are comprised predominantly of diploid hepatocytes, which strongly supports the notion that HCC formation is driven preferentially by diploid hepatocytes (62, 63, 138).

In summary, we identified a functional difference between ploidy subsets within the liver (Fig. 20). Diploid hepatocytes enter the cell cycle earlier, progress through the cell cycle faster and proliferate more extensively than polyploids. There are two major implications of this work. First, diploid hepatocytes are prone to tumorigenesis. Whereas polyploid hepatocytes have multiple copies of tumor suppressors that buffer against inactivating mutations (35), diploid hepatocytes with only 2 copies of each tumor suppressor are much more susceptible to mutational events leading to loss-of-heterozygosity. We speculate that the increased proliferative capacity associated with the diploid state promotes rapid expansion by these cells. Secondly, normal aging and liver diseases such as NAFLD, are associated with increased hepatocyte polyploidy and impaired liver regeneration (60, 92). Although polyploid hepatocytes can proliferate, we suggest that their *reduced* proliferative capacity depresses liver regeneration. Moreover, in the context of cell therapy, we hypothesize that transplantation of hepatocytes that are predominantly diploid rather than a mixture of all ploidy populations could facilitate rapid liver repopulation. Overall, we are just beginning to understand the functional roles played by diploid and polyploid hepatocytes, and a major goal for future work is to exploit these differences to develop new approaches for liver therapy.

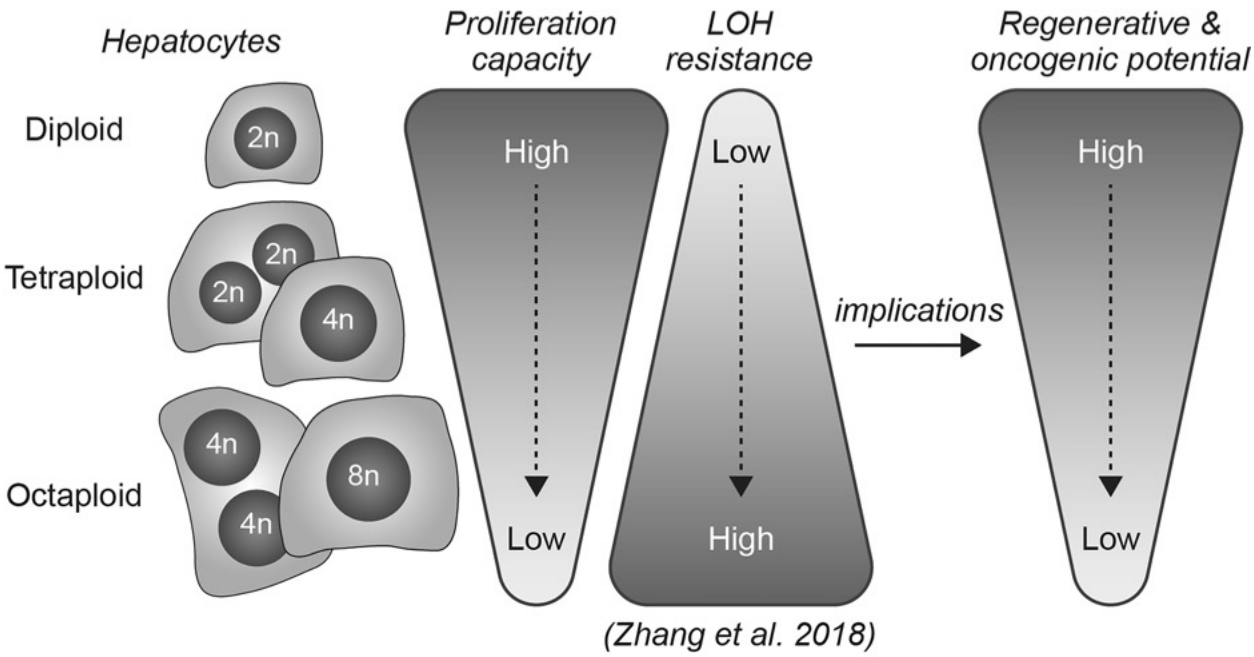

Figure 20. Model illustrating functional differences between diploid and polyploid hepatocytes. Diploid hepatocytes enter the cell cycle earlier and proliferate faster than polyploids, providing diploids with increased capacity for liver regeneration. In terms of liver cancer, diploids are uniquely sensitive to transformation due to tumor suppressor loss-of-heterozygosity (LOH) (35) and, when transformed, they are poised for rapid proliferation.

3.0 Polyploidy in Hepatocyte Aneuploidy and Adaptation to Chronic Liver Injury

Chapter 3 is adapted from one published research manuscript:

Wilkinson PD[1], Alencastro F[1], Delgado ER[1], Leek MP[1], Weirich MP[1], Otero PA[1], Roy N[1], Brown WK[1], Oertel M[1], Duncan AW[1]. Polyploid Hepatocytes Facilitate Adaptation and Regeneration to Chronic Liver Injury. The American Journal of Pathology 2019. 189:1241-1255.

[1] Department of Pathology, McGowan Institute for Regenerative Medicine, Pittsburgh Liver Research Center, University of Pittsburgh, 450 Technology Drive, Suite 300, Pittsburgh, PA 15219.

The liver contains diploid and polyploid hepatocytes (tetraploid, octaploid, etc.), with polyploids comprising ≥90% of the hepatocyte population in adult mice. Polyploid hepatocytes form multipolar spindles in mitosis, which lead to chromosome gains/losses and random aneuploidy. The effect of aneuploidy on liver function is unclear, and the degree of liver aneuploidy is debated, with reports showing aneuploidy affects 5-60% of hepatocytes. To study the relationship between liver polyploidy, aneuploidy and adaptation, we used mice lacking *E2f7* and *E2f8* in the liver (LKO), which have a polyploidization defect. We found polyploids were reduced 4-fold in LKO livers, and LKO hepatocytes remained predominantly diploid following extensive proliferation. Moreover, nearly all LKO hepatocytes were euploid compared to control hepatocytes, suggesting polyploid hepatocytes are required for production of aneuploid progeny. To determine if reduced polyploidy impairs adaptation, we bred LKO mice onto a tyrosinemia background, a disease model where the liver can develop disease-resistant, regenerative nodules. While tyrosinemic LKO mice were more susceptible to morbidities and death associated with

tyrosinemia-induced liver failure, they developed regenerating nodules similar to controls. Analyses revealed that the nodules in the tyrosinemic livers were generated via aneuploidy and inactivating mutations. In summary, we identified new roles for polyploid hepatocytes and demonstrated that they are required for the formation of aneuploid progeny and can facilitate adaptation to chronic liver disease.

3.1 Introduction

Hepatocytes are characterized by variations in polyploidy and aneuploidy. Polyploidy refers to an increase in the number of chromosome sets and, in hepatocytes, is regulated by the number of nuclei per cell (typically 1 or 2) and the DNA content of each nucleus (diploid, tetraploid, octaploid, etc.) (108, 109). At birth, hepatocytes are exclusively diploid, containing 2 copies of each chromosome. During postnatal development in rodents, a subset of proliferating diploid hepatocytes divides by acytokinetic mitosis to generate binucleate tetraploid daughters containing 2 diploid nuclei (25). These daughter cells can then produce a pair of mononucleate tetraploid daughter cells with a round of cell cycling that includes mitosis followed by successful cytokinesis. The cycle of acytokinetic mitosis followed by traditional mitosis continues to generate binucleate and mononucleate octaploids as well as hepatocytes with even higher ploidy (1, 3). More than 50% of adult human hepatocytes are polyploid, and, in adult mice ≥90% are polyploid (22, 26). The polyploid state is also reversible. Proliferating polyploid hepatocytes form multipolar mitotic spindles and, in some cases, cell divisions produce 3 or more daughter cells with reduced ploidy states. Chromosome segregation errors are common during multipolar cell division and lead to random aneuploidy, involving unbiased whole chromosome gains and/or losses (22, 26, 76).

The degree of aneuploidy has been reported to be as low as 5% or as high as 60% in the liver (22, 26, 73, 139). While aneuploidy is strongly correlated with cancer (116, 140), spontaneous liver cancer is extremely rare (141), suggesting that hepatocyte aneuploidy is a normal part of liver homeostasis. Taken together, the adult liver is comprised of a heterogeneous mixture of diploid and polyploid hepatocytes that are either euploid or aneuploid. Despite our understanding of the mechanisms that influence ploidy and aneuploidy in the liver, we are only just beginning to appreciate how these chromosomal alterations affect function and disease.

We previously investigated the role of hepatic aneuploidy in chronic liver injury using *Fah*$^{-/-}$ mice, a model of hereditary tyrosinemia type 1 (78, 81). The *Fah*$^{-/-}$ mouse model has been used in a variety of contexts to study liver function and disease (142, 143). FAH is expressed in the kidney and liver and catalyzes a distal step in the tyrosine catabolic pathway (Fig. 21). Mice lacking FAH accumulate genotoxic intermediates maleylacetoacetate and fumarylacetoacetate in hepatocytes. Cell cycle arrest/death is induced in the hepatocytes, which leads to liver failure and ultimately death of the animal. Blocking the tyrosine pathway upstream of maleylacetoacetate production prevents accumulation of both maleylacetoacetate and fumarylacetoacetate and ameliorates tyrosinemia (82, 144). Treatment with the drug 2-(2-nitro-4-trifluoro- methylbenzoyl)-1,3-cyclo-hexanedione (NTBC), which inhibits the upstream enzyme 4-Hydroxyphenylpyruvate dioxygenase (HPD), prevents liver injury and allows *Fah*$^{-/-}$ mice to be bred and maintained in a healthy state (81). Genetic deletion and inactivation of homogentisate 1,2-dioxygenase (HGD) in the liver has a similar effect (78, 82). In our earlier work, we induced chronic tyrosinemia in *Hgd*$^{+/-}$ *Fah*$^{-/-}$ mice by removal of NTBC. Over 3 months, livers were spontaneously repopulated by subsets of healthy endogenous hepatocytes. These hepatic subsets were resistant to injury via HGD loss-of-function, which provided them with a competitive advantage, compared to injured

hepatocytes, and permitted clonal expansion. It was estimated that half of the regenerating nodules were derived from aneuploid hepatocytes with whole or partial loss of Chromosome 16 (Chr 16), containing the *Hgd* wild-type (WT) locus (78). We, therefore, concluded that aneuploid hepatocytes have the potential to play a major role in liver regeneration and adaptation to long-term injury.

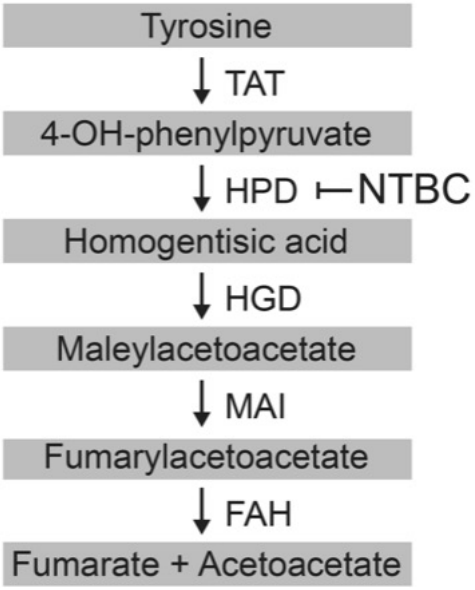

Figure 21. Diagram of the tyrosine catabolic pathway.

Loss of FAH leads to accumulation of fumarylacetoacetate and toxic metabolites. *Fah* deficiency is ameliorated by NTBC treatment or loss of HGD. Abbreviations: tyrosine aminotransferase (TAT); 4-hydroxyphenylpyruvate dioxygenase (HPD); homogentisate 1,2-dioxygenase (HGD); maleylacetoacetate isomerase (MAI); fumarylacetoacetate hydrolase (FAH); 2-(2-nitro-4-trifluoro- methylbenzoyl)-1,3-cyclohexanedione (NTBC).

Transcription factors E2F7 and E2F8, atypical members of the E2F family (145), are highly expressed between weeks 1 and 7 in the developing liver when hepatocyte polyploidization is maximal (32). Recent studies showed liver specific *E2f7/E2f8* double knockout (LKO) mice have a significant reduction of polyploid hepatocytes (31, 32, 146). E2F7 and E2F8 negatively regulate cytokinesis genes, and loss of E2F7 and E2F8 promotes successful cytokinesis of proliferating mononucleate diploid hepatocytes (32). LKO livers have normal development, zonation and function and exhibit normal regeneration and recovery of mass in response to 2/3 partial hepatectomy (32, 146). Moreover, LKO livers respond to DDC diet (32) and high fat diet (146) similar to control mice. It has also been shown that livers deficient in *E2f7* and/or *E2f8* have increased susceptibility to spontaneous tumorigenesis and DEN-induced liver cancer (35, 128,

146). Strikingly, hepatocytes from LKO mice are more proliferative in culture and during liver repopulation and partial hepatectomy-induced regeneration. The increased proliferation of LKO hepatocytes is predominately due to the enriched diploid phenotype as corresponding studies with WT mice demonstrated that diploids are more proliferative than polyploid hepatocytes (146). Since LKO livers are functionally normal and exhibit increased proliferation consistent with diploid enrichment, LKO mice are a robust "polyploidy knockout" model that can be used to study how loss of polyploidy affects liver aneuploidy and adaptation.

It has been challenging to determine if diploid and polyploid hepatocytes have similar roles in liver function and homeostasis because hepatocytes readily increase or decrease their ploidy. Here, we utilized LKO mice to investigate the role of diploids and polyploids in chronic liver injury. In agreement with previous studies, we found that LKO livers have a significant reduction in polyploid hepatocytes (31, 32, 146) and remain predominantly diploid following extensive liver repopulation . Additionally, cytogenetic studies revealed that LKO hepatocytes are mostly euploid, unlike control hepatocytes which are highly aneuploid with chromosome gains/losses occurring in a widespread and unbiased fashion. To test the idea that reduced polyploidy and aneuploidy in LKO mice would impair their ability to adapt to environmental stress, we bred LKO mice onto the $Hgd^{+/-}$ $Fah^{-/-}$ background and withdrew NTBC to induce tyrosinemia (78, 82). Survival was significantly reduced in tyrosinemic LKO mice, compared to controls, but they maintained the ability to form regenerative nodules. Overall, we identify new roles for polyploid hepatocytes — they are required for the formation of aneuploid progeny and are essential mediators that promote adaptation to chronic liver disease.

3.2 Methods

3.2.1 Mouse strains

The Institutional Care and Use Committee of the University of Pittsburgh approved all of the experiments using mice. Optimice cages (AnimalCare Systems, Centennial, CO) with Sani-Chip Coarse bedding (P. J. Murphy, Montville, NJ) were used for housing the mice, which were provided *ad libitum* access to water and standard mouse chow (LabDiet, St. Louis, MO, Purina ISO Pro Rodent 3000) in a standard 12-hour light and 12-hour dark cycle. Huts and running wheels were provided for enrichment. All animals were sacrificed between 9 am and noon daily. *E2f7/E2f8* liver-specific knockout mice (LKO) were a kind gift from Alain deBruin and Gustavo Leone (31, 32). LKO mice, which were a mixed background but predominantly FVB, contained floxed E2f7 and E2f8 alleles, a Rosa26-*lacZ* reporter (R26R-*lacZ*) and Cre recombinase driven by the albumin promoter (Alb-Cre): $E2f7^{loxP/loxP}$ $E2f8^{loxP/loxP}$ $R26R^{lacZ/lacZ}$ $Alb\text{-}Cre^{Tg/0}$. Control mice were negative for Alb-Cre: $E2f7^{loxP/loxP}$ $E2f8^{loxP/loxP}$ $R26R^{lacZ/lacZ}$. FRGN mice ($Fah^{-/-}$ $Rag2^{-/-}$ *Interleukin 2 common Gamma chain*$^{-/-}$ Nod background) were used for liver repopulation flow cytometry and cytogenetic studies (Yecuris, Inc., Tualatin, OR) (112, 113). $Hgd^{+/-}$ $Fah^{-/-}$ mice were acquired from Markus Grompe (78) and bred with the *E2f7/E2f8* liver-specific control and knockout mice to generate T-control and T-LKO mice, respectively. T-control, T-LKO and FRGN mice were maintained on 8 mg/l NTBC in their drinking water (Ark Pharm, Libertyville, IL). Male mice were used for experiments unless otherwise stated.

3.2.2 Hepatocyte isolation

Primary hepatocytes were isolated using a 2-step collagenase perfusion (114). Briefly, following general anesthesia induction, a catheter was inserted into the portal vein or inferior vena cava and 0.3 mg/ml collagenase II (Worthington, Lakewood, NJ) was circulated through the liver. Collagenase-digested livers were placed in DMEM-F12 with 15 mM HEPES (Corning, Corning, NY) + 5% FBS (Sigma-Aldrich, St. Louis, MO), filtered with a 70 μm cell strainer and washed twice using low-speed centrifugation (55g for 2 min.) to remove non-parenchymal cells. Hepatocyte viability, determined by trypan blue staining, was typically >80%. Hepatocytes from FRGN transplantation recipients were isolated as described above, except the collagenase II concentration was increased to 1 mg/ml.

3.2.3 Ploidy analysis

To identify hepatocyte ploidy populations, primary hepatocytes were isolated via 2-step collagenase perfusion, washed with PBS, adjusted to a density of 1-2 million cells/ml and incubated on ice with 2 μl/ml Fixable Viability Dye (FVD) eFluor 780 (eBioscience, San Diego, CA; 65-0865). Following 2 PBS washes, hepatocytes were fixed with 2% PFA, washed an additional 2 times with PBS and incubated with permeabilization buffer (0.1% saponin and 0.5% BSA in PBS) + 15 μg/ml Hoechst 33342 (Life Technologies, Carlsbad, CA; H3570). Cells were then washed twice and stored in PBS until flow cytometry analysis.

Ploidy populations are indicated with *chromatid number* "c" (2c, 4c, 8c). We used *chromatid number* in Fig. 22, Fig. 23 and Fig. 26 because a mixture of quiescent and proliferating

cells comprises the gated cells, even though >99% of adult hepatocytes in mice are quiescent (e.g., a 4c cell is either a diploid in G2/M-phase or a tetraploid in G0/G1-phase).

3.2.4 Liver repopulation using LKO or control hepatocytes

Primary hepatocytes were isolated from 4-month-old male control and LKO mice using a 2-step collagenase perfusion. 300,000 control or LKO donor (FAH^+) hepatocytes were injected into the spleens of 2-month-old female FRGN (FAH^-) recipients. The transplanted FRGN mice were maintained on 8 mg/l NTBC for 4 days following transplantation, and then cycled on/off NTBC for several cycles to stimulate donor cell (FAH^+) expansion. Hepatocytes were isolated from repopulated mice, those whose body weight had stabilized to ~100% of the initial weight, using a 2-step collagenase perfusion as previously described. To identify donor cells, the isolated hepatocytes were washed with PBS, adjusted to a density of 1-2 million cells/ml and incubated on ice with 2 µl/ml Fixable Viability Dye (FVD) eFluor 780. Following 2 PBS washes, cells were incubated with rabbit anti-FAH primary antibody (a gift from Markus Grompe), washed twice with permeabilization buffer (0.5% Saponin in PBS), and incubated with donkey anti-rabbit PE secondary antibody (Ebioscience; 12-4739-81). Following 2 washes in permeabilization buffer, cells were incubated with permeabilization buffer + 15 µg/ml Hoechst 33342, washed again with permeabilization buffer and stored in 0.5% BSA in PBS until flow cytometry analysis.

3.2.5 Cytogenetics

LKO or control hepatocytes from adult mice or fully repopulated FRGN recipients were isolated using a 2-step collagenase perfusion. As >99% of hepatocytes in adult livers are quiescent,

the freshly isolated cells were not actively proliferating. To induce proliferation 300,000 viable cells were seeded in 10-cm Primaria Cell Culture dishes (Corning) in seeding media: DMEM-F12 with 15 mM HEPES (Corning), 5% FBS (Atlanta Biologicals, Atlanta, GA) and Antibiotic-Antimycotic Solution (Corning). After 4 hours, seeding media was replaced with growth media: DMEM-F12 with 15 mM HEPES (Corning), 0.5% FBS (Atlanta Biologicals), Antibiotic-Antimycotic Solution (Corning) and ITS Supplement (containing 1 µg/ml insulin, 0.55 µg/ml transferrin and 0.67 ng/ml sodium selenite; Gibco Life Technologies). Primary mouse hepatocytes are highly proliferative *in vitro* under these and similar conditions as demonstrated through live cell imaging, BrdU incorporation and cyclin gene expression (26, 27, 92, 146). After 44 hours in culture, KaryoMAX Colcemid^{TM} solution (30 ng/ml) was added to the media for 3 hours to arrest dividing cells in metaphase. Proliferating cells must be arrested in metaphase to perform G-banding chromosome staining. Following metaphase arrest, the cells were trypsinized, washed in PBS, incubated in pre-warmed hypotonic swelling solution (56 mM KCl in 5% FBS) for 10 min. and fixed in methanol/acetic acid (3:1 ratio). For each mouse, chromosome G-band staining and karyotype preparation were performed on 14-20 metaphase arrested hepatocytes using a standard trypsin/Wright's staining protocol by the Oregon Health and Science University. For each cell karyotyped, the overall aneuploidy status was determined and all chromosome gains, losses and other abnormalities (deletions, inversions, etc.) were noted.

3.2.6 NTBC cycling

T-control and T-LKO mice were maintained on 8 mg/l NTBC until age 2 to 3 months, at which time it was withdrawn. To induce partial liver repopulation, mice were cycled off NTBC for 1-2 weeks and placed on NTBC for 5 days for approximately 2 to 3 periods. Livers were

harvested from T-control and T-LKO mice when the mice dropped below 80% body weight and expressed high morbidity that could not be improved with placement back on NTBC.

3.2.7 General processing of paraffin embedded tissue

Livers from mice were isolated, fixed in 10% neutral buffered formalin (NBF), embedded in paraffin and sectioned at a thickness of 4 μm. Sections were deparaffinized using xylene and graded ethanol (100-95%) washes and incubated in citric-acid based antigen retrieval (Vector, Burlingame, CA).

3.2.8 Immunofluorescence staining

Following paraffin embedding, sectioning and antigen retrieval, liver sections were stained with Ki-67 and β-catenin to identify regenerating nodules and quantify the mono- and binucleate hepatocytes within the nodules and surrounding tissue. Liver sections were blocked with 2% BSA and stained with rabbit anti-Ki-67 primary antibody (Abcam Cambridge, MA; ab15580) and mouse anti-β-catenin primary antibody (Santa Cruz; sc-7963) followed by species-specific secondary antibodies: goat anti-rabbit AlexaFluor 594 and goat anti-mouse AlexaFluor 488 secondary antibody (both from Life Technologies; A11012 and A11029). The sections were counterstained with Hoechst 33342 to visualize nuclei and mounted with Fluoromount-G (Southern Biotech). A minimum of 100 hepatocytes/sample was counted to determine the percentage of mono- and binucleate hepatocytes in the nodules and surrounding tissue.

3.2.9 Immunohistochemistry

To identify regenerating nodules, tissue sections were first stained for Ki-67 (G1/S/G2/M-phases) as regenerating nodules contained proliferating hepatocytes. Following antigen retrieval, deparaffinized tissue sections were treated with 3% hydrogen peroxide to quench endogenous peroxidase and blocked with Avidin/Biotin blocking solution (Vector SP-2001). Sections were stained with rabbit anti-Ki-67 primary antibody (Abcam; ab15580) followed by biotinylated goat anti-rabbit secondary antibody (Vector; BA-1000) and Avidin-conjugated peroxidase (Vector ABC kit; PK-6100); staining was visualized with ImmPACT DAB Peroxidase Substrate (Vector; SK-4105). Sections were counterstained with hematoxylin, dehydrated with ethanol and xylene washes and mounted with Permount (Fisher). Regenerating nodules were also identified with Hematoxylin and Eosin (H&E) staining, which was performed by the Development Laboratory in the University of Pittsburgh Department of Pathology.

3.2.10 Laser capture microdissection

For laser capture microdissection (LCM), livers were harvested, washed in PBS and frozen. Tissues were cut at a thickness of 8 μm, and individual nodules were isolated directly from unstained tissue sections using an LMD 6500 laser microdissection system (Leica Microsystems, Buffalo Grove, IL) (147).

3.2.11 DNA and RNA isolation and PCR

Total DNA and RNA were extracted from LCM-isolated nodules using an AllPrep DNA/RNA Micro Kit (Qiagen, Germantown, MD). The *Hgd* genotype of the nodules was determined by performing an *Hgd* genotyping PCR reaction (94°C x 3 min.; 45 cycles of 94°C x 30 sec., 56°C x 30 sec., 72°C x 45 sec.; Final extension 72°C x 7 min.) on the total DNA using the forward primer 5'-TTTAGTCGCTGCATCACC-3' and reverse primer 5'-CATTTTCACCGTGCTGAC-3', incubating the PCR product with the restriction enzyme HpyCH4III (Fisher) for 4 hours at 37°C and then running the digested products on a 4% agarose gel. The restriction enzyme HpyCH4III cuts the 290 bp PCR product from the WT allele to generate fragments that are 170 bp and 120 bp long, but the KO allele has a one base mismatch at the HpyCH4III recognition site that prevents cleavage. Therefore, nodules that produce 3 bands following enzyme digestion (290 bp, 170 bp and 120 bp) were considered $Hgd^{+/-}$, and nodules that had lost the *Hgd* WT allele produced a single 290 bp band and were considered *Hgd* null ($Hgd^{-/-}$) (78, 82).

For *Hgd* transcript analysis, total RNA was reverse-transcribed into complementary DNA (cDNA) using Iscript™ Reverse Transcription Supermix (BioRad, Hercules, CA), and a nested PCR reaction was performed to determine the presence or absence of full length and splice variant *Hgd* transcripts in individual nodules. Briefly, the cDNA was run in the first PCR reaction (94°C x 5 min.; 20 cycles of 90°C x 30 sec., 62°C x 30 sec., 72°C x 1 min.; Final extension 72°C x 10 min) using the forward primer 5'-TTTGAGGAGACCAGGGGCTA-3' and reverse primer 5'-TCAATTACAGTAGAGGGCTCCAGTC-3', and following a 50-fold dilution, subjected to a second PCR reaction (94°C x 5 min.; 40 cycles of 90°C x 30 sec., 62°C x 30 sec., 72°C x 1 min.; Final extension 72°C x 10 min.) using the forward primer 5'-

GCCTGGTATGAAGATCGTCGAG-3' and reverse primer 5'-TCAATTACAGTAGAGGGCTCCAGTC-3'. The final products of the second PCR were analyzed on a 2% agarose gel. The *Hgd* WT allele produces a full-length (FL) transcript corresponding to a 665 bp PCR product. The point mutation within the *Hgd* KO allele produces shorter splice variants (SV) approximately 350 bp and 500-550 bp in length that form truncated and defective proteins (82, 148). The nodules were classified based upon their *Hgd* genotype ($Hgd^{+/-}$ or $Hgd^{-/-}$) in combination with their *Hgd* transcript profile (FL only, FL + SV or SV only).

3.2.12 Flow cytometry

All FACS analyses were performed with a FACS Aria II-SORP (BD Biosciences) equipped with a 130 μm nozzle and running DiVa v8.0.2 software. FACS plots were generated using FlowJo 9.9.6 (Treestar, Ashland, OR).

3.2.13 Microscopy

Fluorescent images were acquired with a Nikon TiU fluorescent microscope equipped with a monochrome camera. Non-fluorescent images were acquired with a Nikon TS100 microscope equipped with a color camera. Gross morphology images were taken using a Nikon D3100 DSLR Digital Camera with 18-55mm f/3.5-5.6 Auto Focus-S Nikkor Zoom Lens. Images were processed with Nikon NIS Elements Basic Research 4.13.00, Nikon NIS Elements Freeware 4.00.00, NIH ImageJ 1.49 and Adobe Photoshop CC 20.0.2.

3.2.14 Statistical analysis

Statistical significance was calculated by GraphPad Prism 7.0.a or Microsoft Excel 16.16.6 using 2-tailed Student's *t* test except for the Kaplan-Meier curve (Fig. 26E) where a log-rang (Mantel-Cox) test was performed. *P* values < 0.05 were considered significant.

Additional methods can be found in **Appendix B (page 139)**.

3.3 Results

3.3.1 Livers deficient for *E2f7* and *E2f8* are depleted of polyploid hepatocytes

To confirm the reduced-polyploidy phenotype in mice lacking E2F7 and E2F8, we obtained liver-specific knockout (LKO) mice containing floxed *E2f7*, floxed *E2f8* and a Rosa26-*lacZ* reporter (R26R-*lacZ*) (31, 32). Genes were specifically deleted in LKO livers via Cre recombinase driven by the liver-specific Albumin promoter (Alb-Cre) (149). Cre activity is highly efficient as indicated by expression of the β-galactosidase reporter in LKO hepatocytes and its absence in control cells (Fig. 22A). Hepatocytes were isolated by 2-step collagenase perfusion, stained with the viability marker FVD-780 and loaded with the DNA dye Hoechst 33342. Since >99% of adult hepatocytes are quiescent, cell cycle analysis by flow cytometry provides a precise readout of cellular ploidy. Consistent with previous observations, livers from LKO mice at 3-4 weeks and at 4 months were enriched with diploid hepatocytes and depleted of polyploids (Fig. 22B-D) (31, 32, 146). For example, 4-month-old LKO livers contained 73.0 ± 1.8% diploids, 18.8

± 0.4% tetraploids and 3.2 ± 1.3% octaploids, while control livers contained 6.1 ± 0.6% diploids, 62.4 ± 4.0% tetraploids and 21.7 ± 5.6% octaploids (Fig. 22C).

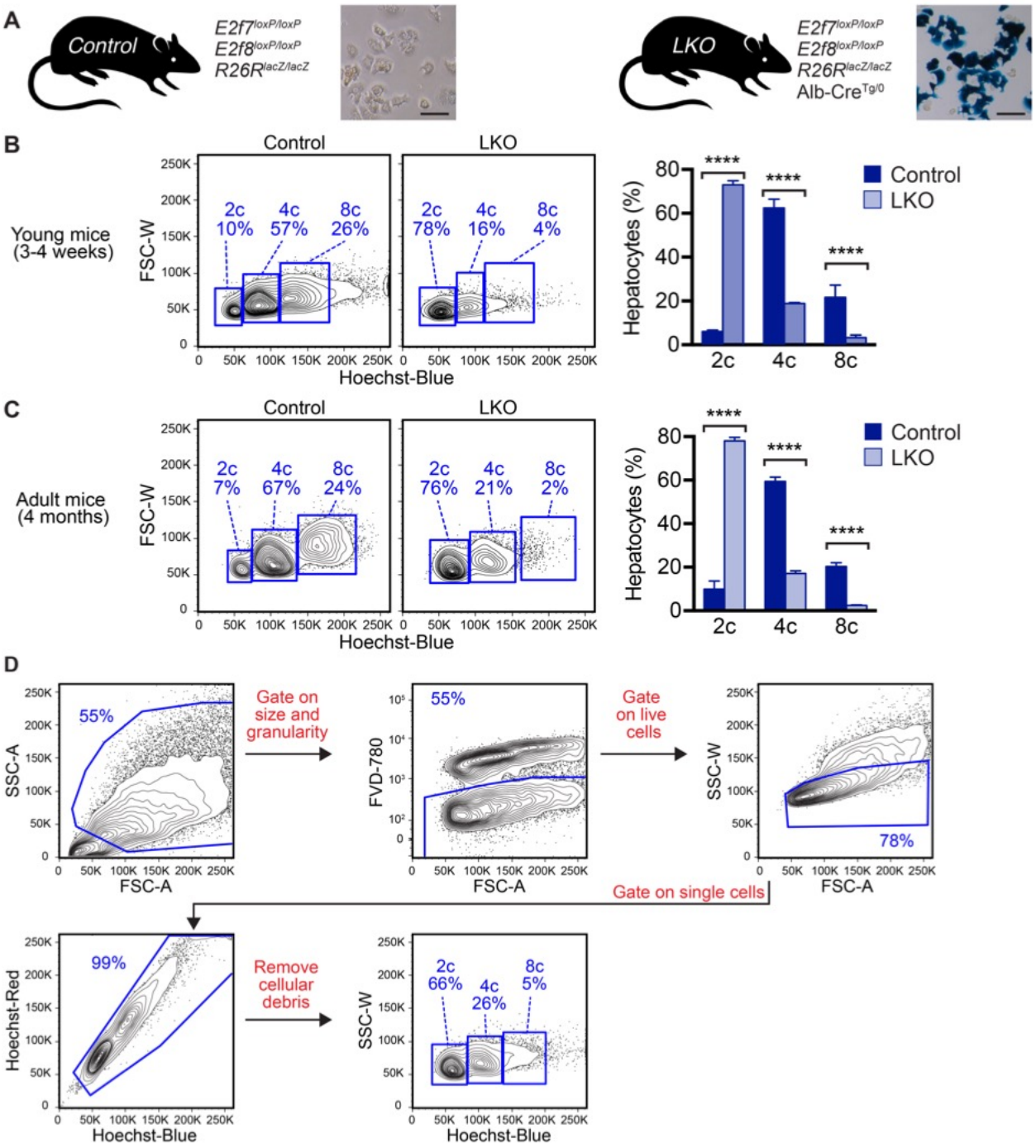

Figure 22. Diploid hepatocytes are increased and polyploid hepatocytes are depleted in *E2f7/E2f8*-deficient livers. (A) Control mice contain floxed alleles of *E2f7/E2f8* and an R26R-*lacZ* reporter but do not contain Cre recombinase. *E2f7/E2f8* liver-specific knockout mice (LKO) also contain Alb-Cre, a liver-specific driver of Cre, which deletes *E2f7/E2f8* and activates the reporter in the liver. Hepatocytes isolated from 2.5-month-old control and LKO livers (n = 3 per genotype) were stained with X-gal, a substrate for β-galactosidase (blue). The presence of blue hepatocytes

confirms Cre expression in LKO livers. (B,C,D) Hepatocytes isolated from control and LKO male mice were stained with the viability dye FVD-780 and the nuclear dye Hoechst. The distribution of live hepatic ploidy populations is shown for 3-4-week-old mice (n = 4-7 per genotype) and 4-month-old adult mice (n = 4 per genotype). Diploid (2c), tetraploid (4c) and octaploid (8c) hepatocytes are indicated on representative flow cytometry plots (left), and the percentage of each population is summarized (right) (B,C). The FACS gating strategy for identification of hepatic ploidy populations is shown. Cells were gated on the basis of size/granularity and viability. Subsequently, single cells were selected and cellular debris removed. Hepatic ploidy populations were determined by separating the cells based on incorporation of Hoechst using the Hoechst-blue channel. Ploidy populations are marked with chromatid number "c" since they contain a mixture of cycling and quiescent cells (although >99% are quiescent). Representative FACS plots are shown for a 4-month-old LKO mouse (D). **** $P < 0.0001$. Graphs show mean ± sem.

To determine if the diploid-enriched phenotype in LKO mice remained stable during liver repopulation, we utilized the FAH repopulation model where transplanted donor cells can expand 500-1000-fold (114). We isolated hepatocytes from control or LKO mice that are FAH^+ and transplanted cells into *Fah*$^{-/-}$ recipients (Fig. 23A). Since control and LKO mice are a mixed background, we used immune-deficient recipients (termed "FRGN" for *Fah*$^{-/-}$ *Rag2*$^{-/-}$ *Interleukin 2 common Gamma chain*$^{-/-}$ Nod background) to prevent graft rejection (112, 113). Four days after transplantation, NTBC was withdrawn to promote proliferation of donor hepatocytes. When the body weight dropped to 80%, the mice were provided NTBC for 5 days and NTBC was subsequently removed again. After several rounds of NTBC cycling (approximately 3 months), livers maintained 100% of body weight in the absence of NTBC, an indicator of complete liver repopulation. FAH^+ control and LKO donor hepatocytes had a survival advantage over the FAH^- FRGN host hepatocytes and were able to proliferate and repopulate host livers over the course of NTBC withdrawal. Following liver repopulation, hepatocytes were isolated from the repopulated livers and analyzed for ploidy. To determine the ploidy distribution of donor-derived hepatocytes

we isolated hepatocytes from repopulated livers and stained for FAH (expressed only by donor cells), FVD-780 and Hoechst. We specifically analyzed the ploidy of FAH^+ donor-derived hepatocytes. Repopulated livers contained ~75% FAH^+ cells, indicating high-level repopulation (Fig. 23B). Similar to the ploidy distribution seen in adults, LKO hepatocytes were predominantly diploid and depleted of polyploid hepatocytes (Fig. 23C). Thus, the diploid-enriched phenotype in LKO mice is stable during normal aging and liver repopulation.

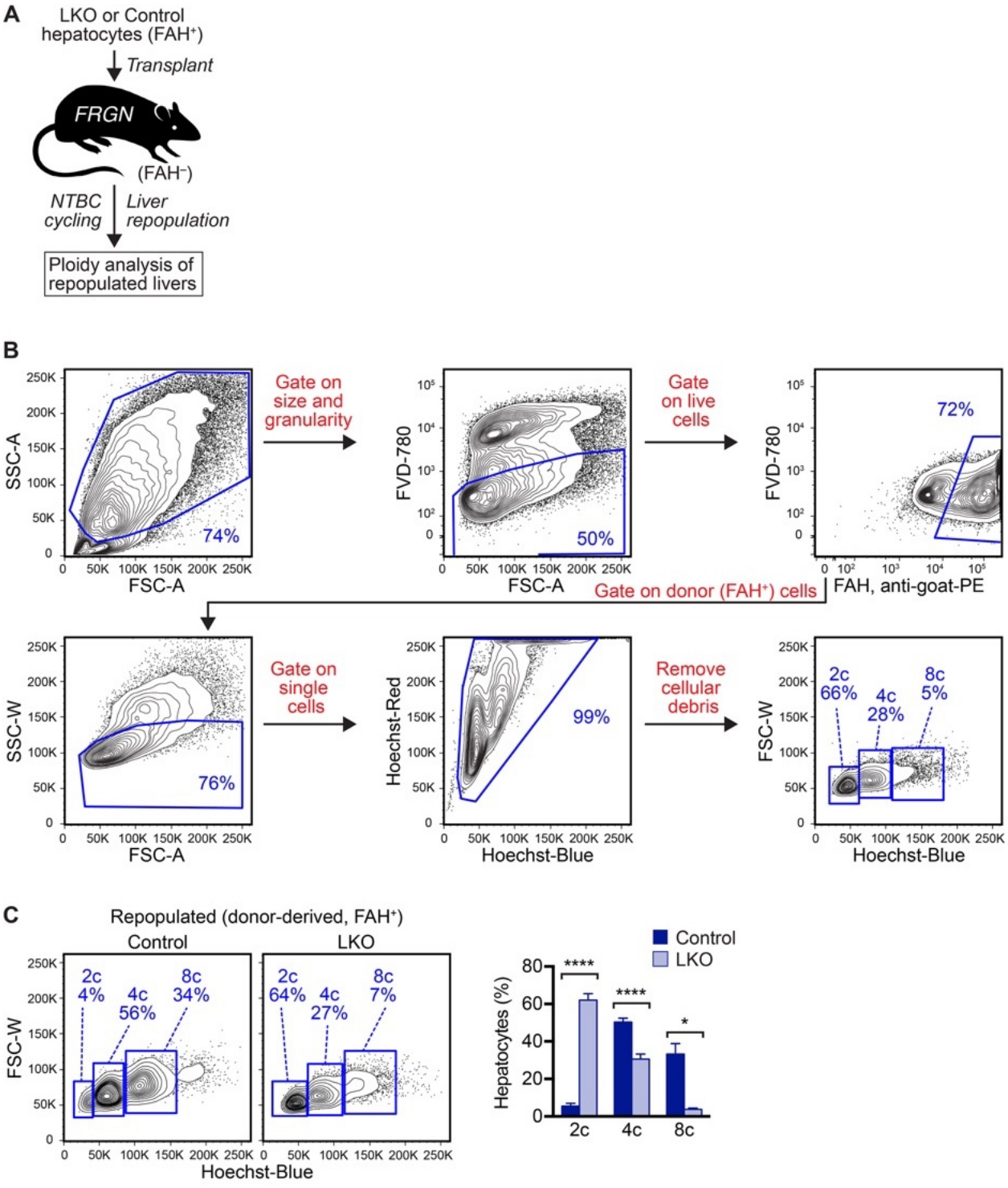

Figure 23. Hepatocytes from *E2f7/E2f8*-deficient livers remain predominantly diploid during extensive *in vivo* proliferation.

(A) Approximately 300,000 hepatocytes from control and LKO mice (males, 4 months old) were transplanted into FRGN recipient mice (females, 2 months old) and subjected to NTBC cycling to promote liver repopulation by

transplanted donor cells. Following completed repopulation, livers containing a mixture of FAH^+ donor hepatocytes and FAH^- host hepatocytes were isolated and stained with FVD-780, Hoechst and FAH antibody (donor marker). (B) Cells were first gated on the basis of size/granularity and viability. Single cells were then selected and cellular debris removed. Donor-derived cells (FAH^+) were selected and hepatic ploidy populations determined. Representative FACS plots are shown for an FRGN mouse repopulated by LKO hepatocytes. (C) The distribution of hepatic ploidy populations of live FAH^+ donor-derived hepatocytes from mice repopulated with control (n = 4 repopulated mice) or LKO (n = 4 repopulated mice) hepatocytes are shown in representative flow cytometry plots and summarized in the graph. * $P < 0.05$, **** $P < 0.0001$. Graph shows mean ± sem.

3.3.2 *E2f7/E2f8*-deficient livers have reduced aneuploidy and are enriched with euploid hepatocytes

Proliferating polyploid hepatocytes undergo chromosome segregation errors to generate aneuploid daughter cells that have gained/lost ≥1 chromosomes (22, 26). We rationalized that LKO hepatocytes, which are depleted of polyploids, would also have fewer aneuploid cells. To test this idea, we isolated hepatocytes from 4-month-old control and LKO mice and karyotyped individual hepatocytes using standard metaphase cytogenetic analysis. Briefly, freshly isolated hepatocytes were cultured for 44 hours and treated with colcemid to arrest proliferating cells in metaphase. Subsequently, metaphase spreads were prepared and chromosomes visualized by G-banding. Consistent with ploidy analysis by flow cytometry, the majority of control hepatocytes were tetraploid or near-tetraploid with ~80 chromosomes, while diploid or near-diploid hepatocytes with ~40 chromosomes were uncommon (Fig. 24A,B). Aneuploid hepatocytes were identified by the presence or absence of chromosomes, leading to chromosome numbers close to, but not exactly, 40, 80 or 160 (Fig. 24B). Aneuploid hepatocytes with a balanced number of gains and losses were also detected. For example, Figure 24A shows a karyogram for a tetraploid control

hepatocyte containing 80 chromosomes with 4 homologues of most autosomes; however, this cell contains 3 homologues of chromosomes 3 and 17 (indicating chromosome losses) and 5 homologues of chromosomes 5 and 13 (indicating chromosome gains). As a whole, chromosome losses outnumbered chromosome gains, and all chromosomes were affected, which is consistent with the random aneuploidy previously observed in WT hepatocytes (Fig. 24A-C and Appendix B Fig. 33). In contrast to control cells, most hepatocytes from LKO mice were diploid and contained exactly 40 chromosomes, and aneuploid karyotypes were rarely observed (Fig. 24A-C and Appendix B Fig. 34). Taken together, 51.8 ± 4.5% of control hepatocytes were aneuploid compared to 7.5 ± 4.3% of LKO hepatocytes (Fig. 24D).

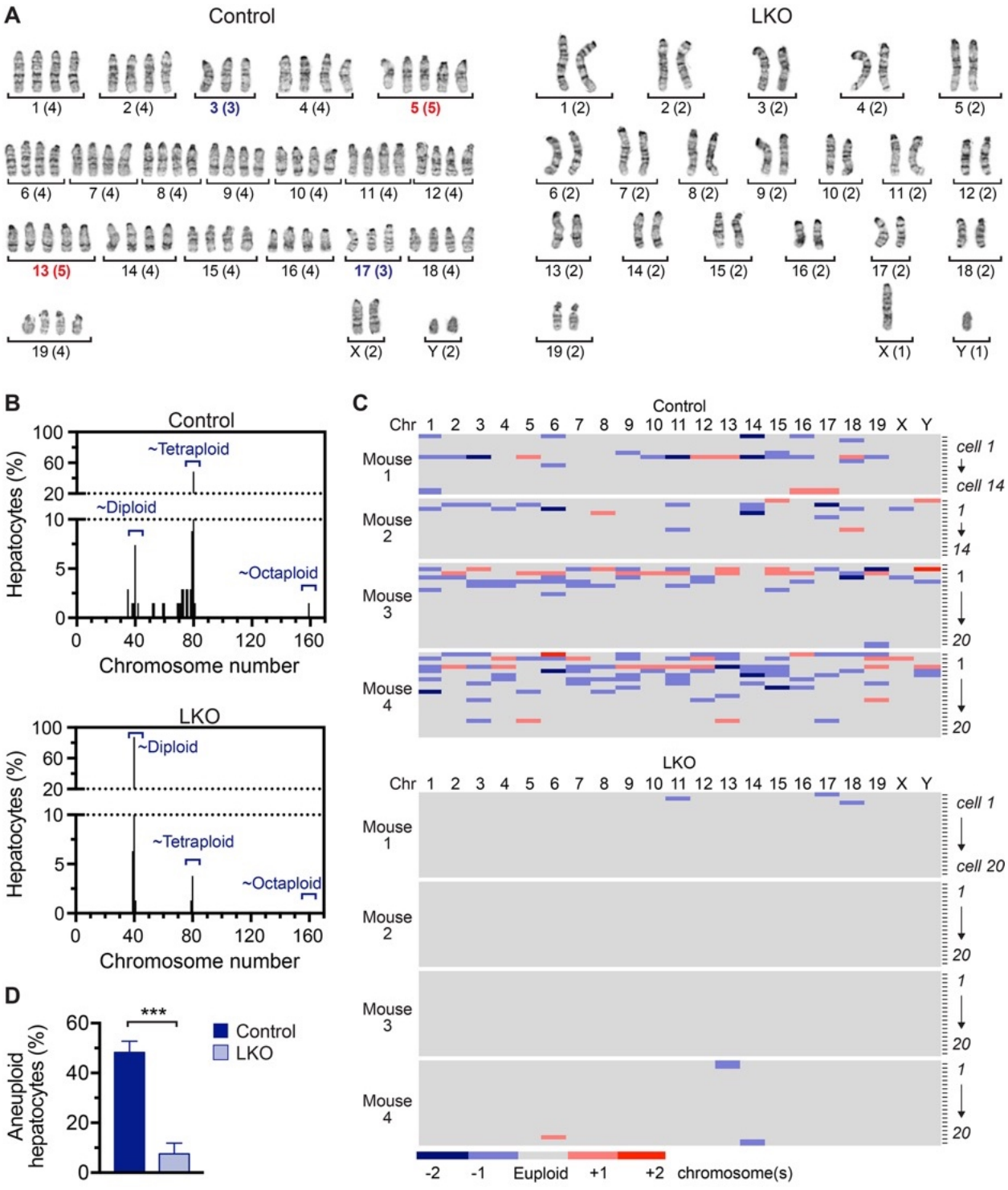

Figure 24. Hepatocytes from LKO livers are predominantly euploid.

(A) Hepatocytes isolated from control or LKO mice (male, n = 4 per genotype) were cultured briefly to stimulate cell division, proliferating hepatocytes were arrested in metaphase and chromosomes from individual cells (n = 14-20 cells per mouse) were identified by G-banding. Representative karyograms are shown for control and LKO hepatocytes.

Chromosome name (i.e., 1-19, X and Y) and number (listed in parentheses) are indicated. Chromosome losses are marked in blue, and chromosome gains are shown in red. The example control hepatocyte is tetraploid and aneuploid with 80 chromosomes (4 copies of most autosomes and 2 copies of each sex chromosome) but lost 1 copy of chromosomes 3 and 17 and gained 1 copy of chromosomes 5 and 13. The example LKO hepatocyte is diploid and euploid (2 copies of all autosomes and 1 copy of each sex chromosome). (B) Chromosome number is shown for control (n = 68) and LKO (n = 80) hepatocytes. Skewed chromosome counts (e.g., hypodiploid, hypotetraploid and hypertetraploid) were frequent in control but not LKO hepatocytes. (C) Chromosome gains and losses are summarized relative to the euploid number of homologous chromosomes. Every row marks an individual cell, and each column corresponds to a different chromosome. Detailed karyotypes are provided in Appendix B Fig. 33 and Fig. 34. (D) The percentage of aneuploid hepatocytes is indicated. *** $P = 0.001$. Graph shows mean ± sem.

To determine if LKO hepatocytes remain diploid and euploid following extensive proliferation, we again used the FAH repopulation model (Fig. 25A and Appendix B Fig. 35). LKO hepatocytes from 4-month-old male mice were transplanted into female FRGN recipients. Mice were cycled off and on NTBC, and, upon complete liver repopulation, hepatocytes were isolated for cytogenetic analysis. The FAH^+ LKO donor hepatocytes had a survival advantage over the FAH^- FRGN host hepatocytes and were able to proliferate and repopulate the FRGN host livers over the course of NTBC withdrawal. Following liver repopulation, hepatocytes were isolated and prepared for metaphase cytogenetic analysis. To measure aneuploidy among donor LKO hepatocytes in the repopulated livers, we focused on metaphase spreads that were positive for the Y chromosome, a marker for donor-derived cells. Most donor-derived hepatocytes contained 40 chromosomes and were euploid (Fig. 25B,C and Appendix B Fig. 35), although there was a trend toward increased aneuploidy in LKO hepatocytes following repopulation (16.3 ± 5.5%) compared to those harvested directly from 4-month-old mice (7.5 ± 4.3%) (Fig. 25D). Taken together, the data show that *E2f7/E2f8* deficiency markedly alters the chromosomal composition of the liver; LKO livers are highly enriched with diploid and euploid hepatocytes whereas control livers are predominantly polyploid and aneuploid.

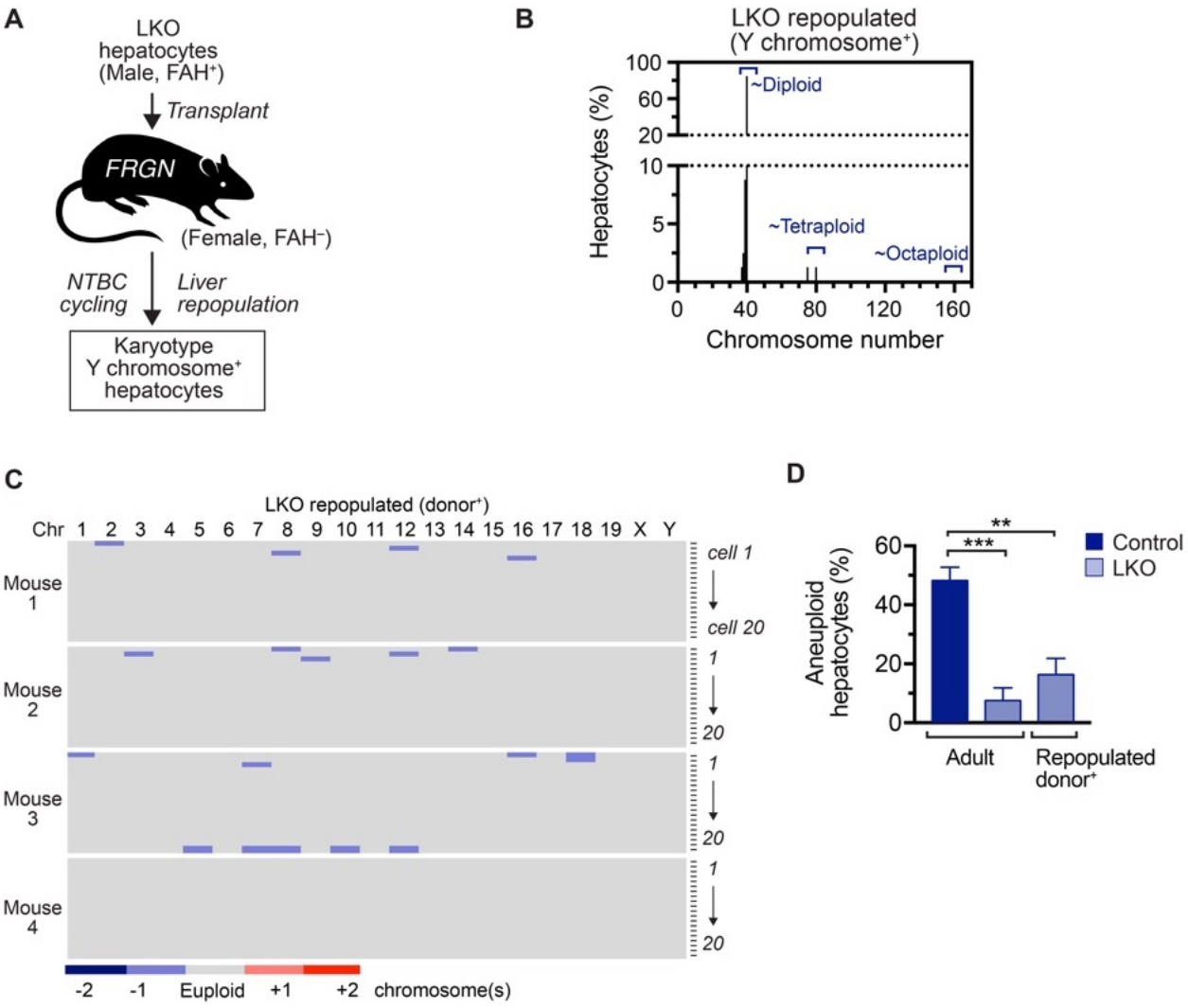

Figure 25. LKO hepatocytes remain predominantly euploid following liver repopulation.

(A) Approximately 300,000 hepatocytes from LKO mice (males, 4 months old) were transplanted into FRGN recipient mice (females, 2 months old) and subjected to NTBC cycling to promote liver repopulation by transplanted donor cells. Following completed repopulation, livers containing a mixture of FAH^+ donor hepatocytes and FAH^- host hepatocytes were isolated. Hepatocytes were cultured briefly to stimulate cell division, proliferating hepatocytes were arrested in metaphase and chromosomes from individual cells (n = 4 repopulated mice; 20 cells per mouse) were identified by G-banding. Karyotypes were determined for donor-derived, male LKO hepatocytes that were Y $chromosome^+$. (B) Chromosome number is shown for LKO-derived hepatocytes (n = 80). Skewed chromosome counts (e.g., hypodiploid, hypotetraploid) were infrequent. (C) Chromosome gains and losses are summarized relative to the euploid number of homologous chromosomes. Every row marks an individual cell, and each column corresponds to

a different chromosome. Detailed karyotypes are provided in Appendix B Fig. 35. (D) The percentage of aneuploid LKO hepatocytes is compared to the degree of aneuploidy in freshly isolated 4-month-old adult control and LKO hepatocytes, which were originally reported in Fig. 24D. ** $P < 0.01$, *** $P < 0.001$. Graph shows mean ± sem.

3.3.3 *E2f7/E2f8*-deficient mice are highly sensitive to chronic tyrosinemia-induced liver injury

Our earlier work demonstrated that chronic tyrosinemia liver injury in $Hgd^{+/-}$ $Fah^{-/-}$ mice resulted in spontaneous liver repopulation by subsets of hepatocytes (78). In this model, loss of functional HGD blocks the tyrosine catabolic pathway upstream of maleylacetoacetate and provides resistance to injury (Fig. 21). It was estimated that half of the tyrosinemia-resistant clones acquired inactivating mutations in the *Hgd* WT allele, and the other regenerating nodules originated from aneuploid hepatocytes lacking the *Hgd* WT locus through whole or partial loss of Chr 16 (78, 82). The data strongly suggested that pre-existing chromosomal variations were required for adaptation to chronic liver injury using an aneuploidy mechanism. We rationalized that *E2f7/E2f8*-deficient mice, with markedly reduced polyploidy and aneuploidy, provided a unique opportunity to test this idea. We, therefore, hypothesized that LKO mice with predominantly diploid and euploid livers are incapable of generating injury-resistant aneuploid clones in the tyrosinemia model of chronic injury, which results in defective liver adaptation and regeneration as well as reduced survival.

$Hgd^{+/-}$ $Fah^{-/-}$ tyrosinemia mice were bred with control and LKO models to generate Tyrosinemia-control (T-control) and Tyrosinemia-LKO (T-LKO) mice, respectively (Fig. 26A). As expected, livers from T-LKO mice contained 16-fold more diploids and 1.5-fold fewer polyploid hepatocytes compared to T-controls (Fig. 26B). Surprisingly, mice bred to the $Hgd^{+/-}$

Fah$^{-/-}$ tyrosinemia background contained more polyploid hepatocytes than non-tyrosinemic mice. For example, <25% of adult LKO hepatocytes were polyploid while nearly 60% of T-LKO hepatocytes were polyploid (compare Fig. 22C with Fig. 26B).

T-control and T-LKO mice were subjected to NTBC withdrawal for up to 7 weeks to induce tyrosinemia and chronic liver injury (Fig. 26C). Experimental mice were monitored throughout the injury period and supplemented with NTBC after 8-11 days. Mice were harvested when body weight dropped 20% below the starting weight or exhibited severe morbidity that could not be alleviated with NTBC. The percentage of T-LKO mice that died prior to harvest (87%) was higher than T-control mice (~72%) (Fig. 26D). Moreover, among the mice that were harvested (Fig. 26E), T-LKO livers were isolated much earlier (21.3 ± 4.4 days) than livers from T-control mice (38.5 ± 2.6 days) (Fig. 26F).

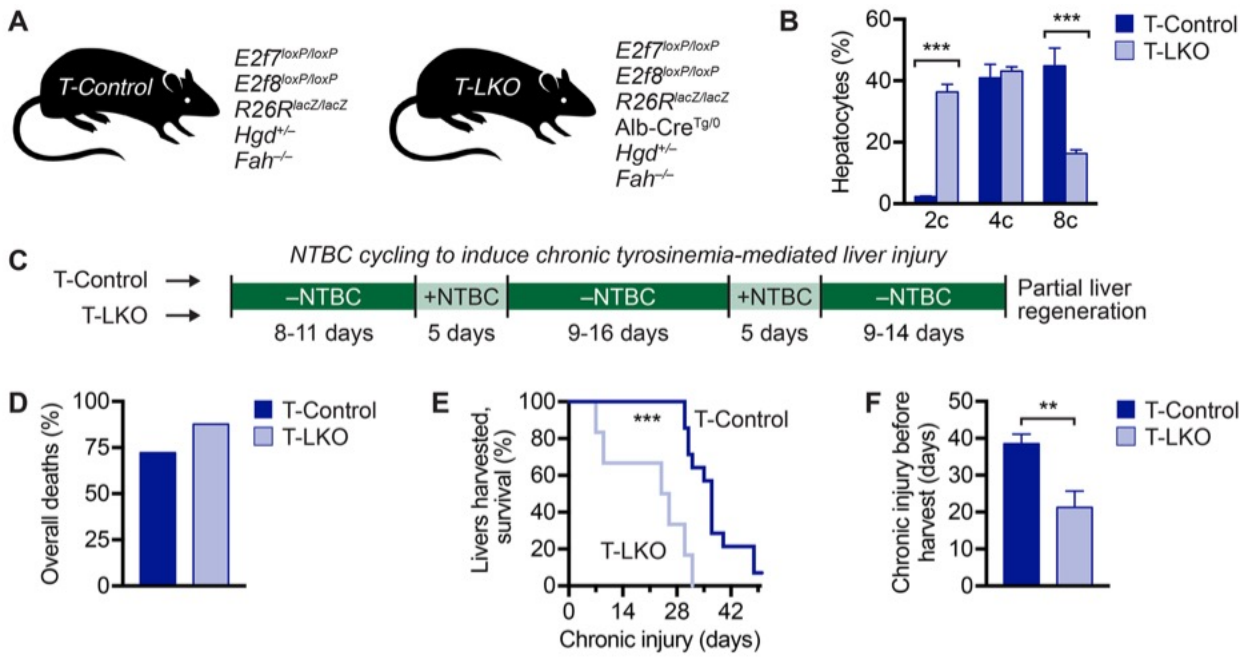

Figure 26. Susceptibility of control and LKO livers to tyrosinemia-induced chronic injury.

(A) Control and LKO mice were mated with *Hgd*$^{+/-}$ *Fah*$^{-/-}$ mice to generate tyrosinemia models: T-control (*E2f7*$^{loxP/loxP}$ *E2f8*$^{loxP/loxP}$ *R26R*$^{lacZ/lacZ}$ *Hgd*$^{+/-}$ *Fah*$^{-/-}$) and T-LKO (*E2f7*$^{loxP/loxP}$ *E2f8*$^{loxP/loxP}$ *R26R*$^{lacZ/lacZ}$ *Alb-Cre*$^{Tg/0}$ *Hgd*$^{+/-}$ *Fah*$^{-/-}$). (B) Hepatocytes were isolated from T-control and T-LKO male mice and stained with the viability dye FVD-780 and the nuclear dye Hoechst. The distribution of live hepatic ploidy populations is shown for 4-month-old T-control and T-LKO mice (n = 3-4 per genotype). (C) At 2.5 months of age, mice were cycled off/on NTBC 3 times, as indicated, to induce chronic injury and promote liver regeneration by proliferation of disease-resistant hepatic clones. (D) Overall survival during injury for T-control (n = 59) and T-LKO (n = 47) mice. (E,F) Kaplan-Meier curve for harvested mice (E) and duration of injury before harvest (F) for T-control (n = 14) and T-LKO (n = 6) mice. ** $P < 0.01$, *** $P < 0.001$. Graphs in B and F show mean ± sem; graph in D shows mean only.

Livers harvested from T-LKO and T-control mice were pale, an indicator of liver damage. Most livers were decorated with red macroscopic regenerating nodules, but nodule size was independent of the duration of chronic injury (Fig. 27A and Appendix B Fig. 36). At the microscopic level, regenerating nodules were apparent in H&E stains by the appearance of large healthy-looking cells with consistent eosin staining and absence of inflammatory cells (Fig. 27B). The healthy and proliferative nature of the nodules was confirmed by the presence of Ki-67^{+} hepatocytes (Fig. 27C). This was expected as hepatocytes within nodules are resistant to tyrosinemia-induced injury and able to proliferate, while hepatocytes in the adjacent tissue are susceptible to tyrosinemia-induced injury and remained quiescent. Nodules were heterogeneous in size and equivalent in number in T-control and T-LKO livers. It has been demonstrated that binucleate hepatocytes can proliferate and that proliferating binucleates generate mononucleate daughters (26, 59). In agreement with these studies, the regenerating nodules in both T-control and T-LKO livers contained fewer binucleate hepatocytes compared to adjacent tissue, indicating the nodules were predominantly comprised of proliferating mononucleate cells (Fig. 27D). Together, the data demonstrate that while both T-control and T-LKO livers were able to develop healthy regenerating nodules in response to NTBC withdrawal, T-LKO mice were more susceptible to morbidity and death associated with chronic tyrosinemia-induced liver injury.

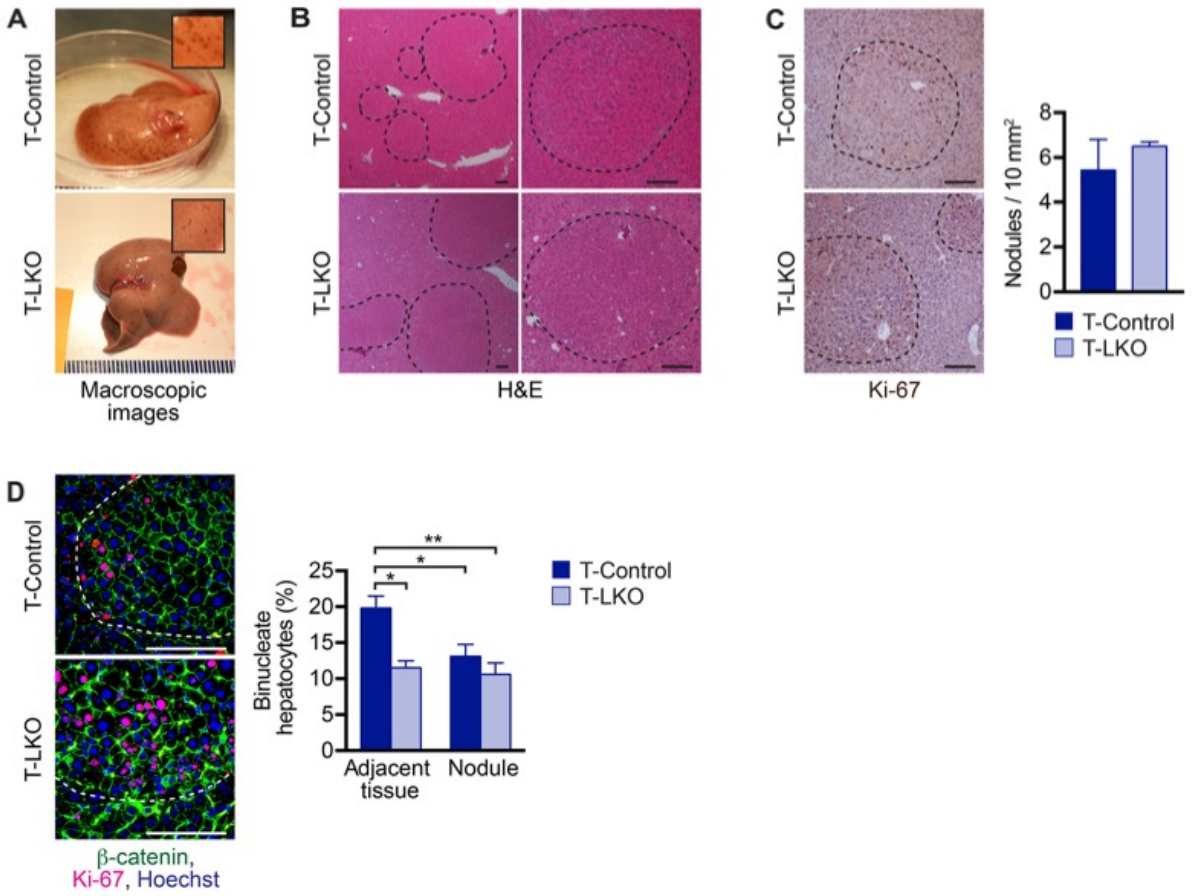

Figure 27. Liver regeneration by control and LKO livers during tyrosinemia-induced chronic injury.

(A) Tyrosinemia-injured livers contained red macroscopic regenerating nodules. Representative images for T-control and T-LKO livers harvested after 37 and 42 days off NTBC, respectively. Insets depict magnified liver images. (B,C): Microscopic nodules are visible by H&E staining (B; low magnification, left; high magnification, right) and presence of proliferating Ki-67^{+} hepatocytes (C, dark brown); the number of nodules is summarized (n = 3-4 mice per genotype). (D) Mono- and binucleate hepatocytes were detected. β-catenin (green) marks cell membranes, Hoechst (blue) marks nuclei and Ki-67 (red) marks proliferating hepatocytes within nodules. The percentage of binucleate cells within nodules and in the tissue adjacent to the nodules is indicated. Dashed lines in B-D indicate nodule boundaries. * $P <$ 0.05, ** $P < 0.01$. Graphs show mean ± sem. Scale bars are 100 μm.

3.3.4 Aneuploidy and inactivating mutations drive formation of regenerating nodules during chronic tyrosinemia-induced liver injury

T-control and T-LKO mice developed regenerating nodules in response to NTBC withdrawal, and these nodules were likely generated by either aneuploidy or gene mutation (78) (Fig. 28A). In terms of aneuploidy, the nodules could arise from pre-existing aneuploid hepatocytes that lost the chromosome containing the *Hgd* WT allele. *Hgd* is located on Chr 16 at position qB3, and we previously showed that loss of the *Hgd* WT allele occurs by whole or partial loss of Chr 16 (78). As $Hgd^{+/-}$ mice contain only one *Hgd* WT allele per diploid genome, cells that have lost this allele lack HGD activity and are, therefore, resistant to tyrosinemia-induced injury (Fig. 21). During chronic injury, these cells have a regenerative advantage and proliferate to restore liver function. The nodules could also be generated by genetic mutation (82). Here, chronic tyrosinemia caused by *Fah* deficiency leads to accumulation of toxic metabolites that can create inactivating mutations in the *Hgd* WT allele (Fig. 21) (82). Once again, these cells become resistant to injury and proliferate to restore liver function. We hypothesized that regenerating nodules from T-control livers are derived from a combination of aneuploid hepatocytes that lost the *Hgd* WT allele and hepatocytes with a mutated WT allele. In contrast, since LKO hepatocytes are euploid, we hypothesized that regenerating nodules from T-LKO livers are derived exclusively from hepatocytes with the mutated WT allele.

To determine the mechanism of nodule formation, individual nodules were isolated by LCM from T-control and T-LKO livers (Fig. 28B). Unstained tissues were used because discrete nodules were easily identified within liver sections. Since nodule size and quantity is independent of the duration of injury (Appendix B Fig. 36), we focused on livers with equivalent sized regenerative nodules from both groups (Fig. 28C). Although not statistically significant, there was

a trend toward smaller nodules in T-LKO livers, compared to T-controls, and this is attributed to the smaller size of LKO hepatocytes (31, 32). LCM-isolated nodules were directly placed into lysis buffer and DNA and RNA isolated simultaneously to permit analysis of the *Hgd* locus and transcript.

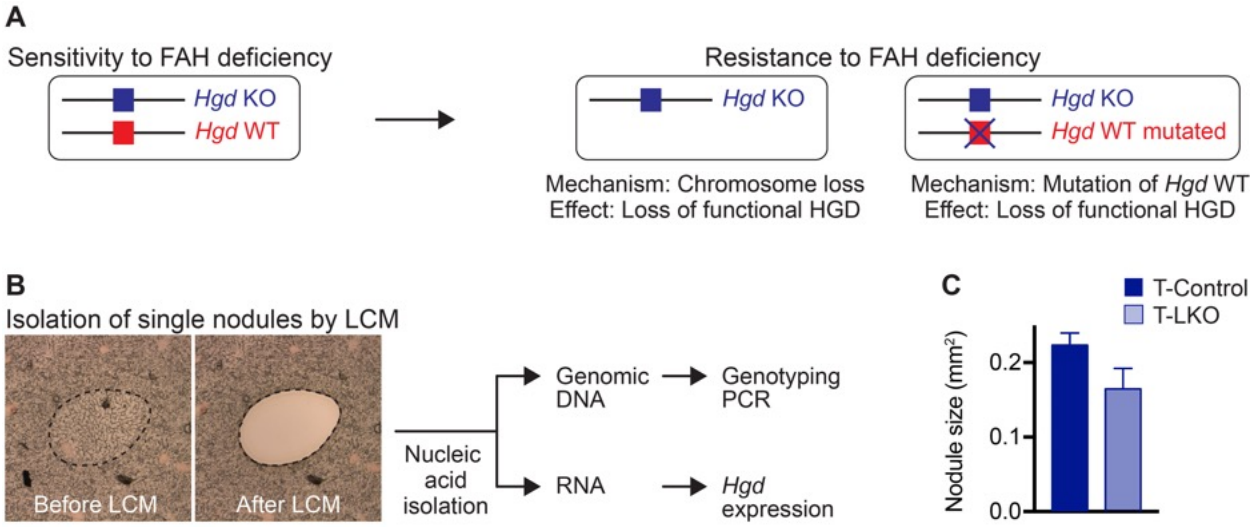

Figure 28. Approach to identify the origin of proliferating nodules.

(A) *Hgd*$^{+/-}$ *Fah*$^{-/-}$ tyrosinemic mice are sensitive to NTBC withdrawal. Hepatocytes that lose the *Hgd* WT allele become resistant to tyrosinemia and can proliferate during tyrosinemia-induced injury. Loss of the *Hgd* WT allele occurs by either loss of Chr 16, which contains the *Hgd* locus, or by inactivating mutations in the *Hgd* WT allele. (B) Individual regenerating nodules were isolated by LCM and genomic DNA and RNA prepared from each nodule for downstream analysis. Dashed lines indicate a representative nodule. (C) The size of nodules in harvested T-control and T-LKO livers subjected to LCM was equivalent (n = 4 mice per genotype; mixed gender).

First, we analyzed the DNA to determine the *Hgd* genotype of the nodules (Fig. 29A). The *Hgd* locus was PCR-amplified and the resulting 290 bp product digested with the restriction enzyme HpyCH4III. This enzyme cuts the 290 bp product for the WT allele to generate fragments that are 170 bp and 120 bp long. The KO allele has a one base mismatch at the HpyCH4III recognition site that prevents cleavage of the 290 bp product. Hence, nodules that produce 3 bands following enzyme digestion (290 bp, 170 bp and 120 bp) are considered $Hgd^{+/-}$, and nodules that have lost the *Hgd* WT allele produce a single 290 bp band and are considered *Hgd* null ($Hgd^{-/-}$) (78, 82). Analysis of nodules from T-control livers revealed that 67.1 ± 9.2% of nodules were $Hgd^{+/-}$ while 32.9 ± 9.2% were $Hgd^{-/-}$ (Fig. 29B,C and Appendix B Fig. 37). Surprisingly, a similar distribution was found in nodules from T-LKO livers where 75.1 ± 15.1% were $Hgd^{+/-}$ and 24.9 ± 15.1% were $Hgd^{-/-}$.

Secondly, to validate the genotyping approach, nodules were interrogated for *Hgd* mRNA expression. Nodules that lost the *Hgd* WT locus are expected to have also lost the full-length (FL) *Hgd* transcript. We converted mRNA to cDNA and PCR-amplified *Hgd* using primers directed to the 3' end of the gene (Fig. 29D). The *Hgd* WT allele produces a FL transcript corresponding to a 665 bp PCR product. The point mutation within the *Hgd* KO allele produces shorter splice variants (SV) approximately 350 bp and 500-550 bp in length that form truncated and defective proteins (82, 148). Most regenerating nodules from T-LKO (50%) and T-control (65%) livers genotyped as $Hgd^{+/-}$ contained the FL transcript with or without SV transcripts (Fig. 29E,F and Appendix B Fig. 37). Manning et al. previously demonstrated that FL transcripts within these nodules acquired gene inactivating alterations (e.g., deletion of 1-31 nucleotides, insertion of up to 27 nucleotides, missense mutations), which resulted in HGD loss-of-function (82). The majority of regenerating nodules genotyped as $Hgd^{-/-}$ contained SV only (T-control, 73%; T-LKO, 78%), which is

consistent with complete loss of the *Hgd* locus (Fig. 29E,F and Appendix B Fig. 37). Thus, as expected, the data suggest that regenerating nodules from T-controls originated from either aneuploid hepatocytes that lost the *Hgd* WT allele or by hepatocytes that acquired inactivating mutations within the WT gene. Although we expected T-LKO nodule formation to be driven exclusively by *Hgd* mutation, the data showed that T-LKO nodules were remarkably similar to T-control nodules as they originated by both the aneuploidy and gene mutation mechanisms.

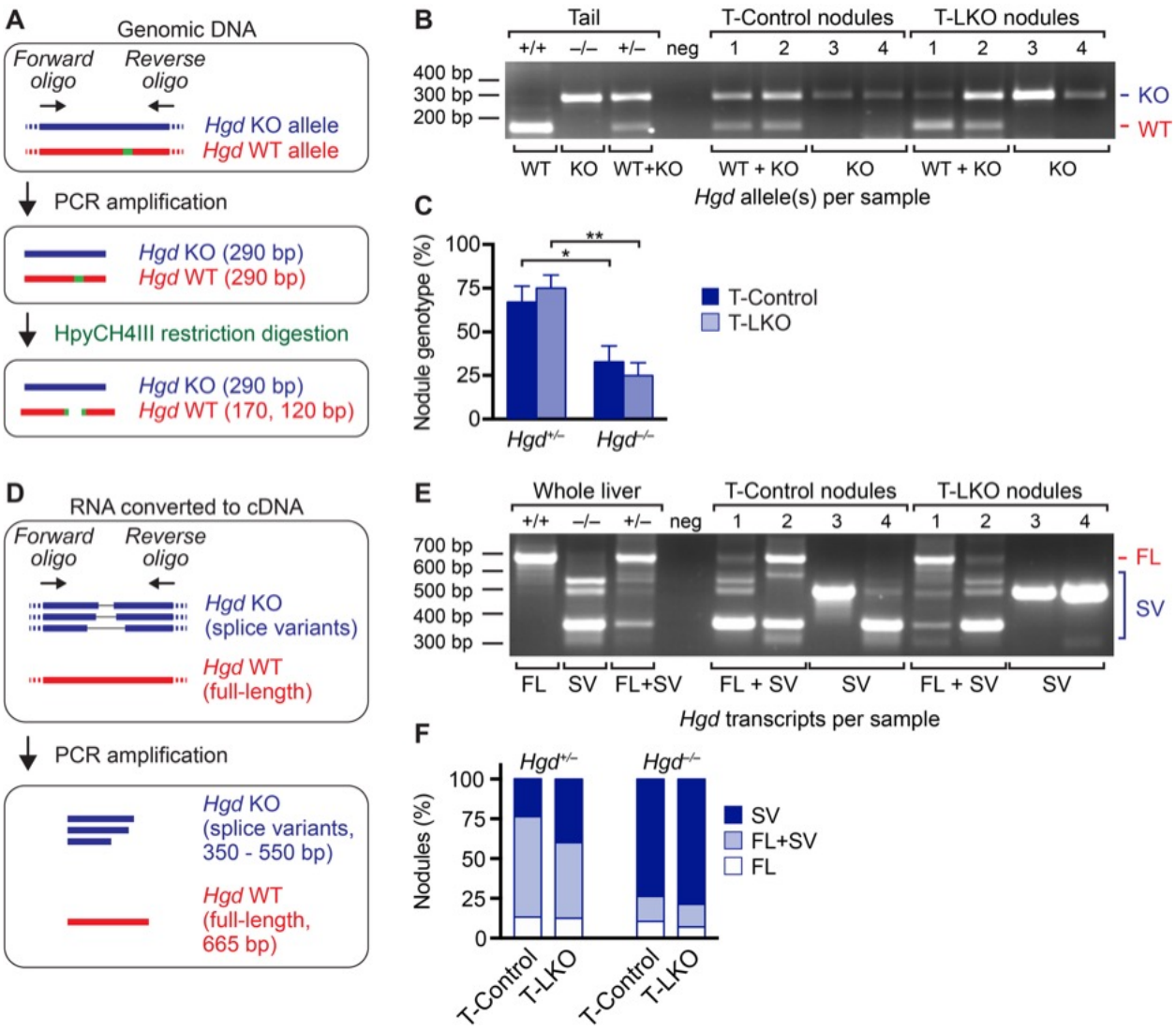

Figure 29. The *Hgd* WT allele is lost by similar mechanisms in equal frequencies by regenerating nodules from T-control and T-LKO livers.

(A-C) Genomic DNA analysis for each nodule (T-control, n = 57 nodules from 4 mice; T-LKO, n = 54 from 4 mice). Strategy for detecting *Hgd* WT and KO alleles in genomic DNA by PCR. Genomic DNA was amplified by PCR and digested with restriction enzyme HpyCH4III (A). Tail tissue DNA isolated from $Hgd^{+/+}$, $Hgd^{-/-}$ and $Hgd^{+/-}$ mice illustrate the WT (170 bp) and KO (290 bp) bands. The 120 bp WT band is not shown. "Neg" is a negative control that did not contain template DNA. Representative nodules from T-control and T-LKO livers depict WT + KO alleles (nodules 1 and 2) and KO alleles (nodules 3 and 4) (B). Nearly 25% of regenerating nodules from T-control and T-LKO livers lost the *Hgd* WT allele and were effectively "$Hgd^{-/-}$" (C). (D-F) Transcriptomic analysis of *Hgd* transcripts in each nodule. Strategy for detecting full-length (FL) transcript from the *Hgd* WT allele or splice variants (SV) from

the *Hgd* KO allele (D). RT-PCR using RNA from whole livers isolated from $Hgd^{+/+}$, $Hgd^{-/-}$ and $Hgd^{+/-}$ mice illustrate FL and SV banding patterns. "Neg" is a negative control that did not contain template cDNA. Representative nodules from T-control and T-LKO livers depict FL + SV *Hgd* transcripts (nodules 1 and 2) and SV *Hgd* transcripts (nodules 3 and 4) (E). The percentage of *Hgd* transcripts is indicated for nodules genotyped as $Hgd^{+/-}$ and $Hgd^{-/-}$. *Hgd* transcripts were expressed similarly in nodules from T-control and T-LKO mice, and, consistent with loss of the WT *Hgd* allele, up to 80% of $Hgd^{-/-}$ nodules contained *Hgd* splice variants only (F). * $P < 0.05$, ** $P < 0.01$. Graph in C shows mean ± sem; graph in F shows mean only.

3.4 Discussion

The "ploidy conveyor" model integrates hepatic polyploidization, ploidy reversal and aneuploidy in the liver, generating widespread genetic heterogeneity and contributing to liver adaptation in response to stress and injury. Here, our goal was to determine if loss of liver polyploidy leads to reduced aneuploidy among hepatocytes and impairs the liver's ability to adapt to chronic injury. We utilized liver-specific *E2f7/E2f8* double knockout (LKO) mice whose livers exhibit reduced hepatic polyploidy (31, 32, 146). In agreement with other studies, we found that hepatocyte polyploidization was disrupted in LKO mice as their livers had a 4-fold reduction of polyploid hepatocytes and a 10-fold enrichment of diploid hepatocytes. Moreover, the polyploidization defect was stable as LKO hepatocytes remained predominantly diploid following extensive proliferation during liver repopulation. Previously, we observed that mice deficient in microRNA-122 (miR-122), another mouse model with a polyploidization defect, had reduced liver polyploidy and few aneuploid hepatocytes (27). To determine if reduced liver polyploidy caused by *E2f7/E2f8* deletion led to decreased hepatic aneuploidy, we karyotyped hepatocytes from LKO and control adult mice. Cytogenetic analysis revealed that almost all hepatocytes from LKO mice

were euploid, while nearly 50% of control hepatocytes were aneuploid. LKO hepatocytes remained mostly euploid even after extensive proliferation during liver repopulation. The low-degree aneuploidy of LKO hepatocytes was within the range of background noise attributed to chromosome loss that occurs during slide preparation, and for the Oregon Health and Science University Cytogenetics Research Service Lab, this affects <15% of cells. Overall, a concomitant reduction of polyploidy and aneuploidy was observed in mice deficient in miR-122 and LKO mice, "polyploidy knockout" models, suggesting that polyploid hepatocytes are required for the generation of aneuploid daughter cells (Fig. 30).

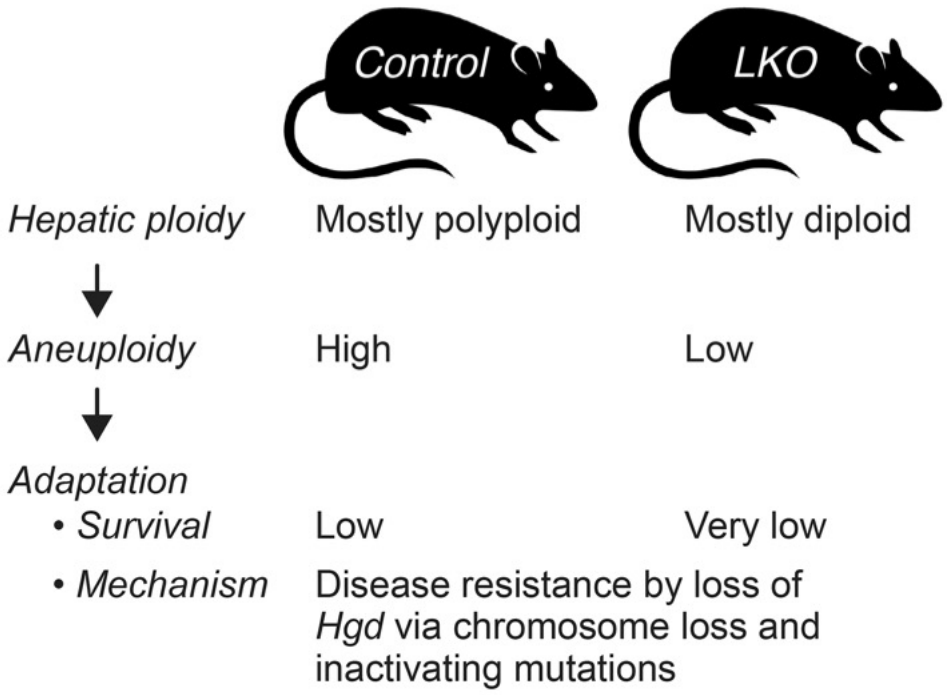

Figure 30. The impact of hepatic polyploidy on liver aneuploidy and adaptation.

LKO mice with reduced polyploidy are mostly euploid and highly sensitive to tyrosinemia-induced chronic liver injury. In contrast, control hepatocytes are predominantly polyploid, enriched with aneuploid karyotypes and are less sensitive to injury.

We have shown in numerous studies that aneuploidy is common among hepatocytes in WT mice, where 50-60% of adult mouse hepatocytes are aneuploid, and humans at various ages (22, 26, 78). In 2014, Knouse et al. subjected hepatic nuclei from 1 mouse and 2 human patients to single-cell DNA sequencing and observed aneuploidy among ~5% of the sequenced hepatocytes (73). A follow-up study in 2018 observed low levels of aneuploidy in hepatocytes with normal tissue organization and cell polarity, but increased chromosome segregation errors in hepatocytes dividing *in vitro* (139). The authors hypothesized that disrupted tissue architecture increased the chance for merotelic microtubule-kinetochore errors to proceed unchecked in dividing polyploid hepatocytes, ultimately leading to aneuploid daughter cells (139). The idea that normal tissue

architecture ensures chromosome segregation fidelity in dividing WT hepatocytes could explain why our metaphase cytogenetic analyses, where hepatocytes are cultured briefly *in vitro*, reveal a higher percentage of aneuploid hepatocytes. Thus, while the actual frequency of aneuploidy could range from 5-60% (26, 73, 139), even the most conservative aneuploidy estimate of 5% indicates that millions of hepatocytes in mice and humans contain random chromosome gains and/or losses, thus highlighting the necessity to understand the role of aneuploidy in liver disease pathology and treatment.

Previously, Manning and colleagues induced chronic tyrosinemia injury in $Hgd^{+/-}$ $Fah^{-/-}$ mice, a model of tyrosinemia, and found livers were spontaneously repopulated by disease-resistant hepatic nodules through complete loss of functional HGD, an enzyme located upstream of FAH in the tyrosine catabolic pathway (Fig. 21). Nearly half of the nodules were derived from hepatocytes containing loss-of-function mutations in the *Hgd* WT allele (82), with the others originating from aneuploid hepatocytes with whole or partial loss of Chr 16 containing the *Hgd* WT locus (78). Here, we determined if polyploidy facilitates adaptation to chronic injury by breeding LKO mice (reduced polyploidy and reduced aneuploidy) onto a tyrosinemia background ($Hgd^{+/-}$ $Fah^{-/-}$), rationalizing that T-LKO mice would be more sensitive to tyrosinemia-induced injury because of a decreased ability to adapt via the aneuploidy mechanism. Indeed, T-LKO mice were more susceptible to morbidities and death associated with tyrosinemia, and it was necessary to harvest T-LKO livers earlier than T-controls for analysis (Fig. 30). Surprisingly, however, livers from both T-control and T-LKO mice contained healthy regenerating nodules that were comparable in size and frequency upon harvest. The percentage of regenerating nodules from T-LKO livers that lost the *Hgd* WT locus via aneuploidy was equivalent to nodules from T-control livers.

Half as many T-LKO mice survived tyrosinemia-induced liver injury compared to T-controls, indicating T-LKOs were much more susceptible to death and morbidities associated with tyrosinemia-induced liver failure (Fig. 26D,E and Fig. 30). We hypothesized T-LKO mice were more susceptible because their livers had reduced hepatic polyploidy, and as a consequence, decreased ability to generate aneuploid hepatocytes that could resist the disease. However, other mechanisms may have contributed to their increased susceptibility. First, gene expression differences associated with loss of *E2f7* and *E2f8* and between diploid and polyploid hepatocytes could have impacted their survival. Several studies, though, demonstrated *E2f7* and *E2f8* deficiency does not disrupt liver architecture or alter gene expression in mice between weeks 3 and 16 (32, 35, 146). Moreover, Lu et al. found gene expression was similar between diploid and polyploid hepatocytes, suggesting ploidy populations are equivalent at the RNA level (54). A second possibility is functional differences between diploid and polyploid hepatocytes. Kreutz et al. found diploids had higher substrate-induced metabolism, measured through esterase activity, and a greater affinity for insulin, indicating that under-appreciated functional differences could specifically affect diploid or polyploid hepatocytes during long-term injury (135). Thus, the increased susceptibility to tyrosinemia-induced liver injury by T-LKO mice may be attributed to multiple mechanisms, including decreased polyploidy and aneuploidy.

Our finding that a similar percentage of regenerating nodules in T-control and T-LKO livers originated by the aneuploidy mechanism was unexpected but could potentially be explained by a combination of factors. First, when LKO mice were bred onto the tyrosinemia background, LKO livers became more polyploid. Specifically, ~40% of the hepatocytes in T-LKO mice were diploid and the remaining ~60% were polyploid (Fig. 26B), compared to ~75% being diploid and ~25% being polyploid in LKO mice (Fig. 22C). The change in ploidy distribution is likely due to

strain differences between the LKO and tyrosinemia models. Consistent with this, control mice (containing *E2f7* and *E2f8*) bred onto the tyrosinemia background also exhibited an increased percentage of polyploid hepatocytes. Note that the ploidy differences are unrelated to hepatic injury since T-LKO and T-control mice were maintained on NTBC continuously (i.e., no tyrosinemia) prior to ploidy analysis. We were unable to karyotype T-LKO hepatocytes because *Fah*-deficient cells die quickly *in vitro* and proliferate poorly, making it difficult to obtain metaphases for G-banding. While we cannot exclude the possibility that T-LKO hepatocytes have unique aneuploid karyotypes that make them more susceptible to tyrosinemia-induced morbidities and death, the aneuploidy data suggests they are highly euploid and exhibit little to no chromosome gains/losses (Fig. 24). Secondly, only a very small number of T-LKO mice were able to be harvested and analyzed, thus potentially biasing the selection for T-LKO livers. We speculate that analysis of only the surviving T-LKO mice inadvertently selected for a unique subset that, randomly, adapted to injury through a combination of aneuploidy and gene inactivation mechanisms. We predict that analysis of T-LKO mice that died and were not able to be harvested would have revealed a failure to generate regenerative nodules via the aneuploidy mechanism entailing loss of the *Hgd* WT allele by Chr 16 aneuploidy.

Recent studies have shed new light on the role of hepatic ploidy in liver function and disease. First, Gentric and Desdouets examined hepatic ploidy in fatty liver disease. Using flow analysis and tissue microscopy, they showed that mouse models of fatty liver disease exhibited increased levels of polyploid hepatocytes and a significant increase in mononucleate cells with high nuclear content. Moreover, patients diagnosed with nonalcoholic fatty liver disease who had undergone liver resections for HCC displayed similar phenotypes (92). Secondly, Zhang and Zhu showed that polyploid hepatocytes protect against liver cancer (35). In a series of elegant

experiments (supported by other studies (128)), polyploid hepatocytes were found to "buffer" against tumor suppressor loss. Inactivation of one tumor suppressor copy in a diploid cell leads to loss-of-heterozygosity and increased potential for transformation. However, in polyploid hepatocytes, the additional chromosome sets effectively provide "backup" tumor suppressor copies, which reduce the likelihood of transformation. Thirdly, we found that, compared to polyploids, diploid hepatocytes have a proliferative advantage . In response to proliferative stimuli, they had faster cell cycle entry and progression than polyploids, suggesting that diploid hepatocytes are immediate drivers of liver regeneration and tumor growth (146). Finally, multiple studies in patients and animal models have shown that hepatocellular carcinomas are enriched with diploid hepatocytes (93-95). Thus, taken together, the polyploid state could provide protection from tumorigenesis by providing extra copies of tumor suppressor genes and by restricting hepatocyte proliferation. The current work identifies another specialized role for hepatocytes based on ploidy. Polyploid hepatocytes perform an essential role in adaptation to tyrosinemia-induced chronic liver injury, with one adaptive mechanism involving production of aneuploid progeny. Thus, together with other studies (25, 59, 60, 146), hepatocyte capabilities are directly influenced by chromosomal content (diploid vs. polyploid; aneuploid vs. euploid), which can dramatically alter cell fate and liver function (Fig. 31).

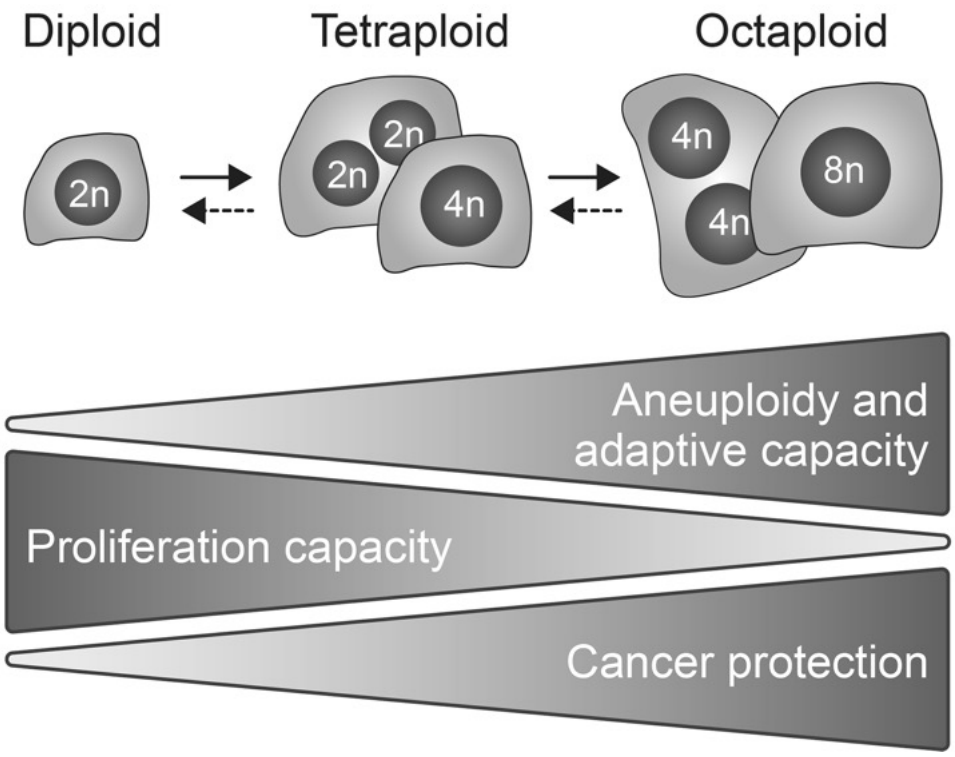

Figure 31. Model summarizing unique capabilities of diploid and polyploid hepatocytes.

Current and recently published findings have shed light on the unique capabilities of diploid and polyploid hepatocytes. Solid arrows indicate polyploidization. Dashed arrows indicate ploidy reversal. Polyploid hepatocytes protect from tumorigenesis associated with tumor suppressor loss (35) , and as demonstrated here, are essential for adaptation to chronic liver injury. In contrast, proliferation capacity is highest among diploid hepatocytes.

Future studies should focus on elucidating the conditions that drive polyploids to generate aneuploid hepatocytes *in vivo* and how this aneuploidy affects liver function and adaptation in homeostasis and disease. For example, transient cell polarity defects are common during liver regeneration induced by partial hepatectomy (150, 151), posing potential aneuploidy-related issues for liver resections and living donor liver transplants. In a cell therapy context, donor hepatocyte isolation involves complete disruption of tissue architecture and cell polarity, which must be re-established post-transplantation in recipients. While the kinetics of "normal" architecture and polarity establishment by donor hepatocytes in a new microenvironment are unknown, we have previously demonstrated donor hepatocyte aneuploidy increased up to 2-fold in liver repopulation post-transplant (26). Additionally, Hepatitis C viral infection has been shown to cause the formation of macroscopic nodules in cirrhotic livers. Interestingly, 25-50% of these nodules have been shown to be monoclonal (152-154), suggesting they were derived from single cells with survival advantages due to unique aneuploid karyotypes. We are only beginning to understand the relationship between polyploidy and aneuploidy in the liver, and therefore future studies are warranted to determine how hepatic polyploidy and aneuploidy can affect liver function and adaptation to injury and stress.

4.0 General Discussion

4.1 Significance in Health and Disease

Chronic liver disease is a significant health concern and affects millions of Americans each year. Among adults aged 45-64 years, deaths attributed to cirrhosis and chronic liver disease increased by 31% between 2000-2015 in the United States (155). Moreover, the number of individuals exhibiting nonalcoholic fatty liver disease and steatohepatitis (NAFLD/NASH) continues to rise, with the two diseases being the second leading cause of liver transplantation in the country (156). As the population ages, the number of individuals necessitating liver transplants will increase and further pressure will be placed on an already strained liver transplantation program, making it even more critical that new treatments for liver pathologies are developed. Since modulations in polyploidy levels have been observed in several liver diseases, it is imperative that studies interrogate the relationship between polyploidy and disease, with the ultimate goal of incorporating polyploidy into liver therapy innovation.

The existence of polyploid hepatocytes has been known for over a century (2), but it is only recently that studies have begun to elucidate the role of polyploidy in liver function, regeneration and disease. First, Desdouets and colleagues examined hepatic ploidy in NAFLD models and patients with NASH (92). Mouse models of NAFLD and patients with NASH exhibited a significant increase in polyploid hepatocytes and dramatic enrichment for mononucleate cells with high nuclear content. While the authors attributed the increased ploidy to oxidative stress brought on by disease, it was unclear whether the highly polyploid hepatocytes were contributing to disease progression or were a protective mechanism (103). Secondly, Zhu and colleagues showed that

polyploid hepatocytes protect against liver cancer (35). By modulating ploidy levels through a variety of mechanisms, they demonstrated polyploid hepatocytes could "buffer" against tumor suppressor loss. In diploid cells, inactivation of one tumor suppressor copy leads to loss-of-heterozygosity and increased potential for transformation. However, polyploid hepatocytes have additional chromosome sets which effectively provide "backup" tumor suppressor copies and reduce the likelihood of transformation.

As detailed in "Chapter 2: Polyploidy in Hepatocyte Proliferation and Liver Regeneration", we showed that compared to polyploid subsets, diploids have a proliferative advantage. We first found that hepatocytes isolated from *E2f7*/*E2f8*-liver specific knockout mice (LKO), where diploid hepatocytes are enriched by 20-fold, proliferated faster *in vitro* and out-competed control hepatocytes in head-to-head competitive repopulation. Diploid cells from wild-type mice also showed a proliferative advantage, entering and progressing through the cell cycle faster than polyploids *in vitro* and during liver regeneration (146). These observations suggest that diploid hepatocytes are one of the first to proliferate in liver regeneration and are immediate drivers of the regenerative process. Even though diploids comprise <10% of the hepatocyte population, their ability to enter and progress through the cell cycle rapidly could be critical in cases of acute liver injury, such as acetaminophen (APAP) overdose or carbon tetrachloride (CCl_4) exposure, where rapid hepatocyte proliferation is necessary to maintain liver function while the liver undergoes complete regeneration. Additionally, it would also be interesting to see if polyploidy plays a role in regulating liver size, which remains a constant size relative to body weight (reviewed in (131)). The signals that cooperate to regulate liver regeneration are collectively called the "hepatostat" (157). Equally important to *initiation* of regeneration is *termination* of regeneration, which is necessary to prevent liver overgrowth. While most hepatocytes – whether they are diploid or

polyploid – are believed to contribute to the regenerative response (59), it is interesting to speculate that rapidly proliferating diploids are important for regeneration *initiation* while less proliferative polyploids play a significant role in regeneration *termination*.

Additionally, we found that LKO livers functioned normally but became highly tumorigenic when challenged with a DEN-PB tumor-promoting regimen. A few different mechanisms could explain the high sensitivity of LKO mice to liver tumorigenesis. First, E2F7 and E2F8 deficiency could affect cell cycle progression and promote oncogenic proliferation. Kent et al. demonstrated LKO mice spontaneously developed liver tumors during aging and developed more tumors than controls in a DEN tumor induction model (128). In fact, E2F8 has been suggested to play a tumor suppressor role, and E2F1, which is upregulated in LKO mice, has exhibited tumor suppressor and oncogenesis functions (128, 137). Secondly, LKO mice are enriched with diploid hepatocytes, which have a greater risk of tumor suppressor loss of heterozygosity and are more susceptible to transformation than polyploid hepatocytes (35). Thirdly, we found that diploid hepatocytes, which are the predominant cell type in LKO mice, are the most proliferative, suggesting that rapidly cycling diploid hepatocytes drive tumorigenesis upon tumor initiation (146). It is likely that the increased tumorigenesis in LKO mice were due to a combination of the aforementioned mechanisms listed. The fact that diploid enrichment has been observed in hepatocellular carcinomas (HCC) in humans and rodents also supports the idea that polyploids protect against liver cancer and diploid hepatocytes prominently contribute to HCC development and progression (62, 63, 138). Future studies should focus on determining the exact ways diploids and polyploids contribute to HCC initiation, development and even advancement. Moreover, it will be important to determine if the response of diploids and polyploids depends on the type of liver cancer in patients. For example, are diploids and polyploids equally susceptible

to liver tumors driven by activating mutations in proliferation genes (i.e., *CTNNB1*) (158), or those characterized by loss of a tumor suppressor (i.e., *TP53*) (159)? Interestingly, Zhu and colleagues observed that while livers with reduced polyploidy were more susceptible to tumorigenesis driven by tumor suppressor loss, those livers were equally susceptible to tumorigenesis driven by Myc oncogene activation compared to livers with high levels of polyploidy (35). Ultimately, the diploid/polyploid ratio within HCC tumors and in surrounding liver tissue may need to be considered, along with other genetic and histological factors, in patient prognosis and treatment design.

In "Chapter 3: Polyploidy in Hepatocyte Aneuploidy and Adaptation to Chronic Liver Injury" we showed that polyploidy is necessary for generating aneuploidy in the liver and promotes adaptation to chronic liver injury (160). Since proliferating polyploid hepatocytes undergo chromosome segregation errors to generate aneuploid daughter cells that have gained/lost ≥1 chromosomes, we hypothesized that LKO livers, which are depleted of polyploid hepatocytes, would also have fewer aneuploid hepatocytes. To test this idea, we isolated hepatocytes from 4-month-old control and LKO mice and karyotyped individual hepatocytes using standard metaphase cytogenetic analysis. We observed that nearly all LKO hepatocytes were euploid compared to control hepatocytes, of which >50% were aneuploid. Additionally, donor-derived LKO hepatocytes remained mostly euploid following repopulation of *Fah*$^{-/-}$ livers. These results, along with the data demonstrating livers deficient in miR-122, another polyploidy depletion model, were predominantly comprised of euploid hepatocytes (27), provides further support to the idea that polyploid hepatocytes are required for production of aneuploid progeny.

In this study and others (22, 26, 33, 76, 160), we have shown that aneuploidy is widespread and random across healthy livers in both mice and humans. We have characterized aneuploidy

primarily using metaphase cytogenetics in which hepatocytes are isolated from livers, cultured briefly and arrested in metaphase so that the first dividing hepatocytes can be karyotyped. Using this method, we have consistently showed that 50-60% of adult hepatocytes in normal mice are aneuploid, and all chromosomes are equally affected. In 2014, Knouse et al used DNA sequencing of individual hepatic nuclei from 1 mouse and 2 human patients and observed random aneuploidy affected ~5% of hepatocytes (73). Furthermore, in a 2018 report, the same authors found high levels of aneuploidy in hepatocytes cultured *in vitro* compared to those located *in vivo*, which exhibited very low aneuploidy (139). The authors hypothesized that proper tissue architecture, which is disrupted when hepatocytes are cultured *in vitro*, promotes bipolar spindle assembly and helps prevent chromosome segregation errors from occurring in dividing polyploid hepatocytes (139). The idea that normal tissue architecture ensures chromosome segregation fidelity in dividing WT hepatocytes could explain why our metaphase cytogenetic analyses, where hepatocytes are cultured briefly *in vitro*, reveal a higher percentage of aneuploid hepatocytes. While the actual frequency of hepatic aneuploidy could range from 5-50% in normal livers, it should be noted that 5% implies that millions of hepatocytes in healthy mice and humans are aneuploid (26, 73, 139, 160).

The implications of liver aneuploidy for liver therapy and disease are numerous. For example, transient cell polarity defects are common during liver regeneration induced by partial hepatectomy (150, 151), posing potential problems for people who undergo liver resections for living donor liver transplantations. Moreover, in 2018 Pradhan-Sunnd et al. showed that mice with livers deficient in beta-catenin and gamma-catenin developed cholestatic liver disease and exhibited disruptions in liver tissue architecture and cell polarity (161). These findings indicate that patients with cholestatic liver disease (CLD), such as progressive familial intrahepatic

cholestasis (PFIC), may have disrupted liver tissue architecture and increased hepatic aneuploidy. Additionally, in the context of cell therapies, donor hepatocytes are isolated from their native environment using techniques that disrupt tissue architecture and cell polarity, and then transplanted into recipient livers where they must integrate and establish proper cell polarity (162, 163). It is unclear as to whether polyploid hepatocytes are more likely to generate aneuploid daughters during this process, and if so, whether this aneuploidy can have negative (or even positive) effects on the recipient liver. Future studies are needed to determine if defects in liver architecture and cell polarity drive chromosome segregation errors in dividing polyploid hepatocytes, and how tissue architecture disruption in liver disease affects hepatic aneuploidy.

While whole chromosome gains/losses have been shown to be random and widespread in the liver, a major unanswered question is the effect this diverse "background" aneuploidy has on liver function and disease. Aneuploidy is typically associated with cancer (116, 140, 164), but spontaneous hepatocellular carcinoma is rare (141), indicating that aneuploidy itself unlikely drives tumorigenesis. Previously, we demonstrated that aneuploid karyotypes could provide protection during chronic liver injury (78). We induced chronic tyrosinemia in $Hgd^{+/-}$ $Fah^{-/-}$ mice, and over 3 months, livers were spontaneously repopulated by subsets of endogenous hepatocytes. These hepatic subsets were resistant to injury, giving them a competitive advantage and permitting clonal expansion. Metaphase cytogenetics and array comparative genomic hybridization (aCGH) indicated half of the regenerating nodules were derived from aneuploid hepatocytes with whole or partial loss of Chromosome 16, thus demonstrating aneuploidy could facilitate liver regeneration and adaptation to chronic liver injury. Here, we induced tyrosinemia in LKO mice, which have reduced polyploidy and almost no aneuploidy, and found that they were much more susceptible to disease-related morbidities and death compared to control mice. Molecular analyses showed that

the regenerative nodules in the tyrosinemic LKO (T-LKO) mice were derived from enzyme-loss-of-function gene mutations and aneuploidy, with frequencies similar to those of regenerative nodules found in T-control mice. However, since our analyses focused only on surviving T-LKO mice, we may have inadvertently biased our analysis for T-LKO mice that, randomly, adapted to injury through a combination of aneuploidy and gene inactivation mechanisms. Ultimately, we predict that T-LKO mice that died and were not able to be harvested would have contained nodules almost exclusively derived from enzyme-loss-of-function gene mutations and hardly any derived from the aneuploidy mechanism entailing loss of Chromosome 16.

Aneuploidy and liver adaptation may play a role in human liver disease, notably Hepatitis C virus (HCV) infection. HCV infection is a major health issue, leading to fibrosis and cirrhosis and at times progressing to liver cancer, liver failure and death (165-168). Studies have shown HCV often disrupts the expression of genes, including tight junction proteins Claudin-1 (*CLDN1*) and occludin (*OCLN*), that regulate hepatocyte cell polarity and liver tissue architecture (169-171). Considering that disrupted tissue architecture promotes chromosome segregation errors and aneuploidy, it is likely that HCV-infected livers have elevated numbers of aneuploid hepatocytes. Notably, several groups observed 25-50% of pre-neoplastic macroscopic nodules from HCV-infected cirrhotic livers were monoclonal (152-154), suggesting they derived from a single cell with a survival advantage. This raises the question of whether aneuploid karyotypes can help hepatocytes resist disease, such as HCV-infection, and proliferate in a clonal manner to aid liver regeneration. Moreover, it will be important to determine if unique aneuploid karyotypes, involving particular chromosome gains/losses, are associated with specific liver diseases and injuries.

4.2 Future Directions and Concluding Remarks

The ploidy conveyor model, which integrates polyploidization, ploidy reversal and aneuploidy, has been used to describe hepatic polyploidy in the liver. The ploidy conveyor demonstrates dividing diploid hepatocytes become binucleate tetraploids through acytokinetic cell division (3), with polyploidization primarily driven through insulin/PI3K/Akt signaling (25) and other genetic regulators including E2F family members, miR-122 and cell cycle regulators (27, 31, 32, 35, 146, 172). These binucleate tetraploids can in turn give rise to mononucleate and binucleate octaploids, and even hepatocytes with higher ploidy through further rounds of cell cycling involving successful and failed cytokinesis (1, 26). Moreover, it was shown *in vitro* and *in vivo* that polyploid hepatocytes could undergo ploidy reversal and generate daughter cells of lower ploidy states, with the daughter cells often being aneuploid (1, 26). The research detailed in this dissertation adds to the ploidy conveyor model, shedding light on the functional capacities of diploid and polyploid hepatocytes, and illustrating the unique, and diverse roles they play in liver function, regeneration and tumorigenesis, as well as aneuploid cell production and effecting adaptation to chronic liver injury.

In "Chapter 2: Polyploidy in Hepatocyte Proliferation and Liver Regeneration", we used the polyploidy-deficient *E2f7*/*E2f8*-liver specific knockout mouse model, in combination with analyses involving wild-type mice, to demonstrate that diploids are the most proliferative, entering and progressing through the cell cycle earlier than polyploids . The results of this study reinforced the idea that all ploidy populations proliferate, but presented the novel finding that proliferative capacity is inversely related to hepatocyte ploidy (146). Going forward, it will be important to determine why diploids are more proliferative than polyploids.

One explanation could involve differences in the transcriptome between ploidy populations. It is possible that individual or specific gene families could be differentially expressed between diploids and polyploids, or mRNA levels could increase proportionally with chromosome content, with tetraploids and octaploids having 2X and 4X the amount of RNA (and even protein), respectively, compared to diploids (1). Interestingly, Itzkovitz and colleagues tracked the switching of promoters from open to closed states among hepatocytes and found promoters stochastically switched between the two states, suggesting normal livers exhibit some degree of cell-to-cell variation in gene expression. Notably, they found polyploid hepatocytes exhibited less transcriptional noise, suggesting gene expression was less random and "bursty" in polyploids than diploids (173). However, a 2007 study by Lu et al. found very few genes were differentially expressed between diploid and tetraploid hepatocytes FACS-isolated from mice, and the magnitude of change was small for those that were expressed differently While this study suggests hepatic ploidy subsets are similar at the RNA level, it is important to note the authors only examined gene expression in quiescent hepatocytes (54). It is possible that diploid and polyploid hepatocytes have similar gene expression under normal conditions but exhibit differential gene expression during high liver activity, liver regeneration and possibly liver trauma. Future studies will need to focus on deciphering the molecular differences between hepatic ploidy populations under normal, healthy conditions as well as times of stress and disease using state-of-the-art techniques (i.e., RNAseq). Moreover, it will be important to determine how epigenetic modifications and chromatin remodeling contribute to molecular differences between diploids and polyploids (174).

Proliferation differences among ploidy populations could also be due to differential growth factor binding by diploid and polyploid hepatocytes. Recently, Kreutz et al. demonstrated insulin

bound with greater affinity to diploid hepatocytes than polyploids, suggesting that hepatic ploidy subsets could have differential responses to insulin stimulation (135). As detailed in this dissertation, we tested the hypothesis that differential growth factor binding by diploid and polyploid hepatocytes drove proliferation differences between ploidy populations. However, we found diploid and tetraploid hepatocytes responded similarly to stimulation by growth factors involved in liver regeneration, including primary mitogens (HGF, EGF and TGFα) and auxiliary mitogens (insulin, FGF1 and FGF2) (134, 136). A caveat to our study was that we tested this hypothesis *in vitro* and did not analyze growth factor binding in octaploids and higher ploidy populations. Future studies will need to focus on comparing growth factor stimulation in all ploidy populations, as well as in hepatocytes from mice of all ages. Additionally, it is possible that proliferation differences among ploidy populations due to growth factor stimulation are only observable *in vivo* or in times of liver injury, both acute and chronic.

In "Chapter 3: Polyploidy in Hepatocyte Aneuploidy and Adaptation to Chronic Liver Injury", we demonstrated that *E2f7*/*E2f8*-liver specific knockout mice, with reduced polyploidy, are almost completely deficient in liver aneuploidy, suggesting polyploid hepatocytes are needed to generate aneuploid hepatocytes. Moreover, we found that *E2f7*/*E2f8*-liver specific knockout mice exhibited increased morbidity and higher mortality than controls when placed on a chronic tyrosinemia injury model, suggesting that reduced polyploidy impairs the ability of the liver to resist chronic liver injury. The results of this study provided further support to the concept that polyploidy drives hepatic aneuploidy, and presented the novel finding that decreased polyploidy increases the susceptibility of the liver to chronic liver injury (160) . Going forward, it will be important to determine how polyploidy regulates hepatic aneuploidy and facilitates adaptation to chronic liver injury.

We demonstrated that LKO mice had livers comprised almost exclusively of euploid hepatocytes, while ~50% of control hepatocytes were aneuploid, exhibiting random chromosome gains/losses. These results show that loss of polyploidy leads to decreased aneuploidy, suggesting that a lack of polyploid hepatocytes precludes the generation of aneuploid hepatocytes. Previous studies demonstrated that polyploid hepatocytes often form multipolar spindles during mitosis, which when left unresolved, often result in aneuploid daughter hepatocytes (1, 26). Future studies should seek to characterize mitosis in LKO hepatocytes, which remain diploid and do not readily polyploidize in culture, focusing on the frequency of multipolar spindle formation and chromosome segregation errors. Moreover, it would be beneficial to karyotype hepatocytes from other polyploidy-deficient mouse models, such as those outlined in Table 1, to see if they are also mostly euploid. Additionally, with recent data suggesting disruptions in cell polarity and tissue architecture interfere with mitosis (139), it will be important to see how hepatic aneuploidy levels are affected by disruptions in liver architecture. For example, it is possible that hepatocytes proliferating during liver regeneration following partial hepatectomy exhibit higher frequencies of lagging chromosomes than hepatocytes that proliferate during normal cell turnover in healthy, uninjured livers. Moreover, it will be important to reconcile the frequency of aneuploidy observed in hepatocytes *in vivo* (~5%) and in those following brief *in vitro* culturing (50-60%) (22, 26, 73, 139).

Additionally, it will be important to see how aneuploidy affects gene expression in hepatocytes. Transcriptomic changes have been observed in aneuploid cancer cells, along with cells isolated from patients with Trisomy 21, suggesting whole chromosome gains can result in altered gene expression (175). Whole gains and losses of chromosomes could affect the expression levels of hundreds of genes in hepatocytes, with the potential to effect genome-wide changes that

influence cell function. Future studies will need to determine if aneuploidy affects gene expression in hepatocytes and how these changes affect hepatocyte function in healthy and diseased states. On the other hand, if aneuploid hepatocytes are found to have transcriptomic profiles similar to those of euploid hepatocytes, it will be important to determine the mechanisms that compensate for extra/reduced copies of genes and prevent significant fluctuations in overall gene expression.

Finally, it will be important to determine the exact mechanisms by which polyploidy and aneuploidy facilitate adaptation to chronic liver injury. We previously demonstrated that aneuploid hepatocytes could protect against chronic liver disease. Specifically, we showed hepatocytes could become resistant to chronic tyrosinemia injury in mice through complete or partial loss of Chromosome 16, and repopulate livers to restore liver function (78). As detailed in this dissertation, we expanded upon these previous results by showing livers severely depleted in polyploid hepatocytes had decreased ability to resist and adapt to chronic tyrosinemia injury. Surprisingly, our analyses showed T-LKO mice, with reduced polyploidy, generated tyrosinemia-resistant nodules through inactivating mutations and aneuploidy in frequencies similar to controls. We hypothesize the percentages were the same because we inadvertently biased our selection for T-LKO mice that contained a sufficient number of aneuploid hepatocytes that allowed them to generate nodules that enabled the mice to survive and make it to harvest. To test this hypothesis, a similar experiment could be conducted in which we would harvest livers from T-control and T-LKO mice after specified intervals following NTBC withdrawal (e.g., 3, 6, 9, 12, 15, 18, 21 days), and then interrogate nodule formation, whole chromosome aneuploidy and gene mutation at each time point. We speculate that analysis of T-LKO mice that died at early time points would have revealed a failure to generate regenerative nodules via the aneuploidy mechanism. Additionally, future studies should focus on determining if polyploidy and aneuploidy can facilitate resistance

to other forms of liver stress. For example, it will be important to determine if polyploidy and aneuploidy can help hepatocytes resist and adapt to other environmental stresses, including other chronic injuries (i.e., cirrhosis) and even repeated instances of acute injury (i.e., APAP).

The development of novel therapies to improve liver health and treat disease requires a better understanding of liver function and regeneration. Here, we showed chromosomal variations play a significant role in liver function, regeneration and disease, demonstrating diploid hepatocytes drive immediate liver regeneration through rapid proliferation and polyploids guard against liver tumorigenesis while also facilitating adaptation to chronic liver injury. However, many questions regarding chromosomal variations remain, such as how polyploidy and aneuploidy affect gene expression, and whether diploids and polyploids exhibit differential activity in healthy and diseased livers. Progress in liver therapy innovation and design hinges on our ability to elucidate the mechanisms driving liver homeostasis and regeneration, incorporating all facets of liver function and physiology, and ultimately deriving treatment stratagems that improve patient health and well-being.

Appendix A – Additional information for chapter 2

A.1 Competitive liver repopulation data

A Group 1: LKO$^{60\%}$ + Control$^{40\%}$

Transplant Recipient	INPUT		OUTPUT	RATIO
	Control β-gal- (%)	LKO β-gal+ (%)	LKO β-gal+ (%)	β-gal+ Output/Input
1	40	60	96.1	1.6
2	40	60	90.9	1.5
3	40	60	93.7	1.6
4	40	60	92.7	1.5
5	40	60	89.2	1.5
mean ± sem	*40*	*60*	*92.5 ± 1.2*	*1.5 ± 0.02*

B Group 2: LKO$^{17\%}$ + Control$^{83\%}$

Transplant Recipient	INPUT		OUTPUT	RATIO
	Control β-gal- (%)	LKO β-gal+ (%)	LKO β-gal+ (%)	β-gal+ Output/Input
1	84	16	94.0	5.9
2	84	16	93.6	5.9
3	84	16	91.4	5.7
4	84	16	92.5	5.8
5	84	16	97.2	6.1
6	80	20	90.1	4.5
7	80	20	85.9	4.3
mean ± sem	*82.9 ± 0.7*	*17.1 ± 0.7*	*92.1 ± 1.3*	*5.4 ± 0.3*

Figure 32. LKO hepatocytes out-compete controls during competitive liver repopulation.

(A,B) LKO (β-gal+) and control (β-gal-) hepatocytes were mixed in defined ratios and transplanted into FRGN recipients, as described in Fig. 14D. Group 1 contained 60% LKO and 40% control (n = 5 recipients); Group 2 contained 17% LKO and 83% control (n = 7 recipients). After complete liver repopulation, the extent of donor

chimerism was determined by β-gal activity. Note that the contribution of β-gal- FRGN hepatocytes was considered negligible because these cells represented <10% of the hepatocyte pool after liver repopulation, as illustrated in Fig. 14E. Tables show the percentage of β-gal- and β-gal+ hepatocytes at the time of transplant (marked as "input") and after liver repopulation (marked as "output") for each transplant recipient. The ratio of "output to input" β-gal+ cells is reported to highlight the fold expansion by LKO cells during liver repopulation. These data are summarized in Fig. 14F.

A.2 Detailed information for select reagents

Table 2. Primer Pairs

Gene	*Forward primer (5′ to 3′)*	*Reverse primer (5′ to 3′)*
Ccna2	TGTCAACCCCGAAAAACTGG	ATGAATGGTGAAGGCAGGCT
Ccnb1	GGCTTTCTCTGATGTAATCCTTGC	TCTTCTTGGGCACACAACTGTTC
Ccnd1	TCAAGACGGAGGAGACCTGT	GGAAGCGGTCCAGGTAGTTC
Ccne1	TGAGTTCCAAGCCCAAGTCC	GGATGAAAGAGCAGGGGTCC
Cyp2e1	TTTCTGCAGGAAAGCGCG	CTGCCAAAGCCAATTGTAACAG
Cyp2b10	CACACGGAGTTCCATCACCA	GCGGTCATCAAGGGTTGGTA
Car	TCAACACGTTTATGGTGCAA	CTGCGTCCTCCATCTTGTAG
E2f7	TCTCCCTAGATGAGGTCGCC	GACCGTGCCAACCATACTGA
E2f8	GAGAAATCCCAGCCGAGTC	CATAAATCCGCCGACGTT
Gapdh	TCCTGCACCACCAACTGCTTAG	TGCTTCACCACCTTCTTGATGTC

Table 3. Primary Antibodies

Epitope	*Antibody with species reactivity*	*Vendor*	*Catalog #*
β-catenin	Rabbit anti-β-catenin	Santa Cruz	sc-7199
β-catenin	Mouse anti-β-catenin	Santa Cruz	sc-7963
BrdU	Mouse anti-BrdU	BD Biosciences	347580
Cyp1A2	Goat anti-Cyp1a2	Santa Cruz	sc-9835
E-cadherin	Mouse anti-E-cadherin	BD Biosciences	610181
FAH	Rabbit anti-FAH	Custom, Grompe Lab	n/a
Glutamine Synthetase	Mouse anti-Glutamine Synthetase	Santa Cruz	sc-74430
Glutamine Synthetase	Rabbit anti-Glutamine Synthetase	Abcam	ab49873
$H2K^q$	Mouse anti-$H2K^q$ AlexaFluor 647	Biolegend	115106
Ki-67	Mouse anti-Ki-67 eFluor660	Invitrogen	50569882
Ki-67	Rabbit anti-Ki-67	Abcam	ab15580
PCNA	Mouse anti-PCNA IgG2a	Santa Cruz	sc-25280
Phospho-histone H3	Rabbit anti-Phospho-histone H3	Invitrogen	PA5-17869

Table 4. Secondary Antibodies

Species reactivity	*Antibody with conjugate*	*Vendor*	*Catalog #*
Goat	Donkey anti-Goat/AlexaFluor 594	Life Technologies	A11058
Mouse	Donkey anti-Mouse/AlexaFluor 647	Life Technologies	A31571
Mouse	Goat anti-Mouse/AlexaFluor 488	Life Technologies	A11029
Mouse	Goat anti-Mouse/AlexaFluor 488 (specific for IgG2a)	Life Technologies	A21131
Mouse	Goat anti-Mouse/AlexaFluor 594	Life Technologies	A11055
Mouse	Goat anti-Mouse/AlexaFluor 594 (specific for IgG1)	Life Technologies	A21125
Rabbit	Donkey anti-Rabbit/AlexaFluor 488	Life Technologies	A11055
Rabbit	Donkey anti-Rabbit/AlexaFluor 555	Life Technologies	A31572
Rabbit	Goat anti-Rabbit/AlexaFluor 594	Life Technologies	A11012
Rabbit	Goat anti-Rabbit/AlexaFluor 647	Life Technologies	A21244
Rabbit	Goat anti-Rabbit/Biotinylated	Vector Laboratories	BA-1000

Appendix B – Additional information for chapter 3

B.1 Karyotypes of control hepatocytes

Control hepatocytes (adult), mouse 1

Aneu-ploid	Nearest Ploidy	Chr Number	Sex Chr	Chr Losses	Chr Gains	Additional Abnormalities
yes	2n	35	XY	1, 6, 14x2, 16		
yes	2n	39	XY	18		
	2n	40	XY			
	2n	40	XY			
yes	2n	40	XY	9	15	
yes	3n	52	XXY	1, 2, 3x2, 10, 11x2, 14x2, 15, 16, 19	5, 12, 13, 18	
yes	4n	79	XXYY	18		
yes	4n	79	XXYY	6		
	4n	80	XXYY			
	4n	80	XXYY			
	4n	80	XXYY			
	4n	80	XXYY			
	4n	80	XXYY			
yes	4n	81	XXYY	1	16, 17	

Control hepatocytes (adult), mouse 2

Aneu-ploid	Nearest Ploidy	Chr Number	Sex Chr	Chr Losses	Chr Gains	Additional Abnormalities
yes	2n	42	XYY		15, Y	Der(11)T(XA6; 11B3)
yes	3n	53	XYY	2, 3, 5, 11, 14, 17x2		
yes	4n	73	XYY	1, 4, 6x2, 14, 18, X		
yes	4n	78	XXYY	14x2	8	Rb(7.8)
yes	4n	79	XXYY	17		
	4n	80	XXYY			
	4n	80	XXYY			
yes	4n	80	XXYY	11	18	
	4n	80	XXYY			
	4n	80	XXYY			
	4n	80	XXYY			
	4n	80	XXYY			
	4n	80	XXYY			
	4n	80	XXYY			

Control hepatocytes (adult), mouse 3

Aneu-ploid	Nearest Ploidy	Chr Number	Sex Chr	Chr Losses	Chr Gains	Additional Abnormalities
	2n	40	XY			
yes	3n	59	XXYYY	1, 7, 9, 11, 17, 19x2	3, 8, 13, 15, XY or YY	
yes	3n	69	XXY	18	2, 5, 6, 9, 10, 11, 13, 15, 16, 19	
yes	4n	71	XYY	1, 2, 6, 8, 9, 12, 18x2, X		
yes	4n	72	XXY	3, 4, 5, 6, 7, 12, 16, Y		
yes	4n	75	XXYY	3, 4, 7, 8, 11		
yes	4n	78	XXYY	1, 15		
yes	4n	79	XXYY	6		
	4n	80	XXYY			
	4n	80	XXYY			
	4n	80	XXYY			
	4n	80	XXYY			
	4n	80	XXYY			
	4n	80	XXYY			
	4n	80	XXYY			
	4n	80	XXYY			
	4n	80	XXYY			
	4n	80	XXYY			
yes	8n	159	XXXXYYYY	19		

Control hepatocytes (adult), mouse 4

Aneu-ploid	Nearest Ploidy	Chr Number	Sex Chr	Chr Losses	Chr Gains	Additional Abnormalities
yes	2n	35	XY	2, 3, 9, 12, 13, 17, 18, 19	6x2, 16	
yes	2n	38	XXY	1, 5, 6, 9, 11, 13, 15	4, 7, 12, 19, X	
	2n	40	XY			
yes	3n	60	XXYY	1, 3, 7, 8, 13x2, 14, 15	2, 4, 9, 10, 11, 12, 19, X or Y	
yes	4n	70	XXY	1, 6x2, 7, 10, 12, 14, 15, 18, Y		
yes	4n	72	XXY	4, 9, 11, 14x2, 15, 17, Y		
yes	4n	73	XXYY	1, 4, 7, 8, 9, 11, 16		
yes	4n	75	XXYY	3, 7, 11, 14, 19		
yes	4n	76	XXYY	9, 15x2, 16		
yes	4n	76	XXYY	1x2, 5, 8		
yes	4n	79	XXYY	13		
yes	4n	79	XXYY	3, 12	19	Dic(7)
	4n	80	XXYY			
	4n	80	XXYY			
	4n	80	XXYY			
	4n	80	XXYY			
yes	4n	80	XXYY	3, 17	5, 13	
	4n	80	XXYY			
	4n	80	XXYY			
	4n	80	XXYY			

Figure 33. Karyotypes of control hepatocytes.

Hepatocytes isolated from 4-month-old control livers were karyotyped by G-banding (n = 4 mice; 14-20 cells per mouse). Cells are arranged based on ascending chromosome number. The nearest ploidy (2n, 3n, 4n, etc.) is indicated according to standard cytogenetic convention, and whole chromosome gains/losses are reported relative to the nearest ploidy. These karyotypes were used for analyses in Fig. 24.

B.2 Karyotypes of LKO hepatocytes

LKO hepatocytes (adult), mouse 1

Aneu-ploid	Nearest Ploidy	Chr Number	Sex Chr	Chr Losses	Chr Gains	Additional Abnormalities
yes	2n	39	XY	17		
yes	2n	39	XY	11		
yes	2n	39	XY	18		
	2n	40	XY			
	2n	40	XY			
	2n	40	XY			
	2n	40	XY			
	2n	40	XY			
	2n	40	XY			
	2n	40	XY			
	2n	40	XY			
	2n	40	XY			
	2n	40	XY			
	2n	40	XY			
	2n	40	XY			
	2n	40	XY			
	2n	40	XY			
	2n	40	XY			
	2n	40	XY			
	2n	40	XY			
	4n	80	XXYY			

LKO hepatocytes (adult), mouse 2

Aneu-ploid	Nearest Ploidy	Chr Number	Sex Chr	Chr Losses	Chr Gains	Additional Abnormalities
	2n	40	XY			
	2n	40	XY			
	2n	40	XY			
	2n	40	XY			
	2n	40	XY			
	2n	40	XY			
	2n	40	XY			
	2n	40	XY			
	2n	40	XY			
	2n	40	XY			
	2n	40	XY			
	2n	40	XY			
	2n	40	XY			
	2n	40	XY			
	2n	40	XY			
	2n	40	XY			
	2n	40	XY			
	2n	40	XY			
	2n	40	XY			Mar
	4n	80	XXYY			
	4n	80	XXYY			

LKO hepatocytes (adult), mouse 3

Aneu-ploid	Nearest Ploidy	Chr Number	Sex Chr	Chr Losses	Chr Gains	Additional Abnormalities
	2n	40	XY			
	2n	40	XY			
	2n	40	XY			
	2n	40	XY			
	2n	40	XY			
	2n	40	XY			
	2n	40	XY			
	2n	40	XY			
	2n	40	XY			
	2n	40	XY			
	2n	40	XY			
	2n	40	XY			
	2n	40	XY			
	2n	40	XY			
	2n	40	XY			
	2n	40	XY			
	2n	40	XY			
	2n	40	XY			
	2n	40	XY			
	2n	40	XY			
	2n	40	XY			

LKO hepatocytes (adult), mouse 4

Aneu-ploid	Nearest Ploidy	Chr Number	Sex Chr	Chr Losses	Chr Gains	Additional Abnormalities
yes	2n	39	XY	13		
yes	2n	39	XY	13		
	2n	40	XY			
	2n	40	XY			
	2n	40	XY			
	2n	40	XY			
	2n	40	XY			
	2n	40	XY			
	2n	40	XY			
	2n	40	XY			
	2n	40	XY			
	2n	40	XY			
	2n	40	XY			
	2n	40	XY			
	2n	40	XY			
	2n	40	XY			
	2n	40	XY			
	2n	40	XY			
	2n	40	XY			
yes	2n	41	XY		6	
yes	4n	79	XXYY	14		

Figure 34. Karyotypes of LKO hepatocytes.

Hepatocytes isolated from 4-month-old LKO livers were karyotyped by G-banding (n = 4 mice; 20 cells per mouse). Cells are arranged based on ascending chromosome number. The nearest ploidy (2n, 3n, 4n, etc.) is indicated according to standard cytogenetic convention, and whole chromosome gains/losses are reported relative to the nearest ploidy. These karyotypes were used for analyses in Fig. 24.

B.3 Karyotypes of LKO hepatocytes following liver repopulation

LKO hepatocytes (donor-derived), repopulated mouse 1

Aneu-ploid	Nearest Ploidy	Chr Number	Sex Chr	Chr Losses	Chr Gains	Additional Abnormalities
yes	2n	39	XY	2		
yes	2n	39	XY	12		
yes	2n	39	XY	8		
yes	2n	39	XY	16		
	2n	40	XY			
	2n	40	XY			
	2n	40	XY			
	2n	40	XY			
	2n	40	XY			
	2n	40	XY			
	2n	40	XY			
	2n	40	XY			
	2n	40	XY			
	2n	40	XY			
	2n	40	XY			
	2n	40	XY			
	2n	40	XY			
	2n	40	XY			
	2n	40	XY			
	2n	40	XY			

LKO hepatocytes (donor-derived), repopulated mouse 2

Aneu-ploid	Nearest Ploidy	Chr Number	Sex Chr	Chr Losses	Chr Gains	Additional Abnormalities
yes	2n	38	XY	8, 14		
yes	2n	38	XY	3, 12		
yes	2n	39	XY	9		
yes	2n	40	XY			Del(12)
yes	2n	40	XY			Inv(7)
	2n	40	XY			
	2n	40	XY			
	2n	40	XY			
	2n	40	XY			
	2n	40	XY			
	2n	40	XY			
	2n	40	XY			
	2n	40	XY			
	2n	40	XY			
	2n	40	XY			
	2n	40	XY			
	2n	40	XY			
	2n	40	XY			
	2n	40	XY			

LKO hepatocytes (donor-derived), repopulated mouse 3

Aneu-ploid	Nearest Ploidy	Chr Number	Sex Chr	Chr Losses	Chr Gains	Additional Abnormalities
yes	2n	37	XY	1, 16, 18		
yes	2n	39	XY	18		T(1;8)
yes	2n	39	XY	7		
	2n	40	XY			
	2n	40	XY			
	2n	40	XY			
	2n	40	XY			
	2n	40	XY			
	2n	40	XY			
	2n	40	XY			
	2n	40	XY			
	2n	40	XY			
	2n	40	XY			
	2n	40	XY			
	2n	40	XY			
	2n	40	XY			
	2n	40	XY			
	2n	40	XY			
yes	4n	75	XXYY	5, 7, 8, 10, 12		

LKO hepatocytes (donor-derived), repopulated mouse 4

Aneu-ploid	Nearest Ploidy	Chr Number	Sex Chr	Chr Losses	Chr Gains	Additional Abnormalities
	2n	40	XY			
	2n	40	XY			
	2n	40	XY			
	2n	40	XY			
	2n	40	XY			
	2n	40	XY			
	2n	40	XY			
	2n	40	XY			
	2n	40	XY			
	2n	40	XY			
	2n	40	XY			
	2n	40	XY			
	2n	40	XY			
	2n	40	XY			
	2n	40	XY			
	2n	40	XY			
	2n	40	XY			
	2n	40	XY			
	2n	40	XY			
	4n	80	XXYY			

Figure 35. Karyotypes of LKO hepatocytes following liver repopulation.

Hepatocytes were isolated from female FRGN livers that were repopulated by male LKO hepatocytes, as described in Fig. 25. Chromosomes were identified by G-banding and karyotypes reported for donor- derived (Y chromosome^{+}) hepatocytes (n = 4 mice; 20 cells per mouse). Cells are arranged based on ascending chromosome number. The nearest ploidy is indicated according to standard cytogenetic convention, and whole chromosome gains/losses are reported relative to the nearest ploidy. These karyotypes were used for analyses in Fig. 25.

B.4 Macroscopic images of livers with regenerating nodules

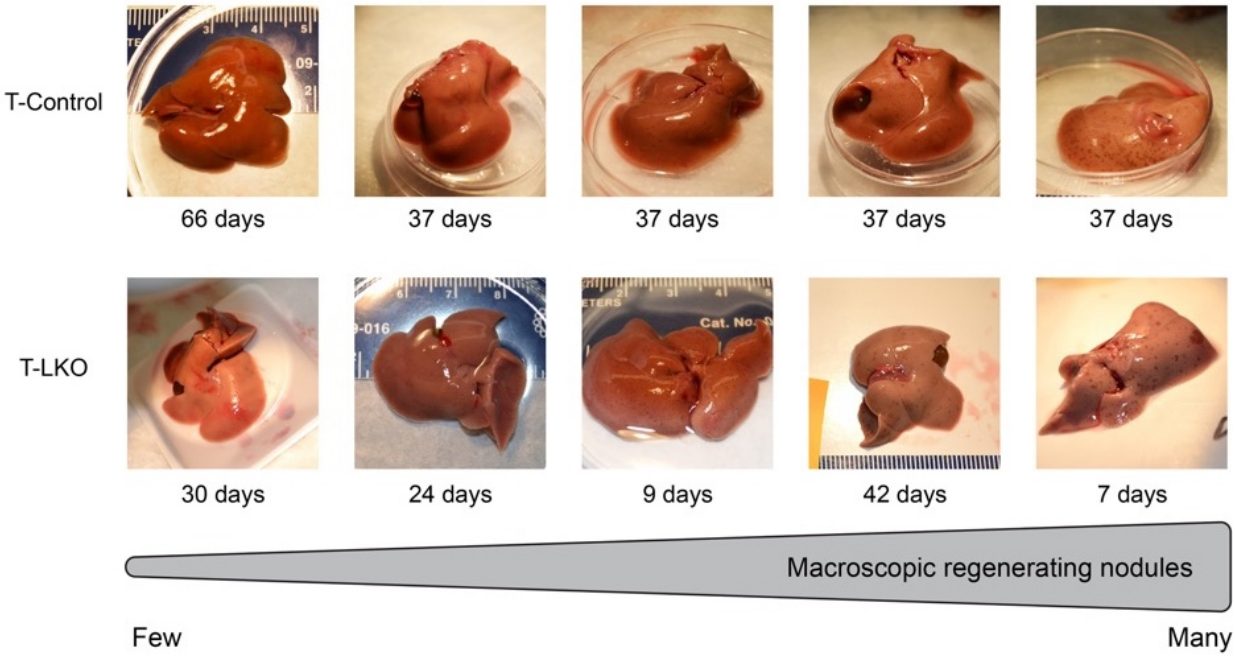

Figure 36. The size of macroscopic regenerating nodules in tyrosinemia-injured livers is independent of the length of injury.

T-control and T-LKO livers were cycled off/on NTBC as described in Fig. 26C. Most livers contained macroscopic regenerating nodules, but nodule size and number varied. Representative images depict liver heterogeneity from T-control and T-LKO livers that were harvested. Livers are arranged from least (left) to most (right) nodules, and the duration of tyrosinemia-induced liver injury (caused by NTBC withdrawal) is indicated beneath each picture.

B.5 Genomic and transcriptomic data for regenerative nodules isolated from T-control and T-LKO mice

T-Control

Mouse	Total Nodules	*Hgd* genotype (DNA)		*Hgd* transcripts (RNA), # Nodules		
		Genotype	# Nodules	FL only	FL + SV	SV only
1	13	+/–	10	2	2	6
		–/–	3	0	0	3
2	15	+/–	12	0	10	2
		–/–	3	1	1	1
3	14	+/–	10	3	7	0
		–/–	4	0	2	2
4	15	+/–	6	0	5	1
		–/–	9	1	0	8
Sum	***57***	***+/–***	***38***	***5***	***24***	***9***
		–/–	***19***	***2***	***3***	***14***

T-LKO

Mouse	Total Nodules	*Hgd* genotype (DNA)		*Hgd* transcripts (RNA), # Nodules		
		Genotype	# Nodules	FL only	FL + SV	SV only
1	16	+/–	9	1	2	6
		–/–	7	0	1	6
2	14	+/–	13	2	6	5
		–/–	1	1	0	0
3	15	+/–	11	0	8	3
		–/–	4	0	1	3
4	9	+/–	7	2	3	2
		–/–	2	0	0	2
Sum	***54***	***+/–***	***40***	***5***	***19***	***16***
		–/–	***14***	***1***	***2***	***11***

Figure 37. Regenerative nodules isolated from T-control and T-LKO mice.

The number of LCM-isolated nodules per mouse genotyped as *Hgd*+/– and *Hgd*–/– is indicated (n = 4 mice/genotype). Furthermore, the number of nodules within each sub-group containing *Hgd* transcripts (FL only, FL + SV, SV only) is noted. Data are summarized in Fig. 29.

B.6 Detailed information for select reagents

Table 5. Primer Pairs

Gene	*Forward primer (5′ to 3′)*	*Reverse primer (5′ to 3′)*
Hgd - DNA	TTTAGTCGCTGCATCACC	CATTTTCACCGTGCTGAC
Hgd - cDNA 1	TTTGAGGAGACCAGGGGCTA	TCAATTACAGTAGAGGGCTCCAGTC
Hgd - cDNA 2	GCCTGGTATGAAGATCGTCGAG	TCAATTACAGTAGAGGGCTCCAGTC

Table 6. Primary Antibodies

Epitope	*Antibody with species reactivity*	*Vendor*	*Catalog #*
β-catenin	Mouse anti-β-catenin	Santa Cruz	sc-7963
Ki-67	Rabbit anti-Ki-67	Abcam	ab15580

Table 7. Secondary Antibodies

Epitope	*Antibody with species reactivity*	*Vendor*	*Catalog #*
Mouse	Goat anti-Mouse/AlexaFluor 488	Life Technologies	A11029
Rabbit	Goat anti-Rabbit/AlexaFluor 594	Life Technologies	A11012
Rabbit	Goat anti-Rabbit/Biotinylated	Vector Laboratories	BA-1000

Bibliography

1. Duncan AW. Aneuploidy, polyploidy and ploidy reversal in the liver. Semin Cell Dev Biol 2013;24:347-356.
2. Milne LS. The histology of liver tissue regeneration. The Journal of Pathology and Bacteriology 1909;13:127-158.
3. Margall-Ducos G, Celton-Morizur S, Couton D, Bregerie O, Desdouets C. Liver tetraploidization is controlled by a new process of incomplete cytokinesis. J Cell Sci 2007;120:3633-3639.
4. Anisimov AP. Endopolyploidy as a morphogenetic factor of development. Cell Biol Int 2005;29:993-1004.
5. Edgar BA, Zielke N, Gutierrez C. Endocycles: a recurrent evolutionary innovation for post-mitotic cell growth. Nat Rev Mol Cell Biol 2014;15:197-210.
6. Lee HO, Davidson JM, Duronio RJ. Endoreplication: polyploidy with purpose. Genes Dev 2009;23:2461-2477.
7. Neiman M, Beaton MJ, Hessen DO, Jeyasingh PD, Weider LJ. Endopolyploidy as a potential driver of animal ecology and evolution. Biol Rev Camb Philos Soc 2015.
8. Orr-Weaver TL. When bigger is better: the role of polyploidy in organogenesis. Trends Genet 2015;31:307-315.
9. Masterson J. Stomatal size in fossil plants: evidence for polyploidy in majority of angiosperms. Science 1994;264:421-424.
10. Meyers LA, Levin DA. On the abundance of polyploids in flowering plants. Evolution 2006;60:1198-1206.
11. Wertheim B, Beukeboom LW, van de Zande L. Polyploidy in animals: effects of gene expression on sex determination, evolution and ecology. Cytogenet Genome Res 2013;140:256-269.
12. Le Comber SC, Smith C. Polyploidy in fishes: patterns and processes. Biological Journal of the Linnean Society 2004;82:431-442.
13. Session AM, Uno Y, Kwon T, Chapman JA, Toyoda A, Takahashi S, Fukui A, et al. Genome evolution in the allotetraploid frog Xenopus laevis. Nature 2016;538:336-343.

14. Abmayr SM, Pavlath GK. Myoblast fusion: lessons from flies and mice. Development 2012;139:641-656.
15. Helming L, Gordon S. Molecular mediators of macrophage fusion. Trends Cell Biol 2009;19:514-522.
16. Edgar BA, Orr-Weaver TL. Endoreplication cell cycles: more for less. Cell 2001;105:297-306.
17. Engel FB, Schebesta M, Keating MT. Anillin localization defect in cardiomyocyte binucleation. J Mol Cell Cardiol 2006;41:601-612.
18. Bohm N, Noltemeyer N. Development of binuclearity and DNA-polyploidization in the growing mouse liver. Histochemistry 1981;72:55-61.
19. Celton-Morizur S, Merlen G, Couton D, Desdouets C. Polyploidy and liver proliferation: central role of insulin signaling. Cell Cycle 2010;9:460-466.
20. Wang X, Montini E, Al-Dhalimy M, Lagasse E, Finegold M, Grompe M. Kinetics of liver repopulation after bone marrow transplantation. Am J Pathol 2002;161:565-574.
21. Wilson JW, Leduc EH. The occurrence and formation of binucleate and multinucleate cells and polyploid nuclei in the mouse liver. Am J Anat 1948;82:353-391.
22. Duncan AW, Hanlon Newell AE, Smith L, Wilson EM, Olson SB, Thayer MJ, Strom SC, et al. Frequent aneuploidy among normal human hepatocytes. Gastroenterology 2012;142:25-28.
23. Wang MJ, Chen F, Lau JTY, Hu YP. Hepatocyte polyploidization and its association with pathophysiological processes. Cell Death Dis 2017;8:e2805.
24. Watanabe T, Tanaka Y. Age-related alterations in the size of human hepatocytes. A study of mononuclear and binucleate cells. Virchows Arch B Cell Pathol Incl Mol Pathol 1982;39:9-20.
25. Celton-Morizur S, Merlen G, Couton D, Margall-Ducos G, Desdouets C. The insulin/Akt pathway controls a specific cell division program that leads to generation of binucleated tetraploid liver cells in rodents. J Clin Invest 2009;119:1880-1887.
26. Duncan AW, Taylor MH, Hickey RD, Hanlon Newell AE, Lenzi ML, Olson SB, Finegold MJ, et al. The ploidy conveyor of mature hepatocytes as a source of genetic variation. Nature 2010;467:707-710.
27. Hsu SH, Delgado ER, Otero PA, Teng KY, Kutay H, Meehan KM, Moroney JB, et al. MicroRNA-122 regulates polyploidization in the murine liver. Hepatology 2016;64:599-615.

28. Seguin L, Liot C, Mzali R, Harada R, Siret A, Nepveu A, Bertoglio J. CUX1 and E2F1 regulate coordinated expression of the mitotic complex genes Ect2, MgcRacGAP, and MKLP1 in S phase. Mol Cell Biol 2009;29:570-581.
29. Huntington JT, Tang X, Kent LN, Schmidt CR, Leone G. The Spectrum of E2F in Liver Disease--Mediated Regulation in Biology and Cancer. J Cell Physiol 2016;231:1438-1449.
30. Conner EA, Lemmer ER, Sanchez A, Factor VM, Thorgeirsson SS. E2F1 blocks and c-Myc accelerates hepatic ploidy in transgenic mouse models. Biochem Biophys Res Commun 2003;302:114-120.
31. Chen HZ, Ouseph MM, Li J, Pecot T, Chokshi V, Kent L, Bae S, et al. Canonical and atypical E2Fs regulate the mammalian endocycle. Nat Cell Biol 2012;14:1192-1202.
32. Pandit SK, Westendorp B, Nantasanti S, van Liere E, Tooten PC, Cornelissen PW, Toussaint MJ, et al. E2F8 is essential for polyploidization in mammalian cells. Nat Cell Biol 2012;14:1181-1191.
33. Kurinna S, Stratton SA, Coban Z, Schumacher JM, Grompe M, Duncan AW, Barton MC. p53 regulates a mitotic transcription program and determines ploidy in normal mouse liver. Hepatology 2013;57:2004-2013.
34. Mayhew CN, Bosco EE, Fox SR, Okaya T, Tarapore P, Schwemberger SJ, Babcock GF, et al. Liver-specific pRB loss results in ectopic cell cycle entry and aberrant ploidy. Cancer Res 2005;65:4568-4577.
35. Zhang S, Zhou K, Luo X, Li L, Tu HC, Sehgal A, Nguyen LH, et al. The Polyploid State Plays a Tumor-Suppressive Role in the Liver. Dev Cell 2018;44:447-459 e445.
36. Diril MK, Ratnacaram CK, Padmakumar VC, Du T, Wasser M, Coppola V, Tessarollo L, et al. Cyclin-dependent kinase 1 (Cdk1) is essential for cell division and suppression of DNA re-replication but not for liver regeneration. Proc Natl Acad Sci U S A 2012;109:3826-3831.
37. Wu H, Wade M, Krall L, Grisham J, Xiong Y, Van Dyke T. Targeted in vivo expression of the cyclin-dependent kinase inhibitor p21 halts hepatocyte cell-cycle progression, postnatal liver development and regeneration. Genes Dev 1996;10:245-260.
38. Baena E, Gandarillas A, Vallespinos M, Zanet J, Bachs O, Redondo C, Fabregat I, et al. c-Myc regulates cell size and ploidy but is not essential for postnatal proliferation in liver. Proc Natl Acad Sci U S A 2005;102:7286-7291.
39. Chipchase MD, O'Neill M, Melton DW. Characterization of premature liver polyploidy in DNA repair (Ercc1)-deficient mice. Hepatology 2003;38:958-966.

40. Nunez F, Chipchase MD, Clarke AR, Melton DW. Nucleotide excision repair gene (ERCC1) deficiency causes G(2) arrest in hepatocytes and a reduction in liver binucleation: the role of p53 and p21. FASEB J 2000;14:1073-1082.
41. Minamishima YA, Nakayama K, Nakayama K. Recovery of liver mass without proliferation of hepatocytes after partial hepatectomy in Skp2-deficient mice. Cancer Res 2002;62:995-999.
42. Kim SH, Jeon Y, Kim HS, Lee JK, Lim HJ, Kang D, Cho H, et al. Hepatocyte homeostasis for chromosome ploidization and liver function is regulated by Ssu72 protein phosphatase. Hepatology 2016;63:247-259.
43. Hagemann S, Wohlschlaeger J, Bertram S, Levkau B, Musacchio A, Conway EM, Moellmann D, et al. Loss of Survivin influences liver regeneration and is associated with impaired Aurora B function. Cell Death Differ 2013;20:834-844.
44. Birchmeier W. Orchestrating Wnt signalling for metabolic liver zonation. Nat Cell Biol 2016;18:463-465.
45. Kietzmann T. Metabolic zonation of the liver: The oxygen gradient revisited. Redox Biol 2017;11:622-630.
46. Asahina K, Shiokawa M, Ueki T, Yamasaki C, Aratani A, Tateno C, Yoshizato K. Multiplicative mononuclear small hepatocytes in adult rat liver: their isolation as a homogeneous population and localization to periportal zone. Biochem Biophys Res Commun 2006;342:1160-1167.
47. Wang B, Zhao L, Fish M, Logan CY, Nusse R. Self-renewing diploid Axin2(+) cells fuel homeostatic renewal of the liver. Nature 2015;524:180-185.
48. Tanami S, Ben-Moshe S, Elkayam A, Mayo A, Bahar Halpern K, Itzkovitz S. Dynamic zonation of liver polyploidy. Cell Tissue Res 2017;368:405-410.
49. Trefts E, Gannon M, Wasserman DH. The liver. Curr Biol 2017;27:R1147-R1151.
50. Galitski T, Saldanha AJ, Styles CA, Lander ES, Fink GR. Ploidy regulation of gene expression. Science 1999;285:251-254.
51. Raslova H, Kauffmann A, Sekkai D, Ripoche H, Larbret F, Robert T, Tronik Le Roux D, et al. Interrelation between polyploidization and megakaryocyte differentiation: a gene profiling approach. Blood 2007;109:3225-3234.
52. Corbel C, Diabangouaya P, Gendrel AV, Chow JC, Heard E. Unusual chromatin status and organization of the inactive X chromosome in murine trophoblast giant cells. Development 2013;140:861-872.

53. Anatskaya OV, Vinogradov AE. Genome multiplication as adaptation to tissue survival: evidence from gene expression in mammalian heart and liver. Genomics 2007;89:70-80.
54. Lu P, Prost S, Caldwell H, Tugwood JD, Betton GR, Harrison DJ. Microarray analysis of gene expression of mouse hepatocytes of different ploidy. Mamm Genome 2007;18:617-626.
55. Rajvanshi P, Liu D, Ott M, Gagandeep S, Schilsky ML, Gupta S. Fractionation of rat hepatocyte subpopulations with varying metabolic potential, proliferative capacity, and retroviral gene transfer efficiency. Exp Cell Res 1998;244:405-419.
56. Gupta S. Hepatic polyploidy and liver growth control. Semin Cancer Biol 2000;10:161-171.
57. Fausto N, Campbell JS. The role of hepatocytes and oval cells in liver regeneration and repopulation. Mech Dev 2003;120:117-130.
58. Bucher NLR, Malt RA. Regeneration of liver and kidney. 1 ed. Boston: Little Brown, 1971: 278.
59. Miyaoka Y, Ebato K, Kato H, Arakawa S, Shimizu S, Miyajima A. Hypertrophy and unconventional cell division of hepatocytes underlie liver regeneration. Curr Biol 2012;22:1166-1175.
60. Sigal SH, Rajvanshi P, Gorla GR, Sokhi RP, Saxena R, Gebhard DR, Jr., Reid LM, et al. Partial hepatectomy-induced polyploidy attenuates hepatocyte replication and activates cell aging events. Am J Physiol 1999;276:G1260-1272.
61. Gandillet A, Alexandre E, Royer C, Cinqualbre J, Jaeck D, Richert L. Hepatocyte ploidy in regenerating livers after partial hepatectomy, drug-induced necrosis, and cirrhosis. Eur Surg Res 2003;35:148-160.
62. Anti M, Marra G, Rapaccini GL, Rumi C, Bussa S, Fadda G, Vecchio FM, et al. DNA ploidy pattern in human chronic liver diseases and hepatic nodular lesions. Flow cytometric analysis on echo-guided needle liver biopsy. Cancer 1994;73:281-288.
63. Rua S, Comino A, Fruttero A, Torchio P, Bouzari H, Taraglio S, Torchio B, et al. Flow cytometric DNA analysis of cirrhotic liver cells in patients with hepatocellular carcinoma can provide a new prognostic factor. Cancer 1996;78:1195-1202.
64. Schwarze PE, Pettersen EO, Shoaib MC, Seglen PO. Emergence of a population of small, diploid hepatocytes during hepatocarcinogenesis. Carcinogenesis 1984;5:1267-1275.
65. Baker DJ, Childs BG, Durik M, Wijers ME, Sieben CJ, Zhong J, Saltness RA, et al. Naturally occurring p16(Ink4a)-positive cells shorten healthy lifespan. Nature 2016;530:184-189.

66. Sturmlechner I, Durik M, Sieben CJ, Baker DJ, van Deursen JM. Cellular senescence in renal ageing and disease. Nat Rev Nephrol 2017;13:77-89.
67. Wang MJ, Chen F, Li JX, Liu CC, Zhang HB, Xia Y, Yu B, et al. Reversal of hepatocyte senescence after continuous in vivo cell proliferation. Hepatology 2014;60:349-361.
68. Bucher NL, Swaffield MN, Ditroia JF. The Influence of Age Upon the Incorporation of Thymidine-2-C14 into the DNA of Regenerating Rat Liver. Cancer Res 1964;24:509-512.
69. Fry M, Silber J, Loeb LA, Martin GM. Delayed and reduced cell replication and diminishing levels of DNA polymerase-alpha in regenerating liver of aging mice. J Cell Physiol 1984;118:225-232.
70. Timchenko NA, Wilde M, Kosai KI, Heydari A, Bilyeu TA, Finegold MJ, Mohamedali K, et al. Regenerating livers of old rats contain high levels of C/EBPalpha that correlate with altered expression of cell cycle associated proteins. Nucleic Acids Res 1998;26:3293-3299.
71. Conboy IM, Conboy MJ, Wagers AJ, Girma ER, Weissman IL, Rando TA. Rejuvenation of aged progenitor cells by exposure to a young systemic environment. Nature 2005;433:760-764.
72. Iakova P, Awad SS, Timchenko NA. Aging reduces proliferative capacities of liver by switching pathways of C/EBPalpha growth arrest. Cell 2003;113:495-506.
73. Knouse KA, Wu J, Whittaker CA, Amon A. Single cell sequencing reveals low levels of aneuploidy across mammalian tissues. Proc Natl Acad Sci U S A 2014;111:13409-13414.
74. Hsu SH, Delgado ER, Otero PA, Teng KY, Kutay H, Meehan KM, Moroney JB, et al. MicroRNA-122 Regulates Polyploidization in the Murine Liver. Hepatology 2016.
75. Kudryavtsev BN, Kudryavtseva MV, Sakuta GA, Stein GI. Human hepatocyte polyploidization kinetics in the course of life cycle. Virchows Arch B Cell Pathol Incl Mol Pathol 1993;64:387-393.
76. Duncan AW, Hickey RD, Paulk NK, Culberson AJ, Olson SB, Finegold MJ, Grompe M. Ploidy reductions in murine fusion-derived hepatocytes. PLoS Genet 2009;5:e1000385.
77. Faggioli F, Vezzoni P, Montagna C. Single-cell analysis of ploidy and centrosomes underscores the peculiarity of normal hepatocytes. PLoS One 2011;6:e26080.
78. Duncan AW, Hanlon Newell AE, Bi W, Finegold MJ, Olson SB, Beaudet AL, Grompe M. Aneuploidy as a mechanism for stress-induced liver adaptation. J Clin Invest 2012;122:3307-3315.
79. Pavelka N, Rancati G, Zhu J, Bradford WD, Saraf A, Florens L, Sanderson BW, et al. Aneuploidy confers quantitative proteome changes and phenotypic variation in budding yeast. Nature 2010;468:321-325.

80. Rancati G, Pavelka N, Fleharty B, Noll A, Trimble R, Walton K, Perera A, et al. Aneuploidy underlies rapid adaptive evolution of yeast cells deprived of a conserved cytokinesis motor. Cell 2008;135:879-893.
81. Grompe M, Lindstedt S, al-Dhalimy M, Kennaway NG, Papaconstantinou J, Torres-Ramos CA, Ou CN, et al. Pharmacological correction of neonatal lethal hepatic dysfunction in a murine model of hereditary tyrosinaemia type I. Nat Genet 1995;10:453-460.
82. Manning K, Al-Dhalimy M, Finegold M, Grompe M. In vivo suppressor mutations correct a murine model of hereditary tyrosinemia type I. Proc Natl Acad Sci U S A 1999;96:11928-11933.
83. Alqahtani SA. Update in liver transplantation. Curr Opin Gastroenterol 2012;28:230-238.
84. Hoyert DL, Xu J. Deaths: preliminary data for 2011. Natl Vital Stat Rep 2012;61:1-51.
85. Habka D, Mann D, Landes R, Soto-Gutierrez A. Future Economics of Liver Transplantation: A 20-Year Cost Modeling Forecast and the Prospect of Bioengineering Autologous Liver Grafts. PLoS One 2015;10:e0131764.
86. ALF. Liver Transplant. In; 2015.
87. Bernal W, Jalan R, Quaglia A, Simpson K, Wendon J, Burroughs A. Acute-on-chronic liver failure. Lancet 2015;386:1576-1587.
88. Duncan AW, Soto-Gutierrez A. Liver repopulation and regeneration: new approaches to old questions. Curr Opin Organ Transplant 2013;18:197-202.
89. Monga SP. Hepatic regenerative medicine: exploiting the liver's will to live. Am J Pathol 2014;184:306-308.
90. Melchiorri C, Bolondi L, Chieco P, Pagnoni M, Gramantieri L, Barbara L. Diagnostic and prognostic value of DNA ploidy and cell nuclearity in ultrasound-guided liver biopsies. Cancer 1994;74:1713-1719.
91. Toyoda H, Bregerie O, Vallet A, Nalpas B, Pivert G, Brechot C, Desdouets C. Changes to hepatocyte ploidy and binuclearity profiles during human chronic viral hepatitis. Gut 2005;54:297-302.
92. Gentric G, Maillet V, Paradis V, Couton D, L'Hermitte A, Panasyuk G, Fromenty B, et al. Oxidative stress promotes pathologic polyploidization in nonalcoholic fatty liver disease. J Clin Invest 2015;125:981-992.
93. Nagasue N, Kohno H, Chang YC, Yamanoi A, Kimoto T, Takemoto Y, Nakamura T. DNA ploidy pattern in synchronous and metachronous hepatocellular carcinomas. J Hepatol 1992;16:208-214.

94. Saeter G, Schwarze PE, Nesland JM, Juul N, Pettersen EO, Seglen PO. The polyploidizing growth pattern of normal rat liver is replaced by divisional, diploid growth in hepatocellular nodules and carcinomas. Carcinogenesis 1988;9:939-945.
95. Schwarze PE, Saeter G, Armstrong D, Cameron RG, Laconi E, Sarma DS, Preat V, et al. Diploid growth pattern of hepatocellular tumours induced by various carcinogenic treatments. Carcinogenesis 1991;12:325-327.
96. Merlo LM, Wang LS, Pepper JW, Rabinovitch PS, Maley CC. Polyploidy, aneuploidy and the evolution of cancer. Adv Exp Med Biol 2010;676:1-13.
97. Nalesnik MA, Tseng G, Ding Y, Xiang GS, Zheng ZL, Yu Y, Marsh JW, et al. Gene deletions and amplifications in human hepatocellular carcinomas: correlation with hepatocyte growth regulation. Am J Pathol 2012;180:1495-1508.
98. Weaver BA, Cleveland DW. Does aneuploidy cause cancer? Curr Opin Cell Biol 2006;18:658-667.
99. Turner PC, Sylla A, Diallo MS, Castegnaro JJ, Hall AJ, Wild CP. The role of aflatoxins and hepatitis viruses in the etiopathogenesis of hepatocellular carcinoma: A basis for primary prevention in Guinea-Conakry, West Africa. J Gastroenterol Hepatol 2002;17 Suppl:S441-448.
100. Slagle BL, Zhou YZ, Butel JS. Hepatitis B virus integration event in human chromosome 17p near the p53 gene identifies the region of the chromosome commonly deleted in virus-positive hepatocellular carcinomas. Cancer Res 1991;51:49-54.
101. Zasadil LM, Britigan EM, Weaver BA. 2n or not 2n: Aneuploidy, polyploidy and chromosomal instability in primary and tumor cells. Semin Cell Dev Biol 2013;24:370-379.
102. Austin LS, Kaushansky A, Kappe SH. Susceptibility to Plasmodium liver stage infection is altered by hepatocyte polyploidy. Cell Microbiol 2014;16:784-795.
103. Hsu SH, Duncan AW. Pathological polyploidy in liver disease. Hepatology 2015;62:968-970.
104. Madra S, Styles J, Smith AG. Perturbation of hepatocyte nuclear populations induced by iron and polychlorinated biphenyls in C57BL/10ScSn mice during carcinogenesis. Carcinogenesis 1995;16:719-727.
105. Yamada T, Sogawa K, Kim JK, Izumi K, Suzuki Y, Muramatsu Y, Sumida T, et al. Increased polyploidy, delayed mitosis and reduced protein phosphatase-1 activity associated with excess copper in the Long Evans Cinnamon rat. Res Commun Mol Pathol Pharmacol 1998;99:283-304.
106. Fleming RE, Ponka P. Iron overload in human disease. N Engl J Med 2012;366:348-359.

107. Gaetke LM, Chow-Johnson HS, Chow CK. Copper: toxicological relevance and mechanisms. Arch Toxicol 2014;88:1929-1938.
108. Gentric G, Desdouets C. Polyploidization in liver tissue. Am J Pathol 2014;184:322-331.
109. Pandit SK, Westendorp B, de Bruin A. Physiological significance of polyploidization in mammalian cells. Trends Cell Biol 2013;23:556-566.
110. Guidotti JE, Bregerie O, Robert A, Debey P, Brechot C, Desdouets C. Liver cell polyploidization: a pivotal role for binuclear hepatocytes. J Biol Chem 2003;278:19095-19101.
111. Xanthoulis A, Tiniakos DG. E2F transcription factors and digestive system malignancies: how much do we know? World J Gastroenterol 2013;19:3189-3198.
112. Azuma H, Paulk N, Ranade A, Dorrell C, Al-Dhalimy M, Ellis E, Strom S, et al. Robust expansion of human hepatocytes in Fah-/-/Rag2-/-/Il2rg-/- mice. Nat Biotechnol 2007;25:903-910.
113. Wilson EM, Bial J, Tarlow B, Bial G, Jensen B, Greiner DL, Brehm MA, et al. Extensive double humanization of both liver and hematopoiesis in FRGN mice. Stem Cell Res 2014;13:404-412.
114. Overturf K, Al-Dhalimy M, Tanguay R, Brantly M, Ou CN, Finegold M, Grompe M. Hepatocytes corrected by gene therapy are selected in vivo in a murine model of hereditary tyrosinaemia type I. Nat Genet 1996;12:266-273.
115. Mitchell C, Willenbring H. A reproducible and well-tolerated method for 2/3 partial hepatectomy in mice. Nat Protoc 2008;3:1167-1170.
116. Ganem NJ, Storchova Z, Pellman D. Tetraploidy, aneuploidy and cancer. Curr Opin Genet Dev 2007;17:157-162.
117. Hanahan D, Weinberg RA. Hallmarks of cancer: the next generation. Cell 2011;144:646-674.
118. Zhang S, Li L, Kendrick SL, Gerard RD, Zhu H. TALEN-mediated somatic mutagenesis in murine models of cancer. Cancer Res 2014;74:5311-5321.
119. Aydinlik H, Nguyen TD, Moennikes O, Buchmann A, Schwarz M. Selective pressure during tumor promotion by phenobarbital leads to clonal outgrowth of beta-catenin-mutated mouse liver tumors. Oncogene 2001;20:7812-7816.
120. Loeppen S, Schneider D, Gaunitz F, Gebhardt R, Kurek R, Buchmann A, Schwarz M. Overexpression of glutamine synthetase is associated with beta-catenin-mutations in mouse liver tumors during promotion of hepatocarcinogenesis by phenobarbital. Cancer Res 2002;62:5685-5688.

121. Moennikes O, Buchmann A, Romualdi A, Ott T, Werringloer J, Willecke K, Schwarz M. Lack of phenobarbital-mediated promotion of hepatocarcinogenesis in connexin32-null mice. Cancer Res 2000;60:5087-5091.
122. Schmid A, Rignall B, Pichler BJ, Schwarz M. Quantitative analysis of the growth kinetics of chemically induced mouse liver tumors by magnetic resonance imaging. Toxicol Sci 2012;126:52-59.
123. Bakiri L, Wagner EF. Mouse models for liver cancer. Mol Oncol 2013;7:206-223.
124. Cieply B, Zeng G, Proverbs-Singh T, Geller DA, Monga SP. Unique phenotype of hepatocellular cancers with exon-3 mutations in beta-catenin gene. Hepatology 2009;49:821-831.
125. Honkakoski P, Zelko I, Sueyoshi T, Negishi M. The nuclear orphan receptor CAR-retinoid X receptor heterodimer activates the phenobarbital-responsive enhancer module of the CYP2B gene. Mol Cell Biol 1998;18:5652-5658.
126. Li L, Bao X, Zhang QY, Negishi M, Ding X. Role of CYP2B in Phenobarbital-Induced Hepatocyte Proliferation in Mice. Drug Metab Dispos 2017;45:977-981.
127. Shirakami Y, Gottesman ME, Blaner WS. Diethylnitrosamine-induced hepatocarcinogenesis is suppressed in lecithin:retinol acyltransferase-deficient mice primarily through retinoid actions immediately after carcinogen administration. Carcinogenesis 2012;33:268-274.
128. Kent LN, Rakijas JB, Pandit SK, Westendorp B, Chen HZ, Huntington JT, Tang X, et al. E2f8 mediates tumor suppression in postnatal liver development. J Clin Invest 2016;126:2955-2969.
129. Bertoli C, Skotheim JM, de Bruin RA. Control of cell cycle transcription during G1 and S phases. Nat Rev Mol Cell Biol 2013;14:518-528.
130. Klochendler A, Weinberg-Corem N, Moran M, Swisa A, Pochet N, Savova V, Vikesa J, et al. A transgenic mouse marking live replicating cells reveals in vivo transcriptional program of proliferation. Dev Cell 2012;23:681-690.
131. Michalopoulos GK. Liver regeneration. J Cell Physiol 2007;213:286-300.
132. Michalopoulos GK, DeFrances MC. Liver regeneration. Science 1997;276:60-66.
133. Higgins G, Anderson GM. Experimental pathology of the liver. Restoration of the liver of the white rat following partial surgical removal. Arch Pathol 1931;12:186-202.
134. Michalopoulos GK. Liver regeneration after partial hepatectomy: critical analysis of mechanistic dilemmas. Am J Pathol 2010;176:2-13.

135. Kreutz C, MacNelly S, Follo M, Waldin A, Binninger-Lacour P, Timmer J, Bartolome-Rodriguez MM. Hepatocyte Ploidy Is a Diversity Factor for Liver Homeostasis. Front Physiol 2017;8:862.
136. Bowen WC, Michalopoulos AW, Orr A, Ding MQ, Stolz DB, Michalopoulos GK. Development of a chemically defined medium and discovery of new mitogenic growth factors for mouse hepatocytes: mitogenic effects of FGF1/2 and PDGF. PLoS One 2014;9:e95487.
137. Johnson DG. The paradox of E2F1: oncogene and tumor suppressor gene. Mol Carcinog 2000;27:151-157.
138. Saeter G, Schwarze PE, Nesland JM, Seglen PO. Diploid nature of hepatocellular tumours developing from transplanted preneoplastic liver cells. Br J Cancer 1989;59:198-205.
139. Knouse KA, Lopez KE, Bachofner M, Amon A. Chromosome Segregation Fidelity in Epithelia Requires Tissue Architecture. Cell 2018.
140. Thompson SL, Bakhoum SF, Compton DA. Mechanisms of chromosomal instability. Curr Biol 2010;20:R285-295.
141. Leenders MW, Nijkamp MW, Borel Rinkes IH. Mouse models in liver cancer research: a review of current literature. World J Gastroenterol 2008;14:6915-6923.
142. Grompe M. Fah Knockout Animals as Models for Therapeutic Liver Repopulation. Adv Exp Med Biol 2017;959:215-230.
143. Nakamura K, Tanaka Y, Mitsubuchi H, Endo F. Animal models of tyrosinemia. J Nutr 2007;137:1556S-1560S; discussion 1573S-1575S.
144. Endo F, Kubo S, Awata H, Kiwaki K, Katoh H, Kanegae Y, Saito I, et al. Complete rescue of lethal albino c14CoS mice by null mutation of 4-hydroxyphenylpyruvate dioxygenase and induction of apoptosis of hepatocytes in these mice by in vivo retrieval of the tyrosine catabolic pathway. J Biol Chem 1997;272:24426-24432.
145. Moon NS, Dyson N. E2F7 and E2F8 keep the E2F family in balance. Dev Cell 2008;14:1-3.
146. Wilkinson PD, Delgado ER, Alencastro F, Leek MP, Roy N, Weirich MP, Stahl EC, et al. The Polyploid State Restricts Hepatocyte Proliferation and Liver Regeneration in Mice. Hepatology 2019;69:1242-1258.
147. Yovchev MI, Locker J, Oertel M. Biliary fibrosis drives liver repopulation and phenotype transition of transplanted hepatocytes. J Hepatol 2016;64:1348-1357.
148. Manning K, Fernandez-Canon JM, Montagutelli X, Grompe M. Identification of the mutation in the alkaptonuria mouse model. Mutations in brief no. 216. Online. Hum Mutat 1999;13:171.

149. Postic C, Magnuson MA. DNA excision in liver by an albumin-Cre transgene occurs progressively with age. Genesis 2000;26:149-150.
150. Odin P, Obrink B. Dynamic expression of the cell adhesion molecule cell-CAM 105 in fetal and regenerating rat liver. Exp Cell Res 1986;164:103-114.
151. Odin P, Obrink B. The cell-surface expression of the cell adhesion molecule cellCAM 105 in rat fetal tissues and regenerating liver. Exp Cell Res 1988;179:89-103.
152. Ochiai T, Urata Y, Yamano T, Yamagishi H, Ashihara T. Clonal expansion in evolution of chronic hepatitis to hepatocellular carcinoma as seen at an X-chromosome locus. Hepatology 2000;31:615-621.
153. Paradis V, Dargere D, Bonvoust F, Rubbia-Brandt L, Ba N, Bioulac-Sage P, Bedossa P. Clonal analysis of micronodules in virus C-induced liver cirrhosis using laser capture microdissection (LCM) and HUMARA assay. Lab Invest 2000;80:1553-1559.
154. Paradis V, Laurendeau I, Vidaud M, Bedossa P. Clonal analysis of macronodules in cirrhosis. Hepatology 1998;28:953-958.
155. QuickStats: Death Rates* for Chronic Liver Disease and Cirrhosis,(dagger) by Sex and Age Group - National Vital Statistics System, United States, 2000 and 2015. MMWR Morb Mortal Wkly Rep 2017;66:1031.
156. Mikolasevic I, Filipec-Kanizaj T, Mijic M, Jakopcic I, Milic S, Hrstic I, Sobocan N, et al. Nonalcoholic fatty liver disease and liver transplantation - Where do we stand? World J Gastroenterol 2018;24:1491-1506.
157. Michalopoulos GK. Hepatostat: Liver regeneration and normal liver tissue maintenance. Hepatology 2017;65:1384-1392.
158. Monga SP. beta-Catenin Signaling and Roles in Liver Homeostasis, Injury, and Tumorigenesis. Gastroenterology 2015;148:1294-1310.
159. Martin J, Dufour JF. Tumor suppressor and hepatocellular carcinoma. World J Gastroenterol 2008;14:1720-1733.
160. Wilkinson PD, Alencastro F, Delgado ER, Leek MP, Weirich MP, Otero PA, Roy N, et al. Polyploid Hepatocytes Facilitate Adaptation and Regeneration to Chronic Liver Injury. Am J Pathol 2019;189:1241-1255.

161. Pradhan-Sundd T, Zhou L, Vats R, Jiang A, Molina L, Singh S, Poddar M, et al. Dual catenin loss in murine liver causes tight junctional deregulation and progressive intrahepatic cholestasis. Hepatology 2018;67:2320-2337.
162. Forbes SJ, Gupta S, Dhawan A. Cell therapy for liver disease: From liver transplantation to cell factory. J Hepatol 2015;62:S157-169.
163. Gupta S, Aragona E, Vemuru RP, Bhargava KK, Burk RD, Chowdhury JR. Permanent engraftment and function of hepatocytes delivered to the liver: implications for gene therapy and liver repopulation. Hepatology 1991;14:144-149.
164. Weaver BA, Cleveland DW. The aneuploidy paradox in cell growth and tumorigenesis. Cancer Cell 2008;14:431-433.
165. Alter MJ. Epidemiology of hepatitis C virus infection. World J Gastroenterol 2007;13:2436-2441.
166. de Martel C, Maucort-Boulch D, Plummer M, Franceschi S. World-wide relative contribution of hepatitis B and C viruses in hepatocellular carcinoma. Hepatology 2015;62:1190-1200.
167. El-Serag HB. Epidemiology of viral hepatitis and hepatocellular carcinoma. Gastroenterology 2012;142:1264-1273 e1261.
168. Pawlotsky JM. New hepatitis C therapies: the toolbox, strategies, and challenges. Gastroenterology 2014;146:1176-1192.
169. Liu S, Yang W, Shen L, Turner JR, Coyne CB, Wang T. Tight junction proteins claudin-1 and occludin control hepatitis C virus entry and are downregulated during infection to prevent superinfection. J Virol 2009;83:2011-2014.
170. Mee CJ, Farquhar MJ, Harris HJ, Hu K, Ramma W, Ahmed A, Maurel P, et al. Hepatitis C virus infection reduces hepatocellular polarity in a vascular endothelial growth factor-dependent manner. Gastroenterology 2010;138:1134-1142.
171. Benedicto I, Molina-Jimenez F, Barreiro O, Maldonado-Rodriguez A, Prieto J, Moreno-Otero R, Aldabe R, et al. Hepatitis C virus envelope components alter localization of hepatocyte tight junction-associated proteins and promote occludin retention in the endoplasmic reticulum. Hepatology 2008;48:1044-1053.
172. Duncan AW: Changes in Hepatocyte Ploidy During Liver Regeneration. In: Apte U, ed. Liver Regeneration: Basic Mechanisms, Relevant Models and Clinical Applications: Elsevier, 2015.
173. Bahar Halpern K, Tanami S, Landen S, Chapal M, Szlak L, Hutzler A, Nizhberg A, et al. Bursty gene expression in the intact mammalian liver. Mol Cell 2015;58:147-156.

174. Schoenfelder KP, Fox DT. The expanding implications of polyploidy. J Cell Biol 2015;209:485-491.
175. Durrbaum M, Storchova Z. Effects of aneuploidy on gene expression: implications for cancer. FEBS J 2016;283:791-802.